Topics in Viscous Shear Flow Dynamics

by

Harry Lee

A dissertation submitted in partial fulfillment
of the requirements for the degree of
Doctor of Philosophy
(Applied and Interdisciplinary Mathematics)
in The University of Michigan
2020

Doctoral Committee:

Professor Charles R. Doering, Co-Chair
Professor Alan S. Wineman, Co-Chair
Professor Silas D. Alben
Professor Anthony M. Bloch
Associate Professor Zaher Hani

Harry Lee

leeharry@umich.edu

ORCID iD: 0000-0001-6392-9894

ACKNOWLEDGEMENTS

First, I want to express my sincere gratitude to my advisor, Charles R. Doering. Words fail to express how lucky I am to grow as a young physicist under his direct supervision. Professor Doering shows a lot of respect on my research endeavors and I owe him a great deal of thanks for his wisdom, encouragements and patience over the years.

Next, I would like to thank my former advisor from the University of Auckland, Shixiao Wang, for his continued support throughout my study here at Michigan. I and him had recently established a novel viscous Arnold's identity for flow stability analysis, our new viscous theory had a nurturing impact on my Ph.D. research.

Additionally, I would like to thank the co-chair of my committee, Alan S. Wineman, a faculty member from the mechanical engineering department who is always ready to meet with me and provide administrative services as requested by the math department. Also, let me thank my dissertation committee members: Silas D. Alben, Anthony M. Bloch, and Zaher Hani.

TABLE OF CONTENTS

LIST OF FIGURES

Figure

ABSTRACT

Improved upper bounds on viscous energy dissipation rates of wall-driven shear flow subject to uniform injection and suction rates are computationally determined. The so-called 'background' variational formulation is implemented via a time-stepping numerical scheme to determine optimal estimates. Shear flow Reynolds numbers range from 50 to 40 000 with injection angles up to 2°. The computed upper bounds for pre-selected angles of injection at high Reynolds numbers significantly improve the rigorously estimated ones. Our results suggest that the steady laminar flow is nonlinearly stable for angles of injection greater than 2°.

A viscous extension of Arnold's inviscid theory for non-inflectional plane shear flows is developed and viscous Arnold's identities are obtained. Special forms of our viscous Arnold's identities have been revealed that are closely related to the perturbation's enstrophy identity derived by Synge [44] [see also 17]. As an application of our enstrophy identities, we quantitatively investigate mechanisms of linear stability/instability within the normal modal framework. The investigation reveals a subtle interaction between a critical layer and its adjacent boundary layer, which governs stability/instability of disturbances. As an implementation of relaxed wall boundary conditions imposed for our enstrophy identity, a control scheme is proposed that transitions wall settings from the no-slip condition to the free-slip condition, through which a flow is stabilized quickly within an early stage of the transition.

CHAPTER I

Introduction

1.1 Energy Dissipation in a Shear Layer

1.1.1 The 'background' method

Turbulence remains to be one of the most difficult unsolved problems in classical physics and mathematics. Research on turbulence can be traced back to more than 120 years ago, since a first experiment conducted by Osborne Reynolds in 1883 [39]. Reynolds demonstrated through his experiment that an initially laminar pipe flow would become turbulent once the flow speed reaches a critical value. Thereafter, a vast amount of research in literature strives to explore the cause of instability (onset of turbulence) for viscous shear flows.

Mathematically, turbulence can be exactly described by solutions to Navier-Stokes equations, a set of nonlinear equations that describe the velocity field of any flow. However, due to the nonlinear nature of these equations, it poses great difficulty for mathematicians to find a complete set of solutions to these equations, especially for the high-Reynolds-number regime in which turbulence may occur. In fact, it remains unknown as to whether the three-dimensional Navier-Stokes equations are well-posed regarding long-time evolution of smooth solutions.

Despite the difficulty of solving Navier-Stokes equations in general, mathemati-

cians developed a few methods to produce rigorous inequality information directly from the equations without solving them explicitly. Among these methods, the 'background' method is a variational approach for rigorously determining upper bounds on the long-time averaged energy dissipation rate (referred to as 'dissipation rate' hereafter) of fluid systems.

The essence of the background method is to split the flow velocity field into two components, a background field and a fluctuation field, in which the background field acts its role to extremize dissipation rates among solutions to Navier-Stokes equations. This method was proposed by Doering and Constantin [10, 11, 9], who adopted a technique of Hopf [21], and it has relations to the energy (nonlinear) stability theory [25].

1.1.2 A shear layer with suction

Flows subject to injection and suction play important roles in industrial and applied science applications. Injection and suction of fluid through a heated/cooled wall is widely used in boundary layer control applications such as film cooling and polymer fiber coating [23]. Suction may reduce drag on an air foil by inhibiting boundary layer separation [5]. Suction is also important astrophysics where matter in accretion disks may be sucked into condensed objects such as black holes [16]. Suction and injection through bounding surfaces can significantly alter fluid flow and, as a consequence, the energy dissipation rate. It is thus of great interest to study effects of injection and suction on viscous laminar/turbulent energy dissipation for wall bounded shear flows.

The plane Couette flow is a classical problem in fluid mechanics that demonstrates shear-driven fluid motion [13]. The flow system consists of two infinite, parallel plates translating in opposite directions with a constant speed. The fluid between the plates is subjected to dynamics due to the relative plate motion. There is a laminar so-

lution to the corresponding Navier-Stokes equations for this flow, which is shown to be nonlinearly stable if $Re < 2\sqrt{1708} \approx 82.66$ (Joseph, 1976). Application of the background method to this flow deduced a rigorous upper bound on the non-dimensionalized dissipation rates to be $\frac{1}{8\sqrt{2}} \approx 0.088$ for $Re \geq 8\sqrt{2} \approx 11.31$ (Doering & Constantin, 1992). Besides, it is proved that the dissipation rates are at least Re^{-1} for this flow, and this lower bound is valid for any level of Re. Subsequent work had been carried out to implement the background method numerically, which estimated an improved upper bound to be 0.0086 as $Re \to \infty$ [37].

Two decades ago Doering, Spiegel, and Worthing [12] carried out an investigation of the effects of uniform injection and suction on the stability and energy dissipation of boundary-driven shear flow, a natural generalization of plane Couette flow. The setup is shown in Figure 1.1 where Re and θ, the Reynolds number and flow injection angle, are the dimensionless control parameters. Steady laminar flows were found and their linear stability and nonlinear energy stability domains were constructed; see Figure 1.2 in which $Re_s(\theta)$ is the marginal energy stability curve and $Re_u(\theta)$ is the marginal linear instability curve. Asymptotic stability of the steady laminar flows in the region enclosed between $Re_s(\theta)$ and $Re_u(\theta)$, most of the region with $Re > 82.66$ and $\theta < 3^\circ$, remained undetermined. Note that the horizontal asymptote of $Re_s(\theta)$ is at $Re = 2\sqrt{1708} \approx 82.66$, the energy stability limit for plane Couette flow [25].

Upper bounds on energy dissipation rates of solutions to the Navier-Stokes equations were also rigorously estimated for arbitrary values of (Re, θ). The bounds were derived using the background method [12]. Unlike the viscous dissipation rate in steady laminar flows, the analytically derived rigorous upper bounds exhibited negligible sensitivity to changes in θ at high Re when $\theta < 1^\circ$. It was also conjectured that the dissipation rate corresponding to the laminar solution is the lowest among all solutions to the governing equations.

In addition to rigorous estimations based on the background method, computa-

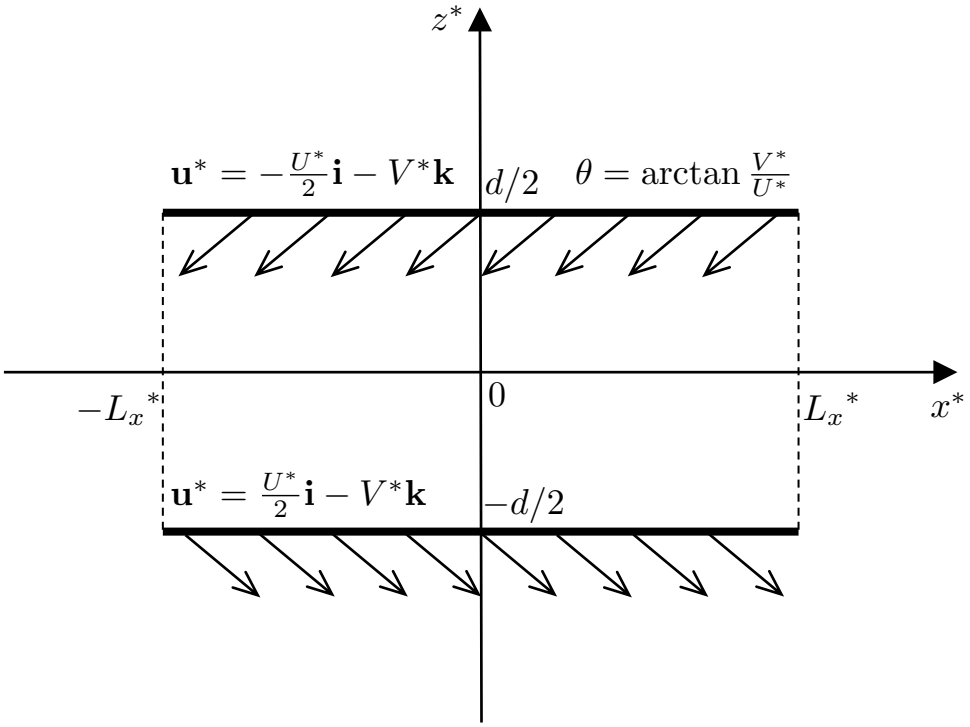

Figure 1.1: A side view of boundaries and boundary conditions for the flow under consideration.

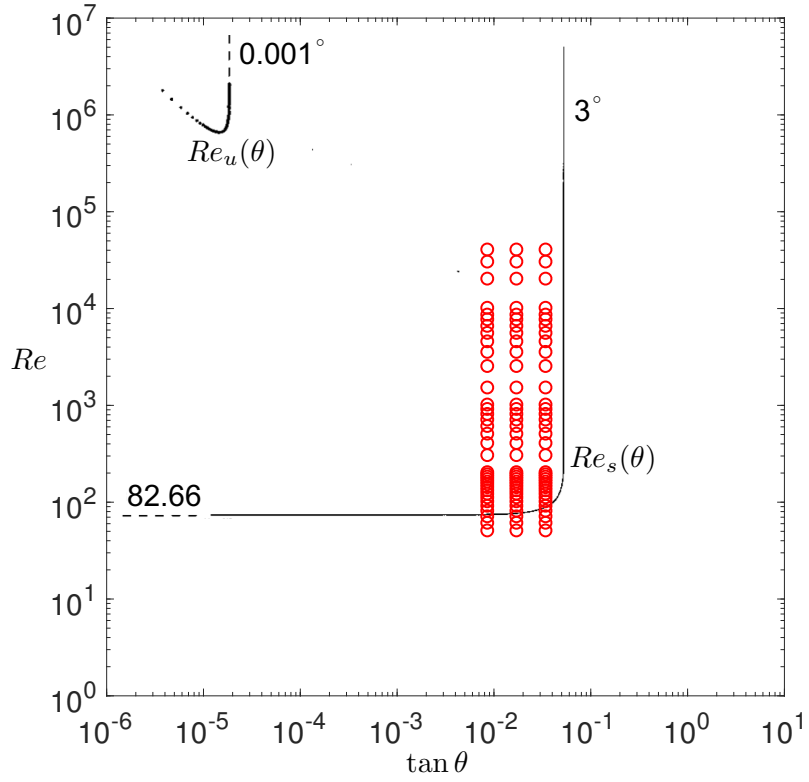

Figure 1.2: Stability boundaries in the $\tan\theta - Re$ plane over logarithmic scales [12].

tional implementations have also been performed for various problems in fluid dynamics [37, 48, 49, 50]. A time-stepping computational scheme was shown to be robust (no restriction on the choice of an initial state) for computing optimal upper bounds within the background variational framework on energy dissipation rates of the Couette flow without injection or suction [49]. The scheme involves a pseudo-time-stepping algorithm for solving the Euler-Lagrange equations derived from the background variational problem.

In Chapter II of this dissertation, we implement the time-stepping numerical scheme [49] to solve Euler-Lagrange equations associated with the optimal background method. We restrict attention to cases with small angles of injection, $\theta \leq 2^\circ$, for which the steady laminar solution might not be energy stable. Pre-selected (Re, θ) combinations for our scope of computation are labeled in Figure 1.2 as circles. Our numerically computed upper bounds for the case with $\theta = 0^\circ$ validates previous numerical results of [37]. We numerically compute upper bounds for $\theta > 0$ at high Re to improve rigorous estimates of [12] by more than 90%.

1.2 Stability of viscous plane shear flows

1.2.1 Viscous extension of Arnold's stability Theory

Stability analysis of plane wall-bounded parallel shear flows forms the basis of modern hydrodynamic stability theory. Within the framework of inviscid linear stability analysis, Rayleigh's inflection-point theorem [38] is one of the fundamental results, it states that a flow is linearly unstable only if its velocity profile has an inflection point. A stronger version of Rayleigh's criterion was established by Fjørtoft [15], in which an additional constraint on the velocity profile of a shear flow was imposed and shown to be necessary for instability.

In studies on nonlinear stability of inviscid planar strictly parallel shear flows,

Arnold [2, 3] was the pioneer to formulate an energy-Casimir function, which is known as the Arnold's function, for examining dynamics of two-dimensional finite-amplitude perturbations, based on which he established conditions for global nonlinear stability that stand as counterparts of Rayleigh's and Fjørtoft's linear stability criteria. In essence, Arnold's approach involves a Lie-Poisson reduction of symmetries in an inviscid shear fluid motion, a process that deeply reflects intrinsic symmetries of the vorticity motion, see [4] for details.

Arnold's theory resides on the Hamiltonian structure of an idealized inviscid flow, and it is not applicable to viscous flows. It is thus of great interest to generalize the theory for inclusion of viscous flows, those with corresponding dynamical systems to be sufficiently close to Hamiltonian systems in their inviscid limits. Pursuing this endeavor, a first extension of Arnold's inviscid theory to viscous flows was carried out by Yau, Wang and Rusak [51] for viscous circular Taylor-Couette flow confined between two concentric rotating cylinders. Through regarding the original inviscid Arnold's function as a Lyapunov function of the associated viscous dissipative system, the viscous extension had led to discovery of a definite flow operation domain in which the Taylor-Couette flow is nonlinearly stable against arbitrary finite-amplitude axisymmetric perturbations. The acquired nonlinear stability operation domain occupies a significant portion of the so-called quasi-Keplerian regime of the Taylor-Couette flow, see the review article by Grossmann, Lohse & Sun [19]. As a comparison, the classical result of Serrin [42] based on the Reynolds-Orr energy equation predicts a stability domain that stays sufficiently close to the solid-body rotation flow, which merely contributes to an infinitesimal fraction of the quasi-Keplerian regime.

In Chapter III of this dissertation, we start off by carrying out a viscous extension of Arnold's inviscid stability theory for strictly parallel non-inflectional shear flows confined between two infinite parallel plates subject to arbitrary two-dimensional perturbations. Through employing the Arnold's inviscid function as a Lyapunov

function (a proposed viscous Arnold's function) for the viscous dissipative system, the extension led to a novel viscous Arnold's identity, it forms the foundation for our study. In Chapter IV of this dissertation, we present another viscous Arnold's identity that is valid for plane shear flows with boundary injection and suction.

1.2.2 Enstrophy-based perspectives on stability/instability

Our viscous Arnold's identity ties in closely with enstrophy of a disturbance field, an important physical quantity in fluid dynamics. An identity that quantifies perturbation's enstrophy of viscous planar shear flows was derived by Synge [44] within the classical normal modal framework. He focused on applying the enstrophy identity to study linear stability of viscous planar Poiseuille flow under no-slip wall condition. With the aid of a variational procedure, Synge obtained a critical Reynolds number corresponding to marginal linear stability to be 155, which is better than the one estimated based on the kinetic energy approach [35].

A variety of identities that involve the disturbance's enstrophy have been reviewed in the lecture notes by Waleffe & Kerswell [47], they extended linear stability theories of Rayleigh's and Fjørtoft's on inviscid shear flows to viscous shear flows. Some enstrophy-based stability criteria and the significance of wall boundary terms therein have also been reviewed and studied in their lectures notes.

In recent years, Fraternale *et al* [17] generalized Synge's enstrophy identity to include general non-modal disturbances. They also improved Synge's approach to study non-modal transient growth of perturbations in viscous planar Poiseuille flow and viscous planar Couette flow.

In this dissertation, we further explore perturbation's enstrophy through using our viscous Arnold's identity. An essential term in the linearized viscous Arnold's identity stands for disturbance's enstrophy scaled by a weight factor, based on which a weighted perturbation's enstrophy identity was naturally obtained. In the special

case of strictly parallel base flows, the weight factor becomes a constant that has reduced the perturbation's enstrophy identity to the one by Synge [44], thus it provides an alternative path to the perturbation's enstrophy identity. We also established a novel weighted perturbation's enstrophy identity in form of Theorem III.2, which is valid for non-inflectional streamwise translation-invariant base shear flows under linear dynamics.

For strictly parallel flows, the validity of the perturbation's enstrophy identity under global nonlinear dynamics imposed with more general wall boundary conditions than the no-slip condition was rigorously examined, and established as Theorem III.4.

Our enstrophy identities serve as grounds for applications. As noted by Theorem III.2 and Theorem III.4, these identities are valid under relaxed wall boundary conditions which include the no-slip condition only as a special case, a fact that allows one to impose active wall boundary settings with controls. We demonstrated in §4.2, that through controlling wall boundary's vorticity disturbance, one may effectively stabilize an originally unstable shear flow.

As enlightened by the earlier works of Synge [44], Waleffe & Kerswell [47] and Fraternale *et al* [17], we seek the potential of applying our enstrophy identities to explore physics underneath the onset of turbulence in planar shear flows. It is evident from the form of a disturbance's enstrophy identity that instability, if there was any, would only be triggered at the walls. To elaborate the physics underneath this vorticity-based observation, we conducted a preliminary investigation in §4.1 to explore the physical mechanism of linear instability and stability for viscous planar Poiseuille flow within classical normal modal framework.

Through our investigation, we found that the production of disturbance's enstrophy at a wall is consistently associated with the viscous damping in disturbance's enstrophy at a near-wall region, and their subtle balance determines the long-term behavior of an unstable perturbation. We also found that the critical layer always

plays a significant role in damping of the perturbation's enstrophy.

As an implementation of those relaxed wall conditions imposed for the enstrophy identity, we proposed a control scheme in §4.2 on wall boundary's vorticity disturbance for viscous plane Poiseuille flow. The control scheme transitions wall settings from the no-slip condition to the free-slip condition. It is observed that an originally linearly unstable mode subject to the no-slip wall condition would quickly be stabilized after a small amount of decrease in its vorticity disturbance at the walls. Evidently, vorticity control schemes of this kind can be potentially applied to general wall-bounded shear flows.

1.3 Outline of the dissertation

My dissertation is organized as follows. In §2.1, we formulate the background variational framework for a shear flow with boundary injection and suction. In §2.2, we numerically implement the background method for deducing new upper bounds on energy dissipation rates.

In §3.1, we formulate the mathematical flow problem and introduce the general mathematical form of base steady state solutions for strictly parallel shear flows. In §3.2 – §3.5, we carry out the viscous extension of Arnold's inviscid theory, based on which we develop a series of perturbation's enstrophy identities that hold under linear or global nonlinear dynamics. In §3.6.1, we provide a new perspective regarding the physical mechanism of linear instability/stability for viscous planar Poiseuille flow based on our enstrophy identity. In §3.6.2, we implement our novel viscous theory by proposing a control scheme on wall boundary's vorticity for viscous planar Poiseuille flow.

In §4.1, we carry out the viscous extension of Arnold's inviscid theory for plane shear flows subject to boundary injection and suction. In §4.2, we derive a novel perturbation's enstrophy identity for the suction problem that holds under global

nonlinear dynamics. In §4.3, we present some enstrophy-based perspectives on the onset of instability for an asymptotic suction profile.

Some future works shall be discussed in §5.

CHAPTER II

Energy dissipation rate for plane shear flow with boundary injection and suction

The material in this chapter comes from *Physics of Fluids* **31**, 085102 (2019) [31].

2.1 Formulation of the problem

We adopt dimensional conventions presented in Section 2 of [37]. We consider a layer of an incompressible (unit density) Newtonian fluid with kinematic viscosity ν confined between parallel rigid plates separated by distance d. The velocity vector field is $\mathbf{u}^* = u_1^*\mathbf{i} + u_2^*\mathbf{j} + u_3^*\mathbf{k}$ where **i, j, k** are the unit vectors in the x^*, y^* and z^* directions, respectively. The bottom plate at $z^* = -d/2$ moves with speed $U^*/2$ while the top plate at $z^* = d/2$ moves with speed $-U^*/2$ in the x^* direction. In addition to the shearing motion of the boundaries, fluid is uniformly injected into the layer with speed V^* at the top plate and uniformly removed at the bottom plate. The boundary conditions are thus

$$\mathbf{u}^* = -\tfrac{1}{2}U^*\mathbf{i} - V^*\mathbf{k} \text{ at } z^* = \tfrac{d}{2}\,, \tag{2.1a}$$

$$\mathbf{u}^* = \tfrac{1}{2}U^*\mathbf{i} - V^*\mathbf{k} \text{ at } z^* = -\tfrac{d}{2}, \tag{2.1b}$$

with all variables periodic in the x^* and y^* directions with periods $2L_x^*$ and $2L_y^*$ respectively. The velocity $\mathbf{u}^*$ and pressure p^* are governed by the Navier-Stokes equations

$$\frac{\partial \mathbf{u}^*}{\partial t^*} + \mathbf{u}^* \cdot \nabla^* \mathbf{u}^* + \nabla^* p^* = \nu \nabla^{*2} \mathbf{u}^* \,, \tag{2.2a}$$

$$\nabla^* \cdot \mathbf{u}^* = 0. \tag{2.2b}$$

The set-up is illustrated in Figure 1.1.

We define two control parameters of this problem, the Reynolds number

$$Re = \frac{U^* d}{\nu} \tag{2.3}$$

and the fluid injection angle θ defined by

$$\tan\theta = \frac{V^*}{U^*}. \tag{2.4}$$

Changing variables in (2.2a) and (2.2b) according to

$$\mathbf{u} = \frac{d}{\nu}\mathbf{u}^*, \;\; (x, y, z) = \frac{1}{d}(x^*, y^*, z^*), \;\; t = \frac{\nu}{d^2} t^*, \;\; p = \frac{d^2}{\nu^2} p^*, \tag{2.5}$$

we obtain the non-dimensional equations

$$\frac{\partial \mathbf{u}}{\partial t} + \mathbf{u} \cdot \nabla \mathbf{u} + \nabla p = \nabla^2 \mathbf{u} \,, \tag{2.6a}$$

$$\nabla \cdot \mathbf{u} = 0, \tag{2.6b}$$

and boundary conditions

$$\mathbf{u} = -\tfrac{1}{2} Re \mathbf{i} - Re \tan\theta \mathbf{k} \text{ at } z = \tfrac{1}{2} \,, \tag{2.7a}$$

$$\mathbf{u} = \tfrac{1}{2} Re \mathbf{i} - Re \tan\theta \mathbf{k} \text{ at } z = -\tfrac{1}{2}. \tag{2.7b}$$

The non-dimensional variables are periodic in the x and y directions, with half periods $L_x = L_x^*/d$ and $L_y = L_y^*/d$.

A steady solution to the system is the laminar flow $\mathbf{u}_l = U_l(z)\mathbf{i} - Re\tan\theta\mathbf{k}$ with horizontal profile

$$U_l(z) := -\frac{Re - Re\exp\left[-Re\tan\theta(z+\frac{1}{2})\right]}{1-\exp(-Re\tan\theta)} + \frac{Re}{2}. \tag{2.8}$$

The dimensionless long-time-averaged energy dissipation rate ϵ for velocity field $\mathbf{u}(\mathbf{x},t)$ is

$$\epsilon := \frac{1}{Re^3}\lim_{T\to\infty}\frac{1}{T}\int_0^T \langle|\nabla\mathbf{u}|^2\rangle \,\mathrm{d}t. \tag{2.9}$$

where horizontal and bulk volume averaging are

$$\overline{(\cdot)} := \frac{1}{4L_xL_y}\int_{-L_x}^{L_x}\mathrm{d}x\int_{-L_y}^{L_y}\mathrm{d}y\;(\cdot), \tag{2.10a}$$

$$\langle\cdot\rangle := \int_{-1/2}^{1/2}\mathrm{d}z\;\overline{(\cdot)}. \tag{2.10b}$$

The energy dissipation rate ϵ_l corresponding to the laminar solution $\mathbf{u}_l$ is

$$\epsilon_l := \frac{\tan\theta}{2\tan\left(\frac{1}{2}Re\tan\theta\right)} \tag{2.11}$$

with limiting behaviors

$$\epsilon_l \sim \frac{1}{Re} \quad \text{as} \quad Re \quad \text{or} \quad \theta\to 0 \tag{2.12}$$

and

$$\epsilon_l \sim \frac{\tan\theta}{2} = \mathcal{O}(1) \quad \text{as} \quad Re\to\infty. \tag{2.13}$$

Using the background variational method, Doering, Spiegel, and Worthing [12] derived a rigorous upper bound on ϵ for all solutions of the Navier-Stokes equations

(2.6a) and (2.6b) with injection-suction-shear boundary conditions (2.7a) and (2.7b):

$$\epsilon \leq \epsilon_B := \frac{1}{2\sqrt{2}} \left[1 + \frac{8}{3} \tan^2 \theta \left(1 - \frac{3\sqrt{2}}{2} \frac{1}{Re} \right) \right] \tag{2.14}$$

for $Re \geq 2\sqrt{2}$ with limiting behavior

$$\epsilon_B \sim \frac{1}{2\sqrt{2}} \left[1 + \frac{8}{3} \tan^2 \theta \right] = \mathcal{O}(1) \quad \text{as} \quad Re \to \infty. \tag{2.15}$$

In view of (2.13), this upper bound displays sharp scaling with respect to the Re as $Re \to \infty$ at fixed $\theta \neq 0$, albeit with a substantially larger prefactor for $\theta \lesssim 3^\circ$ where flows other than $\mathbf{u}_l$ could possibly persist. However, since piecewise linear functions were utilized as background profiles, upper bounds (2.14) and (2.15) are not the most optimal ones within the background variational framework.

To compute sharper upper bound on ϵ in the background scheme for boundary-driven shear flows with injection and suction, we follow the approach of Plasting & Kerswell [37] to numerically solve the full background problem. Consider the functional

$$\mathcal{L} := \lim_{T \to \infty} \frac{1}{T} \int_0^T \left\{ \langle |\nabla \mathbf{u}|^2 \rangle - \left\langle a\mathbf{v} \cdot \left[\frac{\partial \mathbf{u}}{\partial t} + \mathbf{u} \cdot \nabla \mathbf{u} + \nabla p - \nabla^2 \mathbf{u} \right] \right\rangle \right.$$
$$\left. - \langle p \nabla \cdot \mathbf{u} \rangle \right\} \mathrm{d}t, \tag{2.16}$$

defined for flows $\mathbf{u} = u_1 \mathbf{i} + u_2 \mathbf{j} + u_3 \mathbf{k}$ satisfying the injection-suction-shear boundary conditions, where a is a real number and $\mathbf{v}$ is a vector field. The field $a\mathbf{v}$ and the pressure field p play the roles of Lagrange multipliers associated with (2.6a) and (2.6b), respectively. For a standard formulation, we introduce a 'background profile' $\phi(z)$ satisfying

$$\phi \left(\pm \frac{1}{2} \right) = \mp \frac{1}{2} Re \tag{2.17}$$

and choose

$$\mathbf{u}(\mathbf{x},t) := \phi(z)\mathbf{i} + \mathbf{v}(\mathbf{x},t) - Re\tan\theta\ \mathbf{k}. \tag{2.18}$$

Together with (2.6b), (2.7a) and (2.7b) these imply that

$$\nabla\cdot\mathbf{v} = 0\ , \tag{2.19a}$$

$$\mathbf{v} = \mathbf{0} \text{ at } z = \pm 1/2 \tag{2.19b}$$

and $\mathbf{v} = v_1\mathbf{i} + v_2\mathbf{j} + v_3\mathbf{k}$ is periodic in the x and y directions.

(2.6b) implies that

$$\overline{\mathbf{u}} = \overline{u_1}(z)\mathbf{i} - Re\tan\theta\ \mathbf{k}, \tag{2.20}$$

which together with (2.18) implies $\overline{v_2} = 0 = \overline{v_3}$. This suggests decomposing

$$\mathbf{v} = \overline{v_1}(z)\mathbf{i} + \widehat{\mathbf{v}}(\mathbf{x},t) \tag{2.21a}$$

$$p = \overline{p}(z) + \widehat{p}(\mathbf{x},t) \tag{2.21b}$$

in which $\widehat{\mathbf{v}}(\mathbf{x},t)$ and $\widehat{q}(\mathbf{x},t)$ are the mean-free parts of $\mathbf{v}$ and p, respectively. Then, substituting (2.18), (2.21a) and (2.21b) into (2.16), and using (2.17), (2.19a) and (2.19b) we obtain an alternate expression for $\mathcal{L}$,

$$\mathcal{L} = \lim_{T\to\infty}\frac{1}{T}\int_0^T \Big\langle \phi'^2 - a\phi'\widehat{v}_1\widehat{v}_3 - (a-1)|\nabla\widehat{\mathbf{v}}|^2 \\ -(a-1)\overline{v_1}'^2 + (a-2)\phi''\overline{v_1} + aRe\tan\theta\ \phi'\overline{v_1} - \widehat{p}\ \nabla\cdot\widehat{\mathbf{v}}\Big\rangle\ \mathrm{d}t. \tag{2.22}$$

Observe that if ϕ can be selected such that $\mathcal{L}$ has a maximum over all $\mathbf{v}$, then this value will also be an upper bound for ϵ, since any solution $\mathbf{u}$ of the Navier-Stokes equations can also be represented by some $\mathbf{v}$. Thus, minimizing the maximum over all allowable ϕ would generate the least upper bound on ϵ: this is the essence of

the background formulation. The optimization procedure described above can be implemented by considering only stationary fluctuation fields $\mathbf{v}$ that fulfill (2.19a) and (2.19b) [37]. Therefore, hereafter we release the time-dependence of all variables.

Euler-Lagrange equations for the stationary fields $\mathcal{L}$ are

$$\frac{\delta\mathcal{L}}{\delta a} := -\langle|\nabla\widehat{\mathbf{v}}|^2 + \overline{v_1}'^2 + \phi'\widehat{v_1}\widehat{v_3} - \phi''\overline{v_1} - Re\tan\theta\ \phi'\overline{v_1}\rangle = 0, \tag{2.23a}$$

$$\frac{\delta\mathcal{L}}{\delta\phi} := -2\phi'' + a\overline{\widehat{v_1}\widehat{v_3}}' - aRe\tan\theta\ \overline{v_1}' + (a-2)\overline{v_1}'' = 0, \tag{2.23b}$$

$$\frac{\delta\mathcal{L}}{\delta\overline{v_1}} := 2(a-1)\overline{v_1}'' + (a-2)\phi'' + aRe\tan\theta\ \phi' = 0, \tag{2.23c}$$

$$\frac{\delta\mathcal{L}}{\delta\widehat{\mathbf{v}}} := 2(a-1)\nabla^2\widehat{\mathbf{v}} - a\phi'\begin{pmatrix}\widehat{v_3}\\0\\\widehat{v_1}\end{pmatrix} + \nabla\widehat{p} = \begin{pmatrix}0\\0\\0\end{pmatrix}, \tag{2.23d}$$

$$\frac{\delta\mathcal{L}}{\delta\widehat{p}} := \nabla\cdot\widehat{\mathbf{v}} = 0. \tag{2.23e}$$

Note that (2.23c) may be solved for $\overline{v_1}$ yielding

$$\overline{v_1} = -\frac{a-2}{2(a-1)}(\phi + Re\ z) - \frac{aRe\tan\theta}{2(a-1)}\left[\int_{-1/2}^{z}\phi\ \mathrm{d}z' - \left(z+\frac{1}{2}\right)\int_{-1/2}^{1/2}\phi\ \mathrm{d}z'\right]. \tag{2.24}$$

Let $(a, \overline{v_1}, \phi, \widehat{\mathbf{v}}, \widehat{p})$ be a stationary point of $\mathcal{L}$ obtained via solving (2.23a–2.23e). The time-independent form of (2.22) evaluated at a stationary point reads

$$\begin{aligned}\mathcal{L}\,(a, \overline{v_1}, \phi, \widehat{\mathbf{v}}, \widehat{p}) = \langle\phi'^2 - (a-1)\overline{v_1}'^2 + (a-2)\phi''\overline{v_1} + aRe\tan\theta\ \phi'\overline{v_1}\rangle\\ -(a-1)\mathcal{H}_{\phi,a}(\widehat{\mathbf{v}})\end{aligned} \tag{2.25}$$

where

$$\mathcal{H}_{\phi,a}(\widehat{\mathbf{v}}) := \langle|\nabla\widehat{\mathbf{v}}|^2\rangle + \frac{a}{a-1}\langle\phi'\widehat{v_1}\widehat{v_3}\rangle. \tag{2.26}$$

A global upper bound on ϵ is thereon established to be

$$\epsilon \leq \epsilon_N := \langle \phi'^2 - (a-1)\overline{v_1}'^2 + (a-2)\phi''\overline{v_1} + aRe\tan\theta\ \phi'\overline{v_1}\rangle \tag{2.27}$$

provided that $a > 1$ and $\mathcal{H}_{\phi,a}(\widehat{\mathbf{v}}) \geq 0$. The latter assumption is so-called the 'spectral constraint', it would be manifestly fulfilled if $\mathcal{H}_{\phi,a}(\widehat{\mathbf{w}}) \geq 0$ for all $\widehat{\mathbf{w}} \in \{\mathbf{w} \mid \nabla \cdot \mathbf{w} = 0,\ \overline{\mathbf{w}} = \mathbf{0},\ \mathbf{w}(x, y, \pm 1/2) = \mathbf{0}\}$.

2.2 The time-stepping numerical scheme

In the following we assume, as in previous studies [37], that optimal solutions of the Euler-Lagrange equations do not have x dependence, that is, $\partial_x \equiv 0$. Justification for the assumption dates back to Joseph [24] in the context of energy stability, which was also adopted and partially verified by Busse [8]. We would like to remark that the background method contains different information than linear stability/instability analysis, and above assumption does not apply to the latter case [34, 27].

The time-stepping algorithm proposed by Wen *et al* [49] is adopted for solving the Euler-Lagrange equations of $\mathcal{L}$. Specifically, an artificial time evolution scheme is imposed for (2.23a), (2.23b) and (2.23d) as follows:

$$\frac{\partial a}{\partial \tau} = -\frac{\delta \mathcal{L}}{\delta a},\quad \frac{\partial \phi}{\partial \tau} = -\frac{\delta \mathcal{L}}{\delta \phi},\ \text{and}\ \frac{\partial \widehat{\mathbf{v}}}{\partial \tau} = \frac{\delta \mathcal{L}}{\delta \widehat{\mathbf{v}}} \tag{2.28}$$

where τ is the artificial time variable. These evolution equations are coupled with (2.23e) and (2.24) to form a closed system.

The time-stepping scheme was shown to be numerically stable for solving a class of flow equations, including system (2.28) [49]. A subroutine is incorporated into the scheme for ensuring the positivity of $\mathcal{H}$, which is enforced by (2.26). The algorithm is implemented for pre-selected Fourier modes of $\widehat{\mathbf{v}}$ and $\widehat{p}$, with application of the

following Chebyshev collocation scheme.

Rescaling variables as $\phi \to \phi/Re,\ \widehat{\mathbf{v}} \to \widehat{\mathbf{v}}/Re,\ \overline{v_1} \to \overline{v_1}/Re,\ \widehat{p} \to \widehat{p}/(a-1)Re$ in Euler-Lagrange equations (2.23a), (2.23b) and (2.23d), substituting them into (2.28), and coupling them with (2.23e) and (2.24) to obtain the following set of equations

$$\frac{\partial a}{\partial \tau} = \langle |\nabla \widehat{\mathbf{v}}|^2 + \overline{v_1}'^2 + Re\phi' \widehat{v_1}\widehat{v_3} - \phi'' \overline{v_1} - Re \tan\theta\ \phi' \overline{v_1} \rangle, \tag{2.29a}$$

$$\frac{\partial \phi}{\partial \tau} = 2\phi'' - aRe\ \overline{\widehat{v_1}\widehat{v_3}}' + aRe \tan\theta\ \overline{v_1}' - (a-2)\overline{v_1}'', \tag{2.29b}$$

$$\frac{\partial \widehat{\mathbf{v}}}{\partial \tau} = 2\nabla^2 \widehat{\mathbf{v}} - \frac{a}{a-1} Re\phi' \begin{pmatrix} \widehat{v_3} \\ 0 \\ \widehat{v_1} \end{pmatrix} + \nabla \widehat{p}, \tag{2.29c}$$

$$\nabla \cdot \widehat{\mathbf{v}} = 0, \tag{2.29d}$$

$$\overline{v_1} = -\frac{a-2}{2(a-1)}(\phi + z) - \frac{aRe \tan\theta}{2(a-1)} \left[\int_{-1/2}^{z} \phi\ \mathrm{d}z' - \left(z + \frac{1}{2}\right) \int_{-1/2}^{1/2} \phi\ \mathrm{d}z' \right], \tag{2.29e}$$

under boundary conditions

$$\phi\left(\pm\frac{1}{2}\right) = \mp\frac{1}{2},\ \widehat{\mathbf{v}}\Big|_{z=\pm 1/2} = \mathbf{0}. \tag{2.30}$$

For a solution that is translation invariant along the x direction (i.e. $\partial_x = 0$), we propose forms on $\widehat{\mathbf{v}}$ and $\widehat{p}$ to be

$$\widehat{\mathbf{v}} = \sum_{m=1}^{M} \begin{pmatrix} \widehat{v_{1m}}(z) \cos m\pi y \\ \widehat{v_{2m}}(z) \sin m\pi y \\ \widehat{v_{3m}}(z) \cos m\pi y \end{pmatrix},\ \widehat{p} = \sum_{m=1}^{M} \widehat{p_m}(z) \cos m\pi y, \tag{2.31}$$

where M is a pre-selected integer, that is big enough for including all critical wave numbers which contribute to the optimal solution.

For the numerical implementation, we discretize the interval $[-1/2, 1/2]$ into $N+1$ grid points according to the standard Chebyshev collocation method [7]. The corresponding differentiation matrix realizing the zero Dirichlet boundary conditions at $z = \pm 1/2$ is denoted by D_N. In the following description, every z dependent variable is assumed to be a column vector with $N + 1$ entries.

We denote the state τ as a superscript in each variable hereafter. Given the initial states ϕ^0, $\widehat{v_{3m}}^0$ and a^0, one obtains $\overline{v_1}^0$ based on (2.29c). Besides, $\widehat{v_{1m}}^0, \widehat{v_{2m}}^0$ and $\widehat{p_m}^0$ are determined in accordance with (2.29c), (2.29d) and (2.31) as

$$\widehat{v_{1m}}^0 = \frac{a^0 Re}{2(a^0 - 1)} \left[D_N^2 - (m\pi)^2 I_N\right]^{-1} \left(D_N \phi^0 \odot \widehat{v_{3m}}^0\right), \tag{2.32a}$$

$$\widehat{v_{2m}}^0 = -\frac{1}{m\pi} D_N \widehat{v_{3m}}^0, \tag{2.32b}$$

$$\widehat{p_m}^0 = \frac{2}{m\pi} \left[D_N^2 - (n\pi)^2 I_N\right] \widehat{v_{2m}}^0, \tag{2.32c}$$

in which I_N is the $(N + 1) \times (N + 1)$ identity matrix, and the binary operation $\odot$ stands for the entry-wise vector multiplication.

Suppose the time-step in τ is Δs, and suppose that we have the variables at $\tau = s$ computed for some $s \geq 0$. The variables corresponding to $\tau = s + \Delta s$ are to be computed as the following.

First, we impose time stages to variables in (2.29c) and (2.29d) as follows

$$\frac{\widehat{\mathbf{v}}^{s+\Delta s} - \widehat{\mathbf{v}}^s}{\Delta s} = 2\nabla^2 \widehat{\mathbf{v}}^{s+\Delta s} - \left\{ \frac{a}{a-1} Re \phi' \begin{pmatrix} \widehat{v_3} \\ 0 \\ \widehat{v_1} \end{pmatrix} \right\}^s + \nabla \widehat{p}^{s+\Delta s} \tag{2.33a}$$

$$\nabla \cdot \widehat{\mathbf{v}}^{s+\Delta s} = 0. \tag{2.33b}$$

Based on (2.33a) and (2.33b), variables $\widehat{\mathbf{v}_m}^{s+\Delta s}$ and $\widehat{p_m}^{s+\Delta s}$ are computed to be

$$\widehat{v_{1m}}^{s+\Delta s}(2:N) = A(2:N,2:N)^{-1}\left[\widehat{v_{1m}}(2:N) - \Delta s\frac{aRe}{a-1}\left(D_N\phi \odot \widehat{v_{3m}}\right)(2:N)\right]^s, \tag{2.34a}$$

$$\begin{bmatrix} \widehat{v_{2m}}(2:N) \\ \widehat{v_{3m}}(2:N) \\ \widehat{p_m}(1:N+1) \end{bmatrix}^{s+\Delta s} = \begin{bmatrix} A(2:N,2:N) & O_{(N-1)\times(N-1)} & m\pi\Delta s I_N(2:N,1:N+1) \\ O_{(N-1)\times(N-1)} & A(2:N,2:N) & -\Delta s D_N(2:N,1:N+1) \\ -m\pi I_N(1:N+1,2:N) & -D_N(1:N+1,2:N) & O_{(N+1)\times(N+1)} \end{bmatrix}^{-1} \times \begin{bmatrix} \widehat{v_{2m}}(2:N) \\ \widehat{v_{3m}}(2:N) - \Delta s\frac{aRe}{a-1}D\phi \odot \widehat{v_{1m}}(2:N) \\ O(N+1,1) \end{bmatrix}^s, \tag{2.34b}$$

where $A := [1 + 2(n\pi)^2\Delta s]\, I_N - 2\Delta s D_N^2$.

Secondly, let $\widehat{\phi} := \phi + z$, we have then $\widehat{\phi}(\pm 1/2) = 0$ according to (2.30). Assigning time stages to variables in (2.29b) as follows

$$\frac{\widehat{\phi}^{s+1} - \widehat{\phi}^s}{\Delta s} = 2\frac{\mathrm{d}^2}{\mathrm{d}z^2}\widehat{\phi}^{s+1} - \left[aRe\ \overline{\widehat{v_1}\widehat{v_3}}' + (a-2)\overline{v_1}'' - aRe\tan\theta\ \overline{v_1}'\right]^s. \tag{2.35}$$

(2.35) implies that

$$\widehat{\phi}^{s+1}(2:N) = B(2:N,2:N)^{-1}\times \left\{\widehat{\phi} - \Delta s\left[aReD_N\left(\frac{1}{2}\sum_{m=1}^{M}\widehat{v_{1m}}\odot\widehat{v_{3m}}\right) + (a-2)D_N^2\overline{v_1} - aRe\tan\theta\ D_N\overline{v_1}\right]\right\}^s(2:N), \tag{2.36}$$

where $B := I_N - 2\Delta s D_N^2$.

Then, $\overline{v_1}^{s+1}$ is obtained by substituing $\phi = \phi^{s+1}$ and $a = a^s$ into (2.29e).

Next, (2.29a) and the marginal case of the stability constraint (2.26) imply the following

$$\begin{aligned} a^{s+1} =& a^s + \Delta s \left\langle -\frac{Re}{a^s - 1} \left(\frac{1}{2} \sum_{m=1}^{M} \widehat{v_{1m}}^s \odot \widehat{v_{3m}}^s \right) \odot D_N \phi^s \right\rangle \\ &+ \Delta s \left\langle D_N \overline{v_1}^s \odot D_N \overline{v_1}^s + D_N \overline{v_1}^s \odot D_N \phi^s - Re \tan\theta \overline{v_1}^s \odot D_N \phi^s \right\rangle \ . \end{aligned} \tag{2.37}$$

Above routine is kept running until the absolute difference between successive time stages of a, ϕ and $\widehat{\mathbf{v}}$ are within 10^{-8}.

Finally, once after a set of stationary solutions of $\mathcal{L}$ are computed, we need to verify $a > 1$ and the spectral constraint that (2.26) ≥ 0, by numerically solving the following eigenvalue problem in $(\lambda, \mathbf{w})$, in which we had applied the scaling $\mathbf{w} \to \mathbf{w}/Re$

$$-2\nabla^2 \mathbf{w} + \frac{aRe}{a-1} \phi' \begin{pmatrix} w_3 \\ 0 \\ w_1 \end{pmatrix} - \nabla p = \lambda \mathbf{w} \ , \tag{2.38a}$$

$$\nabla \cdot \mathbf{w} = 0 \ , \tag{2.38b}$$

$$\mathbf{w}\Big|_{z=\pm\frac{1}{2}} = 0. \tag{2.38c}$$

By proposing $\mathbf{w}$ to be of the same form as $\mathbf{v}$ given by (2.31), one may again use the Chebyshev collocation scheme described for solving (2.29c), to solve for the components of $\mathbf{w}$ corresponding to each wave number. The spectral constraint is met if the smallest eigenvalue corresponding to each wave number is non-negative.

2.3 Computational outcome

Results for $\theta = 0^\circ,\ 0.5^\circ,\ 1^\circ,\ 2^\circ$ are shown in Figure 2.1 and Figure 2.1(b). The dotted blue curve at the top of each subfigure stands for previously established rigor-

ous upper bounds ϵ_B given by (2.14); there is very little sensitivity of this bound to changes in the angle of injection for $\theta < 1^\circ$. Our numerically computed upper bounds ϵ_N from (2.27) are shown as circles (connected by the black solid curve). The red dashed curve is ϵ_l given by (2.11). Note that ϵ_N approaches a finite asymptotic value for $Re > 10\ 000$ at each fixed angle of injection in agreement with the zeroth law of turbulence which states that the dissipation rate becomes independent of viscosity as the viscosity tends to zero. In particular, for the case with $\theta = 0^\circ$, ϵ_N approaches 0.0086 for $Re > 10\ 000$, reconfirming the results of Plasting and Kerswell [37]. For $Re > 10\ 000$, the asymptotic values of ϵ_N are all well over an order of magnitude less than than the analytical bounds (ϵ_B) at $\theta = 0^\circ, 0.5^\circ, 1^\circ, 2^\circ$, respectively: the computed bounds significantly improve the rigorous estimates at high Reynolds numbers.

Results presented in Figure 2.1 suggest new insights about stability of the laminar solution U_l. As illustrated in Figure 1.2, the laminar flow is energy stable for $Re < 2\sqrt{1708} \approx 82.66$ at any angle of injection, a fact supported by the match of ϵ_N with ϵ_l (the dashed curve) for the same range of Re at each pre-selected θ. Fig. 1.2 also shows that the laminar solution is energy stable for $\theta > 3^\circ$, but it is still unknown about whether the flow is absolutely stable for $\theta < 3^\circ$ at high Re. Observe that the gap between asymptotic values of ϵ_N and ϵ_l in Fig. 2 diminishes as θ increases. In particular, the difference between ϵ_N is just 1.7% above ϵ_l for $\theta = 2^\circ$. This small difference suggests that U_l might actually be the unique asymptotically stable solution of equations (2.23a)- (2.23e) for θ only a small amount larger than 2°, perhaps significantly lower than the 3° energy stability limit.

The streamwise mean velocity components $\overline{u_1}$ of the optimizing fields corresponding to $Re = 10\ 000$ are shown in Figure 2.2. In accordance with (2.18), $\overline{u_1} = \phi + \overline{v_1}$. Note that the gap between $\overline{u_1}$ (the solid curve) and U_l (the dashed curve) shrinks substantially as $\theta \to 2^\circ$. This further supports the hypothesis that the base laminar flow is stable for $\theta \gtrsim 2^\circ$.

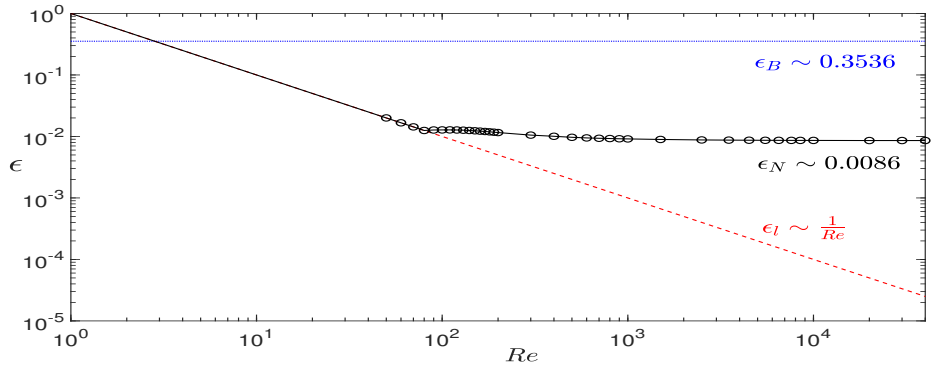

(a) $\theta = 0°$.

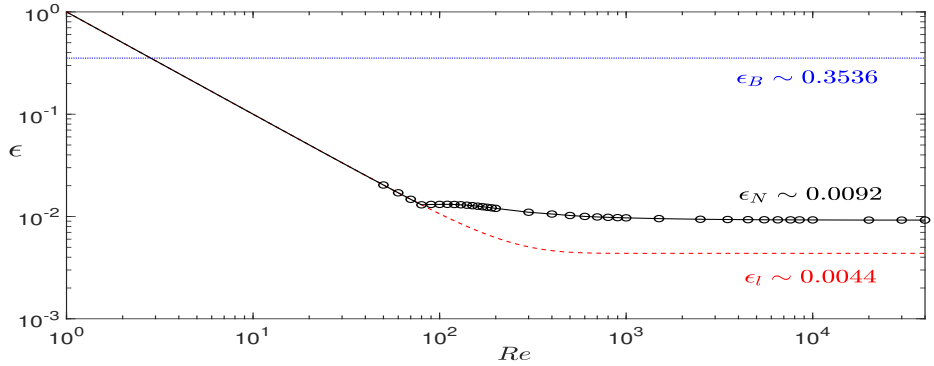

(b) $\theta = 0.5°$.

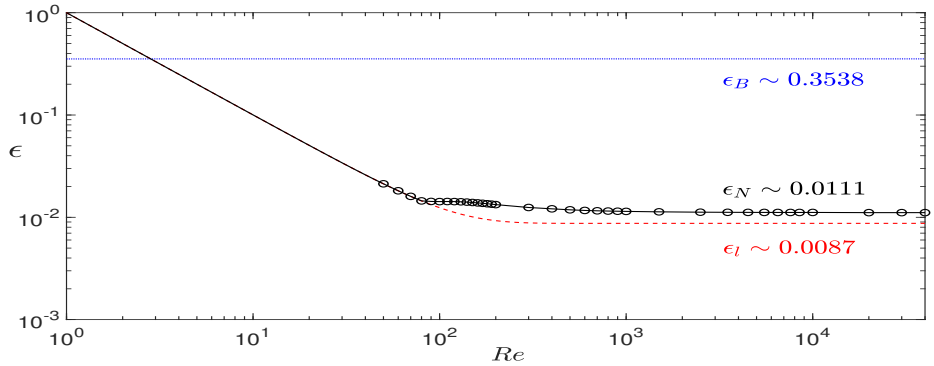

(c) $\theta = 1°$.

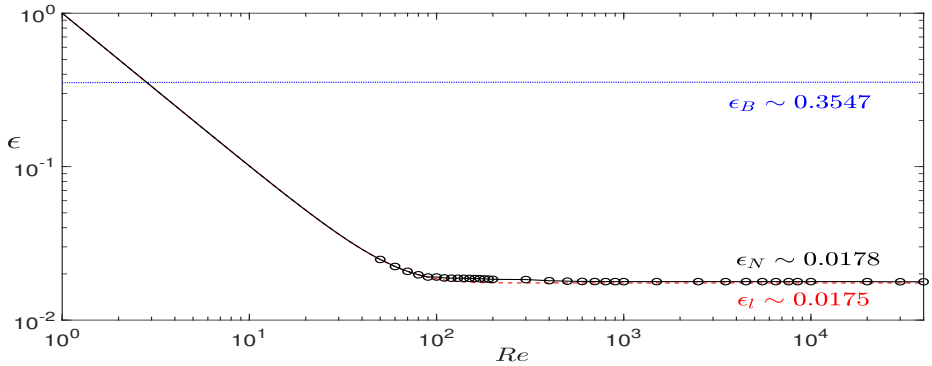

(d) $\theta = 2°$.

Figure 2.1: Upper bounds of ϵ versus Re for various values of θ.

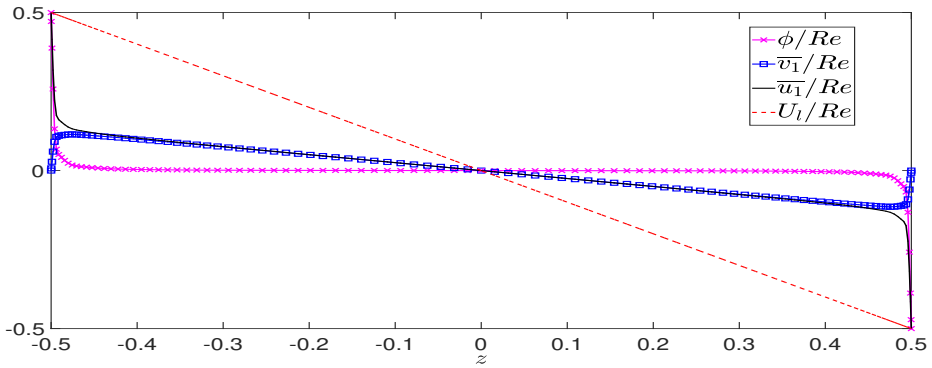

(a) $\theta = 0°$.

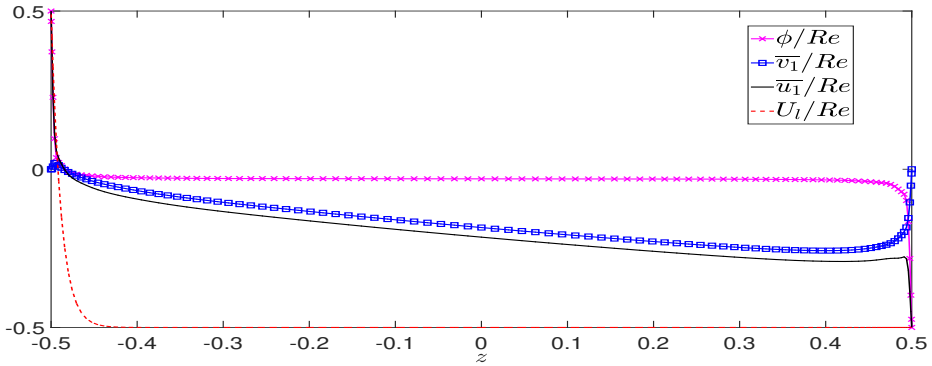

(b) $\theta = 0.5°$.

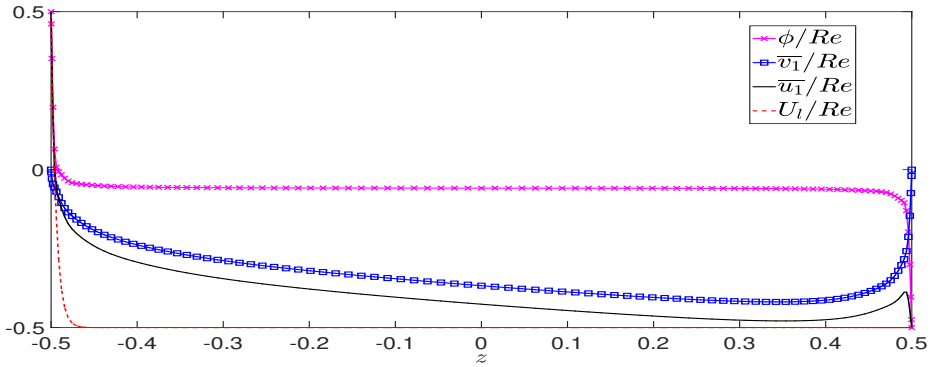

(c) $\theta = 1°$.

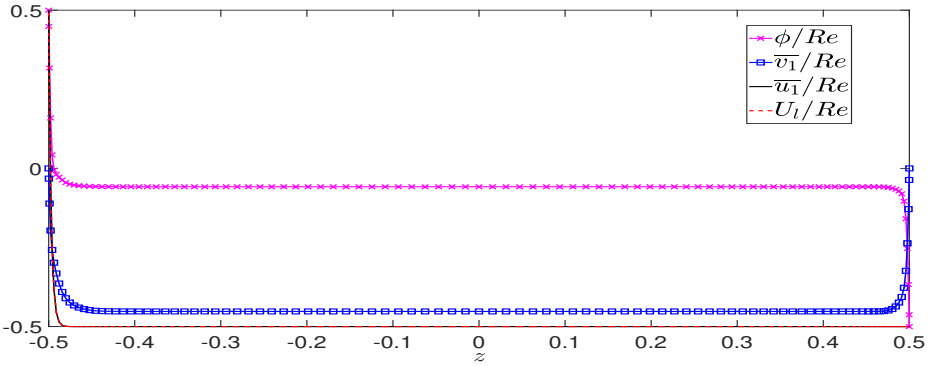

(d) $\theta = 2°$.

Figure 2.2: Optimized ϕ/Re, $\overline{v_1}/Re$, $\overline{u_1}/Re$ and $\overline{U_l}/Re$ versus z at $Re = 10\ 000$

2.4 Discussion

We computed improved upper bounds on energy dissipation rates ϵ of the Couette flow with wall injection and suction. The scope of numerical computations included a pre-selected set of Reynolds numbers $Re \in [50, 40\ 000]$ for angles of injection $\theta \in \{0^\circ, 0.5^\circ, 1^\circ, 2^\circ\}$. These (Re, θ) combinations mostly lie in a sub-region of the $Re - \theta$ plane in which absolute stability nature of the steady laminar flow U_l remains unknown.

For each (Re, θ) combination, a time-stepping numerical optimization scheme was imposed via equations derived from the background variational formulation to solve for optimal solutions that lead to an upper bound on ϵ. Computed upper bounds for $\theta = 0^\circ$ validated previous numerical results for shear flow in the absence of injection and suction [37]. Our numerically computed upper bounds for $\theta > 0$ at high Re significantly improves rigorously estimated ones by more than an order of magnitude.

It was also observed that our computed upper bounds approach to those of U_l as θ approaches 2°, supported by the convergence of the computed optimal background profile and the laminar solution for $\theta = 2^\circ$. This suggests that the true absolute stability limit of the steady laminar solution is closer to $\theta \approx 2^\circ$, about a degree lower than the energy stability limit [12].

The success of this computational approach to deduce improved bounds on ϵ signals its potential for applications to other fundamental fluid flow problems. A closely related problem that remains open regards cylindrical Taylor-Couette flow with injection and suction [18, 22]. In that case analytical application of the background method fails to produce bounds on the flow's viscous dissipation rate at (even moderately) high Reynolds number and injection-suction flux rates. This mathematical shortcoming is subtle [28] and computational studies employing the time-stepping numerical scheme may help guide alternative analysis techniques [45].

CHAPTER III

Viscous extension of Arnold's non-viscous stability theory for plane shear flows

The material in this chapter comes from *Journal of Fluid Mechanics* **877**, 1134–1162 (2019) [30].

3.1 Mathematical formulation

We adopt following conventions [see 13, 37]. The dimensional velocity field is designated as $\mathbf{u}^* = u^*\mathbf{i} + v^*\mathbf{j}$, where $\mathbf{i}$, $\mathbf{j}$ are the canonical unit vectors of x^*- (streamwise) and y^*- (spanwise) directions, respectively. The velocity field is governed by following two-dimensional incompressible Navier-Stokes equations, in which t^* is the dimensional time, p^* is the dimensional pressure normalized by constant density of the fluid, and ν is the kinematic viscosity

$$\begin{cases} \frac{\partial \mathbf{u}^*}{\partial t^*} + \mathbf{u}^* \cdot \nabla^* \mathbf{u}^* + \nabla^* p^* = \nu \nabla^{*2} \mathbf{u}^*, \\ \nabla^* \cdot \mathbf{u}^* = 0. \end{cases} \tag{3.1}$$

We confine the domain to be over the finite cell $(x^*, y^*) \in [-L_x, L_x] \times \left[-\frac{h}{2}, \frac{h}{2}\right]$, in which the streamwise direction is periodic with half-period L_x.

We consider an arbitrary non-zero strictly parallel base steady state of the form

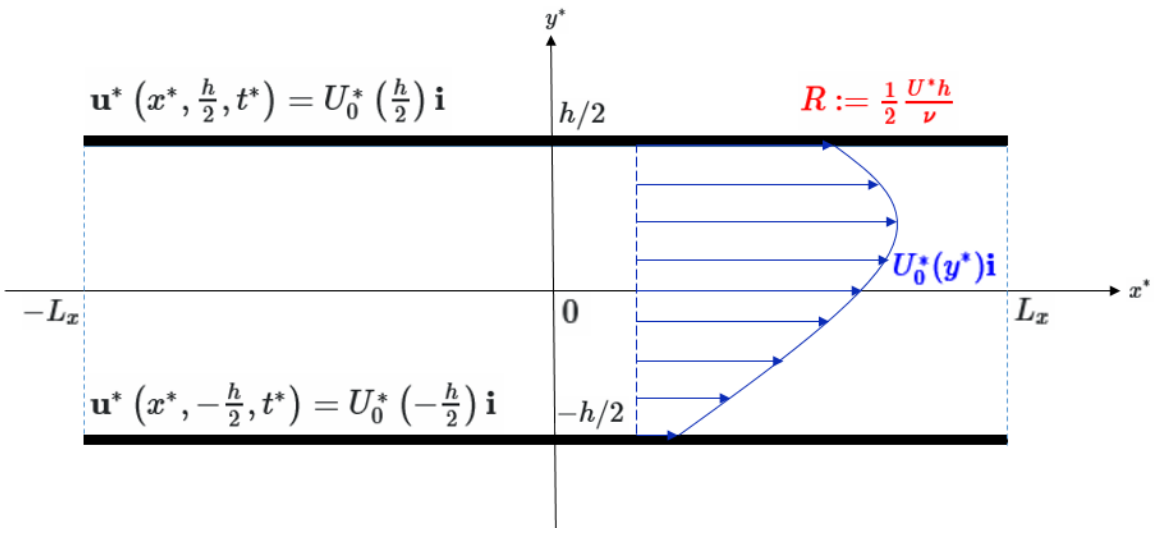

Figure 3.1: The dimensional flow system with boundary conditions, in which $U_0^*(y^*)\mathbf{i}$ is an arbitrary base steady state that satisfies (3.1).

$\mathbf{u}_0^* := U_0^*(y^*)\mathbf{i}$ and denote

$$U^* := \max_{y^* \in \left[-\frac{h}{2}, \frac{h}{2}\right]} |U_0^*(y^*)|. \tag{3.2}$$

Flow velocities at the walls are the following

$$\mathbf{u}^*\left(x^*, \pm\frac{h}{2}, t^*\right) = U_0^*\left(\pm\frac{h}{2}\right)\mathbf{i}, \tag{3.3}$$

as illustrated in Figure 3.1.

Introducing following dimensionless quantities, in which R is the Reynolds number

$$\mathbf{u} = \begin{pmatrix} u \\ v \end{pmatrix} := \frac{1}{U^*}\mathbf{u}^*, \quad \begin{pmatrix} x \\ y \end{pmatrix} := \frac{2}{h}\begin{pmatrix} x^* \\ y^* \end{pmatrix}, \quad t := \frac{2U^*}{h}t^*, \quad p := \frac{p^*}{U^{*2}}, \quad R := \frac{U^* h}{2\nu}. \tag{3.4}$$

Substituting (3.4) into (3.1) to obtain non-dimensionalized equations

$$\begin{cases} \frac{\partial \mathbf{u}}{\partial t} + \mathbf{u} \cdot \nabla \mathbf{u} + \nabla p = \frac{1}{R} \nabla^2 \mathbf{u}, \\ \nabla \cdot \mathbf{u} = 0. \end{cases} \tag{3.5}$$

Let $L := \frac{2L_x}{h}$ and let $U_0 := \frac{U_0^*}{U^*}$, note that we have $|U_0(y)| \leq 1$ for $y \in [-1, 1]$. The periodic domain is $\Omega := [-L, L] \times [-1, 1]$, and $\mathbf{u}$ is imposed with following rigid wall boundary condition

$$\mathbf{u}(x, \pm 1, t) = \begin{pmatrix} U_0(\pm 1) \\ 0 \end{pmatrix}. \tag{3.6}$$

Let p_0 be the pressure field corresponding to the base steady state $U_0(y)\mathbf{i}$. It is evident from (3.5), that

$$\frac{\partial p_0}{\partial x} = \frac{1}{R} U_0''(y), \ \frac{\partial p_0}{\partial y} = 0. \tag{3.7}$$

Thus we have

$$p_0''(x) = 0 = U_0'''(y). \tag{3.8}$$

It implies that $U_0(y)$ is in general a quadratic function, among which $U_0(y) = 1 - y^2$ is the viscous planar Poiseuille flow. We restrict our attention to cases where $U_0''(y)$ does not change its sign for every $y \in (-1, 1)$, namely non-inflectional flows. Without loss of generality, we assume that $U_0'' < 0$ throughout this study, with a note that all results presented henceforth are also valid for the category of flows with $U_0'' > 0$. In particular, the viscous planar Couette flow has its $U_0(y) = y$, hence it is precluded from the scope of our study. However, as we shall see, that Theorem III.4 is also applicable to the viscous planar Couette flow.

Suppose following decomposition for a solution $\mathbf{u}$ of (3.5)

$$\mathbf{u} = \begin{pmatrix} U_0(y) \\ 0 \end{pmatrix} + \begin{pmatrix} \widetilde{u}(x,y,t) \\ \widetilde{v}(x,y,t) \end{pmatrix}, \; p = p_0(x) + \widetilde{p}(x,y,t). \tag{3.9}$$

In accordance with (4.4), wall boundary conditions on the perturbed fields are

$$\begin{pmatrix} \widetilde{u} \\ \widetilde{v} \end{pmatrix} \Bigg|_{y=\pm 1} = \begin{pmatrix} 0 \\ 0 \end{pmatrix} \tag{3.10}$$

together with streamwise periodicity.

For a vorticity form of (3.5), we introduce a stream function $\psi(x,y)$ such that $u = \frac{\partial \psi}{\partial y}$ and $v = -\frac{\partial \psi}{\partial x}$, the corresponding vorticity is $\omega := \frac{\partial v}{\partial x} - \frac{\partial u}{\partial y} = -\nabla^2 \psi$. The vorticity formulation of (3.5) is hence

$$\frac{\partial \omega}{\partial t} + \{\psi, \omega\} = \frac{1}{R} \nabla^2 \omega, \tag{3.11}$$

in which $\{\psi, \omega\} := \frac{\partial \psi}{\partial y}\frac{\partial \omega}{\partial x} - \frac{\partial \psi}{\partial x}\frac{\partial \omega}{\partial y}$.

Let ψ_0 be the stream function associated with the base flow $U_0\mathbf{i}$ and let $\omega_0 := -U_0' = -\psi_0''$. Suppose a decomposition for a solution (ψ, ω) of (3.11) to be $\psi = \psi_0(y) + \widetilde{\psi}(x,y,t)$ and $\omega = \omega_0(y) + \widetilde{\omega}(x,y,t)$. We enforce streamwise periodicity on $\widetilde{\psi}$. Besides, following boundary conditions on $\widetilde{\psi}$ are consistent with (3.10)

$$\widetilde{\psi}\Big|_{y=\pm 1} = 0, \; \frac{\partial \widetilde{\psi}}{\partial y}\Big|_{y=\pm 1} = 0. \tag{3.12}$$

Remark: Note that the wall boundary condition (3.10) is directly inherited from the rigid wall condition (3.6). From now on, we shall refer the term 'no-slip' wall boundary condition to be the one defined by (3.10). Besides, as we shall demonstrate, that our major results in forms of Theorem III.2 and Theorem III.4 are both valid

under more general wall boundary conditions including but not limited to the no-slip wall condition.

3.2 Viscous extension of Arnold's inviscid theory for strictly parallel shear flows

In this section, we extend nonlinear stability theory of Arnold [2] on inviscid planar shear flows to viscous planar shear flows subject to two-dimensional disturbances under the no-slip wall condition. As a reminder that for our scope of study on non-inflectional shear flows, we assume without loss of generality that $\omega_0' = -U_0'' > 0$ throughout this work.

Denoting the total kinetic energy of a flow field $\mathbf{u}$ as $\mathcal{E} := \frac{1}{2}\int_\Omega \mathbf{u}\cdot\mathbf{u}\ \mathrm{d}\Omega$, the kinetic energy of a base steady state $U_0\mathbf{i}$ is thus $\mathcal{E}_0 := \frac{1}{2}\int_\Omega U_0^2\ \mathrm{d}\Omega$. Let $\widetilde{\mathcal{E}} := \mathcal{E} - \mathcal{E}_0$. We define an associated Casimir function to be $\mathcal{C}_s := \int_\Omega F(\omega)\ \mathrm{d}\Omega$, where F is an arbitrary smooth function. In particular, let $\mathcal{C}_{s0} := \int_\Omega F(\omega_0)\ \mathrm{d}\Omega$ and $\widetilde{\mathcal{C}_s} := \mathcal{C}_s - \mathcal{C}_{s0}$.

By following the approach used in Arnold's study on inviscid shear flows, we need to choose a suitable function F that relates $\mathcal{E} + \mathcal{C}_s$ to the perturbation fields. Based on the definition of $\widetilde{\mathcal{E}}$ and the Taylor expansion

$$F(\omega_0 + \widetilde{\omega}) = F(\omega_0) + F'(\omega_0)\widetilde{\omega} + F''(\omega_0 + \eta\widetilde{\omega})\frac{\widetilde{\omega}^2}{2},\ \text{for some } \eta \in (0,1), \tag{3.13}$$

we choose F to be the function that satisfies the following condition for eliminating first-order terms in $\widetilde{\mathcal{E}} + \widetilde{\mathcal{C}_s}$

$$U_0 + F''(\omega_0)\omega_0' = 0, \tag{3.14}$$

from which we obtain

$$\widetilde{\mathcal{E}} + \widetilde{\mathcal{C}}_s = \int_{\Omega} \frac{1}{2}\widetilde{u}^2 + \frac{1}{2}\widetilde{v}^2 + F''(\omega_0 + \eta\widetilde{\omega})\frac{\widetilde{\omega}^2}{2}\ \mathrm{d}\Omega. \tag{3.15}$$

For the purpose of conclusive stability analysis, the quadratic form (3.15) needs to be positive definite. This is guaranteed if F'' is a positive-valued function, a requirement that may be fulfilled by the introduction of an appropriate velocity shift onto U_0, as described below.

We introduce a constant velocity shift $\overline{U}$ that is to be added into the base steady state's streamwise velocity profile U_0, with the observation that ω_0 as well as all perturbation fields are preserved under such a shift. As such, it enables us to modify (3.14) for it to become

$$U_0 + \overline{U} + F''(\omega_0)\omega_0' = 0, \tag{3.16}$$

from which we obtain

$$F''(\omega_0) = -\frac{U_0(y) + \overline{U}}{\omega_0'}. \tag{3.17}$$

The positivity of F'' can hence be guaranteed by selecting a sufficiently negative constant shift $\overline{U}$.

Besides the goal of matching for the fixed sign condition on F'', the inclusion of $\overline{U}$ into $F''(\omega_0)$ reviews a fact, that $F''(\omega_0)$ has a freedom due to an arbitrary constant shift. This is built upon the idea of a travelling coordinate system that is moving with a constant velocity relative to the original (stationary) coordinate system. We will base our arguments on this fact in the next section.

Up to this stage, to continue our viscous extension of Arnold's inviscid theory, we need to ensure also that all first-order terms of the temporal rate of change of $\widetilde{\mathcal{E}} + \widetilde{\mathcal{C}}_s$

cancel each other out under the same F chosen according to (3.14).

The total kinetic energy of a flow is $\mathcal{E} = \frac{1}{2}\int_\Omega \mathbf{u}\cdot\mathbf{u}\ \mathrm{d}\Omega$. In accordance with (3.5), we have the following identity

$$\frac{\mathrm{d}\mathcal{E}}{\mathrm{d}t} + \frac{1}{2}\int\limits_{\partial\Omega} |\mathbf{u}|^2\mathbf{u}\cdot\mathrm{d}\mathbf{S} + \int\limits_{\partial\Omega} p\mathbf{u}\cdot\mathrm{d}\mathbf{S} = \frac{1}{R}\left(\int\limits_{\partial\Omega} u\nabla u\cdot\mathrm{d}\mathbf{S} + \int\limits_{\partial\Omega} v\nabla v\cdot\mathrm{d}\mathbf{S} - \int\limits_{\Omega} |\nabla\mathbf{u}|^2\ \mathrm{d}\Omega\right). \tag{3.18}$$

Recall that $\mathcal{E}_0 = \frac{1}{2}\int_\Omega U_0^2\ \mathrm{d}\Omega$ and $\widetilde{\mathcal{E}} = \mathcal{E} - \mathcal{E}_0$. Substituting (3.9) into (3.18), and using (3.8), (3.10), (3.12) together with streamwise periodicity to obtain the following

$$\begin{aligned}
\frac{\mathrm{d}\widetilde{\mathcal{E}}}{\mathrm{d}t} &= \frac{\mathrm{d}\mathcal{E}}{\mathrm{d}t} - \frac{\mathrm{d}\mathcal{E}_0}{\mathrm{d}t} \\
&= -\int_{-1}^{1}[p_0(L) - p_0(-L)]\widetilde{u}(L,y)\ \mathrm{d}y - \int_\Omega U_0\frac{\partial\widetilde{p}}{\partial x}\ \mathrm{d}\Omega \\
&\quad + \frac{1}{R}\int_{-L}^{L}\left[U_0(1)\frac{\partial\widetilde{u}}{\partial y}(x,1) - U_0(-1)\frac{\partial\widetilde{u}}{\partial y}(x,-1)\right]\mathrm{d}x \\
&\quad - \frac{1}{R}\int_\Omega |\nabla\widetilde{u}|^2 + |\nabla\widetilde{v}|^2 + 2U_0'\frac{\partial\widetilde{u}}{\partial y}\ \mathrm{d}\Omega \\
&= -\int_\Omega U_0\frac{\partial\widetilde{p}}{\partial x}\ \mathrm{d}\Omega + \frac{1}{R}\int_\Omega U_0\frac{\partial^2\widetilde{u}}{\partial y^2} + U_0'\frac{\partial\widetilde{u}}{\partial y}\ \mathrm{d}\Omega - \frac{1}{R}\int_\Omega |\nabla\widetilde{u}|^2 + |\nabla\widetilde{v}|^2 + 2U_0'\frac{\partial\widetilde{u}}{\partial y}\ \mathrm{d}\Omega \\
&= -\int_\Omega U_0\frac{\partial\widetilde{p}}{\partial x}\ \mathrm{d}\Omega + \frac{1}{R}\int_\Omega U_0\frac{\partial^2\widetilde{u}}{\partial y^2}\ \mathrm{d}\Omega + \frac{1}{R}\int_\Omega U_0''\widetilde{u}\ \mathrm{d}\Omega - \frac{1}{R}\int_\Omega |\nabla\widetilde{u}|^2 + |\nabla\widetilde{v}|^2\ \mathrm{d}\Omega \\
&= -\int_\Omega U_0\frac{\partial\widetilde{p}}{\partial x}\ \mathrm{d}\Omega + \frac{1}{R}\int_\Omega U_0\frac{\partial^2\widetilde{u}}{\partial y^2}\ \mathrm{d}\Omega - \frac{1}{R}\int_\Omega |\nabla\widetilde{u}|^2 + |\nabla\widetilde{v}|^2\ \mathrm{d}\Omega,
\end{aligned} \tag{3.19}$$

in which we have used the fact that $\int_\Omega \widetilde{u}\ \mathrm{d}\Omega = \int_\Omega \frac{\partial\widetilde{\psi}}{\partial y}\ \mathrm{d}\Omega = \int_{-L}^{L}[\widetilde{\psi}]_{y=-1}^{y=1}\ \mathrm{d}x = 0$.

The associated Casimir function was defined to be $\mathcal{C}_s = \int_\Omega F(\omega)\ \mathrm{d}\Omega$. Recall that $\mathcal{C}_{s0} = \int_\Omega F(\omega_0)\ \mathrm{d}\Omega$ and $\widetilde{\mathcal{C}}_s = \mathcal{C}_s - \mathcal{C}_{s0}$. In accordance with (3.11), the streamwise periodicity of ψ and ω, and the conditions $v|_{y=\pm1} = -\frac{\partial\psi}{\partial x}\Big|_{y=\pm1} = 0$, we arrive at the

following identity

$$\begin{aligned}\frac{\mathrm{d}\mathcal{C}_s}{\mathrm{d}t} &= \frac{1}{R}\left[\int\limits_{\partial\Omega} F'(\omega)\nabla\omega\cdot\ \mathrm{d}\mathbf{S} - \int\limits_{\Omega}\nabla F'(\omega)\cdot\nabla\omega\ \mathrm{d}\Omega\right] \\ &\quad - \int\limits_{\Omega} F'(\omega)\frac{\partial\psi}{\partial y}\frac{\partial\omega}{\partial x}\ \mathrm{d}\Omega + \int\limits_{\Omega} F'(\omega)\frac{\partial\psi}{\partial x}\frac{\partial\omega}{\partial y}\ \mathrm{d}\Omega \\ &= \frac{1}{R}\int\limits_{-L}^{L}\left[F'(\omega)\frac{\partial\omega}{\partial y}\right]_{y=-1}^{y=1}\mathrm{d}x - \frac{1}{R}\int\limits_{\Omega} F''(\omega)|\nabla\omega|^2\ \mathrm{d}\Omega \\ &\quad - \int\limits_{-1}^{1}\left[F(\omega)\frac{\partial\psi}{\partial y}\right]_{x=-L}^{x=L}\mathrm{d}y + \int\limits_{-L}^{L}\left[F(\omega)\frac{\partial\psi}{\partial x}\right]_{y=-1}^{y=1}\mathrm{d}x \\ &= \frac{1}{R}\int\limits_{-L}^{L}\left[F'(\omega)\frac{\partial\omega}{\partial y}\right]_{y=-1}^{y=1}\mathrm{d}x - \frac{1}{R}\int\limits_{\Omega} F''(\omega)|\nabla\omega|^2\ \mathrm{d}\Omega. \end{aligned} \tag{3.20}$$

Recall that $\omega = \omega_0 + \widetilde{\omega}$. In order to re-express (3.20) in terms of ω_0 and $\widetilde{\omega}$ with the first- and the second-order terms explicitly shown, we proceed with the following auxiliary function g in $s \in \mathbb{R}$, regarding ω_0 and $\widetilde{\omega}$ as constant terms herein,

$$g(s) := \frac{1}{R}\int\limits_{-L}^{L}\left[F'(\omega_0 + s\widetilde{\omega})\frac{\partial(\omega_0 + s\widetilde{\omega})}{\partial y}\right]_{y=-1}^{y=1}\mathrm{d}x - \frac{1}{R}\int\limits_{\Omega} F''(\omega_0 + s\widetilde{\omega})|\nabla(\omega_0 + s\widetilde{\omega})|^2\ \mathrm{d}\Omega. \tag{3.21}$$

It is evident that $g(1) = \frac{\mathrm{d}\mathcal{C}_s}{\mathrm{d}t}$ and $g(0) = \frac{\mathrm{d}\mathcal{C}_{s0}}{\mathrm{d}t}$.

Direct computation leads to the following derivatives of g

$$\begin{aligned} g'(s) &= \frac{1}{R}\int\limits_{-L}^{L}\left[F''(\omega_0 + s\widetilde{\omega})\widetilde{\omega}\left(\omega_0' + s\frac{\partial\widetilde{\omega}}{\partial y}\right) + F'(\omega_0 + s\widetilde{\omega})\frac{\partial\widetilde{\omega}}{\partial y}\right]_{y=-1}^{y=1}\mathrm{d}x \\ &\quad - \frac{1}{R}\int\limits_{\Omega} F'''(\omega_0 + s\widetilde{\omega})\widetilde{\omega}\left[\left(s\frac{\partial\widetilde{\omega}}{\partial x}\right)^2 + \left(\omega_0' + s\frac{\partial\widetilde{\omega}}{\partial y}\right)^2\right]\ \mathrm{d}\Omega \\ &\quad - \frac{1}{R}\int\limits_{\Omega} F''(\omega_0 + s\widetilde{\omega})\left[2s\left(\frac{\partial\widetilde{\omega}}{\partial x}\right)^2 + 2\left(\omega_0' + s\frac{\partial\widetilde{\omega}}{\partial y}\right)\frac{\partial\widetilde{\omega}}{\partial y}\right]\ \mathrm{d}\Omega, \end{aligned} \tag{3.22}$$

$$
\begin{aligned}
g''(s) = \frac{1}{R}\int_{-L}^{L}\Bigg[F'''(\omega_0+s\widetilde{\omega})\widetilde{\omega}^2\left(\omega_0'+s\frac{\partial\widetilde{\omega}}{\partial y}\right)+2F''(\omega_0+s\widetilde{\omega})\widetilde{\omega}\frac{\partial\widetilde{\omega}}{\partial y}\Bigg]_{y=-1}^{y=1}\mathrm{d}x \\
-\frac{1}{R}\int_{\Omega}F''''(\omega_0+s\widetilde{\omega})\widetilde{\omega}^2\left[\left(s\frac{\partial\widetilde{\omega}}{\partial x}\right)^2+\left(\omega_0'+s\frac{\partial\widetilde{\omega}}{\partial y}\right)^2\right]\,d\Omega \\
-\frac{4}{R}\int_{\Omega}F'''(\omega_0+s\widetilde{\omega})\widetilde{\omega}\left[s\left(\frac{\partial\widetilde{\omega}}{\partial x}\right)^2+\left(\omega_0'+s\frac{\partial\widetilde{\omega}}{\partial y}\right)\frac{\partial\widetilde{\omega}}{\partial y}\right]\,d\Omega \\
-\frac{2}{R}\int_{\Omega}F''(\omega_0+s\widetilde{\omega})|\nabla\widetilde{\omega}|^2\,d\Omega. \qquad (3.23)
\end{aligned}
$$

Taylor's expansion of g up to the second order centered at $s=s_0$ with increment Δs reads

$$
g(s_0+\Delta s)=g(s_0)+g'(s_0)\Delta s+\frac{1}{2}g''(\xi)\Delta s^2, \qquad (3.24)
$$

where $\xi\in(s_0,s_0+\Delta s)$ is a constant. In particular, set $s_0=0$ and $\Delta s=1$ in (3.24) to obtain

$$
\frac{\mathrm{d}\widetilde{\mathcal{C}}_s}{\mathrm{d}t}=g(1)-g(0)=g'(0)+\frac{1}{2}g''(\xi). \qquad (3.25)
$$

Substituting (3.22) into (3.25) with $s=0$ to obtain

$$
\begin{aligned}
\frac{\mathrm{d}\widetilde{\mathcal{C}}_s}{\mathrm{d}t}=\frac{1}{R}\int_{-L}^{L}\left[F''(\omega_0)\omega_0'\widetilde{\omega}+F'(\omega_0)\frac{\partial\widetilde{\omega}}{\partial y}\right]_{y=-1}^{y=1}\mathrm{d}x \\
-\frac{1}{R}\int_{\Omega}F'''(\omega_0)\omega_0'^2\widetilde{\omega}+2F''(\omega_0)\omega_0'\frac{\partial\widetilde{\omega}}{\partial y}\,\mathrm{d}\Omega+\frac{1}{2}g''(\xi) \qquad (3.26)
\end{aligned}
$$

Using integration by parts and the relationship $\widetilde{\omega}=\frac{\partial\widetilde{v}}{\partial x}-\frac{\partial\widetilde{u}}{\partial y}$ to further manipulate (3.26) as follows

$$
\begin{aligned}
\frac{\mathrm{d}\widetilde{\mathcal{C}}_s}{\mathrm{d}t} &= \frac{1}{R}\int\limits_{\Omega} F'''(\omega_0)\omega_0'^2\widetilde{\omega} + F''(\omega_0)\omega_0''\widetilde{\omega} + F''(\omega_0)\omega_0'\frac{\partial\widetilde{\omega}}{\partial y}\ \mathrm{d}\Omega \\
&\quad + \frac{1}{R}\int\limits_{\Omega} F''(\omega_0)\omega_0'\frac{\partial\widetilde{\omega}}{\partial y} + F'(\omega_0)\frac{\partial^2\widetilde{\omega}}{\partial y^2}\ \mathrm{d}\Omega \\
&\quad - \frac{1}{R}\int\limits_{\Omega} F'''(\omega_0)\omega_0'^2\widetilde{\omega} + 2F''(\omega_0)\omega_0'\frac{\partial\widetilde{\omega}}{\partial y}\ \mathrm{d}\Omega + \frac{1}{2}g''(\xi) \\
&= \frac{1}{R}\int\limits_{\Omega} F'(\omega_0)\frac{\partial^2\widetilde{\omega}}{\partial y^2}\ \mathrm{d}\Omega + \frac{1}{2}g''(\xi) \\
&= -\frac{1}{R}\int\limits_{\Omega} F'(\omega_0)\frac{\partial^3\widetilde{u}}{\partial y^3}\ \mathrm{d}\Omega + \frac{1}{2}g''(\xi) \\
&= -\frac{1}{R}\int\limits_{-L}^{L}\left[F'(\omega_0)\frac{\partial^2\widetilde{u}}{\partial y^2}\right]_{y=-1}^{y=1}\mathrm{d}x + \frac{1}{R}\int\limits_{\Omega} F''(\omega_0)\omega_0'\frac{\partial^2\widetilde{u}}{\partial y^2}\ \mathrm{d}\Omega + \frac{1}{2}g''(\xi) \\
&= -\int\limits_{-L}^{L}\left[F'(\omega_0)\frac{\partial\widetilde{p}}{\partial x}\right]_{y=-1}^{y=1}\mathrm{d}x + \frac{1}{R}\int\limits_{\Omega} F''(\omega_0)\omega_0'\frac{\partial^2\widetilde{u}}{\partial y^2}\ \mathrm{d}\Omega + \frac{1}{2}g''(\xi) \\
&= -\int\limits_{\Omega} F''(\omega_0)\omega_0'\frac{\partial\widetilde{p}}{\partial x} + F'(\omega_0)\frac{\partial^2\widetilde{p}}{\partial x\partial y}\ \mathrm{d}\Omega + \frac{1}{R}\int\limits_{\Omega} F''(\omega_0)\omega_0'\frac{\partial^2\widetilde{u}}{\partial y^2}\ \mathrm{d}\Omega + \frac{1}{2}g''(\xi) \\
&= -\int\limits_{\Omega} F''(\omega_0)\omega_0'\frac{\partial\widetilde{p}}{\partial x}\ \mathrm{d}\Omega + \frac{1}{R}\int\limits_{\Omega} F''(\omega_0)\omega_0'\frac{\partial^2\widetilde{u}}{\partial y^2} + \frac{1}{2}g''(\xi). \qquad (3.27)
\end{aligned}
$$

Notice that the fact $\omega_0'' = 0$ and the following equation had been applied

$$
\frac{1}{R}\frac{\partial^2\widetilde{u}}{\partial y^2}(x,\pm 1) = \frac{\partial\widetilde{p}}{\partial x}(x,\pm 1), \qquad (3.28)
$$

which holds due to (3.5) and the no-slip wall boundary condition $\widetilde{u} = \widetilde{v} = 0$. Notice also that the presence of viscosity had made above derivations much more complicated than Arnold's original derivations for the non-viscous case, as in the latter case one did not need to apply any constraint (e.g. equations of motion) other than the boundary conditions.

Moreover, the higher-order remainder in (3.27) is evaluated based on (3.23) to be

$$\begin{aligned}\frac{1}{R}h(\widetilde{\omega},\xi) :&= \frac{1}{2}g''(\xi)\\ &= \frac{1}{2R}\int_{-L}^{L}\left[F'''(\omega_0+\xi\widetilde{\omega})\widetilde{\omega}^2\left(\omega_0'+\xi\frac{\partial\widetilde{\omega}}{\partial y}\right)+2F''(\omega_0+\xi\widetilde{\omega})\widetilde{\omega}\frac{\partial\widetilde{\omega}}{\partial y}\right]_{y=-1}^{y=1}\mathrm{d}x\\ &-\frac{1}{2R}\int_{\Omega}\left\{F''''(\omega_0+\xi\widetilde{\omega})\widetilde{\omega}^2\left[\left(\xi\frac{\partial\widetilde{\omega}}{\partial x}\right)^2+\left(\omega_0'+\xi\frac{\partial\widetilde{\omega}}{\partial y}\right)^2\right]\right.\\ &+4F'''(\omega_0+\xi\widetilde{\omega})\widetilde{\omega}\left[\xi\left(\frac{\partial\widetilde{\omega}}{\partial x}\right)^2+\left(\omega_0'+\xi\frac{\partial\widetilde{\omega}}{\partial y}\right)\frac{\partial\widetilde{\omega}}{\partial y}\right]\\ &\left.+2F''(\omega_0+\xi\widetilde{\omega})|\nabla\widetilde{\omega}|^2\right\}\,d\Omega. \end{aligned} \tag{3.29}$$

As the final step of the derivations, we need to validate that first-order terms in (3.19) and (3.27) cancel each other out upon summed together under the same function F defined by (3.16), but this is evidently true.

Therefore, the summation of (3.19) and (3.27) consists of perturbation terms of at least a second-order, which gives rise to the following Theorem.

Theorem III.1. *(The viscous Arnold's identity) The following identity is valid for a strictly parallel viscous planar non-inflectional shear flow $U_0(y)\boldsymbol{i}$ under global nonlinear dynamics enforced by the no-slip wall boundary condition* (3.10)

$$\frac{1}{2}\frac{\mathrm{d}}{\mathrm{d}t}\int_{\Omega}\left[\widetilde{u}^2+\widetilde{v}^2+F''(\omega_0+\eta\widetilde{\omega})\widetilde{\omega}^2\right]\mathrm{d}\Omega=-\frac{1}{R}\int_{\Omega}|\nabla\widetilde{u}|^2+|\nabla\widetilde{v}|^2\,\mathrm{d}\Omega+\frac{1}{R}h(\widetilde{\omega},\xi), \tag{3.30}$$

where F is a function that obeys (3.17) *for a sufficiently negative constant $\overline{U}$ such that $F''>0$, $\frac{1}{R}h(\widetilde{\omega},\xi)$ is defined by* (3.29) *and $\eta(x,y,t),\xi(x,y,t)$ are two functions that depend upon $\widetilde{\omega}$ with range $(0,1)$.*

We have so far extended Arnold's nonlinear stability theory of inviscid parallel

shear flows to viscous parallel shear flows. The basic physics revealed by Arnold's inviscid theory indicates that there is no physical mechanism which is capable to support the growth of perturbation's energy and vorticity, as shown by the Arnold's function on the left-hand side of (3.30). Above result demonstrates that the same holds true for viscous shear flows, namely all terms related to the inviscid mechanism cancelled each other out perfectly and remaining terms are explicitly viscous. Theorem III.1 is novel and it serves as a basis for a number of results presented in subsequent sections.

3.3 An alternative path to the enstrophy identity by J. L. Synge

Let us reduce the complexity of the remainder term $h(\widetilde{\omega}, \xi)$ in Theorem III.1 for a moment by considering its linearized form, with those disturbance terms that are higher than the second-order removed. Thereafter, we obtain the following

$$\begin{aligned}
\frac{1}{2}\frac{\mathrm{d}}{\mathrm{d}t}\int\limits_{\Omega}\left[\widetilde{u}^2+\widetilde{v}^2+F''(\omega_0)\widetilde{\omega}^2\right]\mathrm{d}\Omega &= -\frac{1}{R}\int\limits_{\Omega}|\nabla\widetilde{u}|^2+|\nabla\widetilde{v}|^2\ \mathrm{d}\Omega \\
&+\frac{1}{2R}\int\limits_{-L}^{L}\left[F'''(\omega_0)\widetilde{\omega}^2\omega_0'+2F''(\omega_0)\widetilde{\omega}\frac{\partial\widetilde{\omega}}{\partial y}\right]_{y=-1}^{y=1}\mathrm{d}x \\
&-\frac{1}{2R}\int\limits_{\Omega}\left\{F''''(\omega_0)\omega_0'^2\widetilde{\omega}^2+4F'''(\omega_0)\omega_0'\widetilde{\omega}\frac{\partial\widetilde{\omega}}{\partial y}+2F''(\omega_0)|\nabla\widetilde{\omega}|^2\right\}\mathrm{d}\Omega, \qquad (3.31)
\end{aligned}$$

For further simplification of (3.31), we elaborate the observation made through (3.17) that $F''(\omega_0)$ has a freedom due to an arbitrary constant shift $\overline{U}$, together with the fact that ω_0' is a positive constant due to the strict parallelism assumption on U_0 as enforced by (3.8).

Specifically, as we observed through (3.17), that $F''(\omega_0)$ has a freedom due to an arbitrary constant shift $\overline{U}$. Differentiating both sides of (3.17) with respect to y, with

the observation that ω_0' is a constant, we have

$$F'''(\omega_0) = \frac{\omega_0}{\omega_0'^2},\ F''''(\omega_0) = \frac{1}{\omega_0'^2}. \tag{3.32}$$

Substituting (3.17) and (3.32) into (3.31), and dividing both sides of the resulting identiy by $-\overline{U}$ to obtain

$$\begin{aligned}
&\frac{1}{2}\frac{\mathrm{d}}{\mathrm{d}t}\int\limits_{\Omega}\left[-\frac{\widetilde{u}^2+\widetilde{v}^2}{\overline{U}}+\frac{U_0(y)+\overline{U}}{\omega_0'(y)\overline{U}}\widetilde{\omega}^2\right]\mathrm{d}\Omega = \frac{1}{R}\int\limits_{\Omega}\frac{|\nabla\widetilde{u}|^2+|\nabla\widetilde{v}|^2}{\overline{U}}\,\mathrm{d}\Omega \\
&+\frac{1}{2R}\int\limits_{-L}^{L}\left[-\frac{\omega_0(y)}{\omega_0'(y)\overline{U}}\widetilde{\omega}^2+2\frac{U_0(y)+\overline{U}}{\omega_0'(y)\overline{U}}\widetilde{\omega}\frac{\partial\widetilde{\omega}}{\partial y}\right]_{y=-1}^{y=1}\mathrm{d}x \\
&-\frac{1}{2R}\int\limits_{\Omega}\left\{-\frac{\widetilde{\omega}^2}{\overline{U}}-4\frac{\omega_0(y)}{\omega_0'(y)\overline{U}}\widetilde{\omega}\frac{\partial\widetilde{\omega}}{\partial y}+2\frac{U_0(y)+\overline{U}}{\omega_0'(y)\overline{U}}|\nabla\widetilde{\omega}|^2\right\}\mathrm{d}\Omega.
\end{aligned} \tag{3.33}$$

Taking the limit as $\overline{U}\to-\infty$ in (3.33) and then dividing out the constant common weight factor $1/\omega_0'$ on both sides of the resulting equality leads us to the following identity

$$\frac{1}{2}\frac{\mathrm{d}}{\mathrm{d}t}\int\limits_{\Omega}\widetilde{\omega}^2\,\mathrm{d}\Omega = \frac{1}{R}\int\limits_{-L}^{L}\left[\widetilde{\omega}\frac{\partial\widetilde{\omega}}{\partial y}\right]_{y=-1}^{y=1}\mathrm{d}x-\frac{1}{R}\int\limits_{\Omega}|\nabla\widetilde{\omega}|^2\,\mathrm{d}\Omega, \tag{3.34}$$

where $\widetilde{\omega}$ is determined by linear dynamics under the no-slip wall condition (3.10).

Identity (3.34) was first discovered by Synge [44] within the framework of the classical normal-mode analysis in which perturbations are restricted to exponential growth/decay modes. Fraternale *et al* [17] recently extended Synge's result to include transient infinitesimal disturbances, and obtained (3.34) explicitly. Our alternative derivation presented above establishes a natural connection between the viscous Arnold's identity and (3.34). Moreover, our alternative derivation signals the potential of using the viscous Arnold's identity to find new identities that quantify the perturbation's enstrophy. With regards such potential as a strategy, it gives rise

to much of the work presented in the next two sections.

The quantity $\frac{1}{2}\int_\Omega \widetilde{\omega}^2 \, \mathrm{d}\Omega$ is commonly referred to as the perturbation's enstrophy over the domain Ω. It is worth mentioning that there is rather limited study in literature that aims to explore the physical mechanism of shear flow stability from the perspective of enstrophy [17].

An evident observation that can be made immediately based on (3.34) is that the perturbation's enstrophy can only generate at the walls, and it dissipates inside the fluid bulk. However, one cannot draw further conclusion based on (3.34) alone about the production/dissipation of the perturbation's enstrophy. With the aid of numerical computation, we will take a step of addressing this question in §4.1 in the context of viscous planar Poiseuille flow.

We have restricted our attention so far to strictly parallel shear flows under the no-slip wall condition. In the next two sections, we will relax the parallelism assumption and/or relax the no-slip wall condition to arrive at two additional novel results of this study. As we shall see, both of the upcoming results have their roots in Theorem III.1.

3.4 A weighted disturbance's enstrophy identity for non-parallel shear flows

As we observed in the derivation procedure for (3.34), we needed to divide out the constant common weight factor $1/\omega_0'$ on both sides of the resulting equality to finally obtain (3.34). Apparently, the constant weight factor $1/\omega_0'$ that originally presented on both sides of (3.34) played no practical role. However, it suggests a weighted enstrophy identity that might be valid for a broader category of shear flows which are not strictly parallel. Note that such weight factor corresponding to a non-parallel shear flow is no longer a constant.

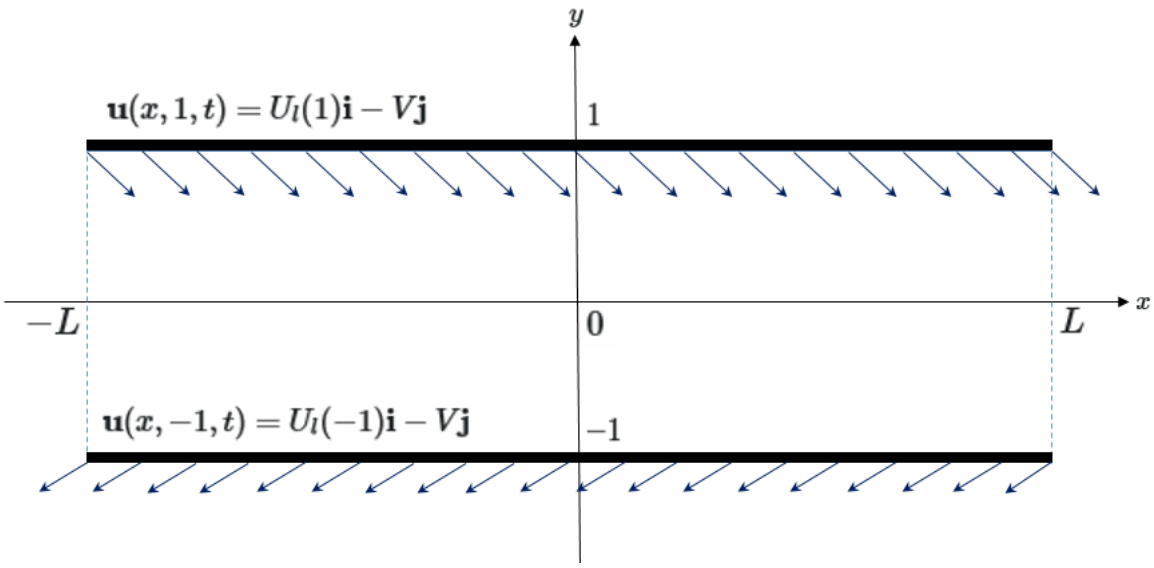

Figure 3.2: Sketch of boundaries and wall boundary conditions for a streamwise translation-invariant non-parallel shear flow imposed with uniform boundary injection and suction. The streamwise velocity component is $U_l(y)$, and the constant rate of injection (through the top wall) and suction (through the bottom wall) are both $-V$.

For a streamwise translation-invariant shear flow that is not strictly parallel, such as a shear layer subject to uniform injection and suction of fluid through its walls, its streamwise velocity profile is in general non-inflectional. A sketch of the boundaries and wall boundary conditions for a flow of this kind is illustrated in Figure 3.2. We present the following weighted perturbation's enstrophy identity for such flows, which is inspired by the viscous Arnold's identity (3.30).

Theorem III.2. *(A weighted perturbation's enstrophy identity) Let $U_l(y)\boldsymbol{i} - V\boldsymbol{j}$ be a steady-state velocity field of a viscous shear flow that fulfills* (3.5)*, where V is a constant. Suppose that at each wall, either of the following two categories of boundary conditions are imposed*

1. *$\widetilde{v} = 0$ and another arbitrarily prescribed condition on a perturbation field.*

2. *$\widetilde{u} = 0$ and another arbitrarily prescribed condition on a perturbation field.*

Denote its vorticity by $\omega_l := -U_l'$*, assuming that* $\omega_l' \neq 0$ *for* $y \in (0,1)$*. We have*

$$\frac{1}{2}\frac{\mathrm{d}}{\mathrm{d}t}\int\limits_{\Omega}\frac{1}{\omega_l'}\widetilde{\omega}^2\ \mathrm{d}\Omega = \frac{1}{R}\int\limits_{-L}^{L}\left[\frac{1}{\omega_l'}\widetilde{\omega}\frac{\partial\widetilde{\omega}}{\partial y}\right]_{y=-1}^{y=1}\mathrm{d}x - \frac{1}{R}\int\limits_{\Omega}\frac{1}{\omega_l'}|\nabla\widetilde{\omega}|^2\ \mathrm{d}\Omega, \tag{3.35}$$

in which the perturbation's vorticity $\widetilde{\omega}$ *is determined by linear dynamics.*

Proof. Recall that $u = \frac{\partial\psi}{\partial y}$ and $v = -\frac{\partial\psi}{\partial x}$. Linearizing (4.7) about the base steady state $U_l(y)\mathbf{i} - V\mathbf{j}$ to obtain

$$\frac{\partial\widetilde{\omega}}{\partial t} + U_l(y)\frac{\partial\widetilde{\omega}}{\partial x} - V\frac{\partial\widetilde{\omega}}{\partial y} + \omega_l'(y)\widetilde{v} = \frac{1}{R}\nabla^2\widetilde{\omega} \tag{3.36}$$

subject to either $\widetilde{u} = 0$ or $\widetilde{v} = 0$ at the walls (as we shall see, that following derivations rely on only one of these wall boundary conditions).

Multiplying both sides of (3.36) by $\widetilde{\omega}/\omega_l'$, then integrating which over Ω to obtain

$$\frac{1}{2}\frac{\mathrm{d}}{\mathrm{d}t}\int\limits_{\Omega}\frac{\widetilde{\omega}^2}{\omega_l'}\ \mathrm{d}\Omega + \frac{1}{2}\int\limits_{\Omega}\frac{U_l}{\omega_l'}\frac{\partial\left(\widetilde{\omega}^2\right)}{\partial x}\ \mathrm{d}\Omega - V\int\limits_{\Omega}\frac{\widetilde{\omega}}{\omega_l'}\frac{\partial\widetilde{\omega}}{\partial y}\ \mathrm{d}\Omega + \int\limits_{\Omega}\widetilde{v}\widetilde{\omega}\ \mathrm{d}\Omega = \frac{1}{R}\int\limits_{\Omega}\frac{\widetilde{\omega}}{\omega_l'}\nabla^2\widetilde{\omega}\ \mathrm{d}\Omega. \tag{3.37}$$

Observe that the second integral on the left-hand side of (3.37) vanishes due to the streamwise periodic condition on $\widetilde{\omega}$. Besides, we have

$$\begin{aligned}\int\limits_{\Omega}\widetilde{v}\widetilde{\omega}\ \mathrm{d}\Omega &= \int\limits_{\Omega}\widetilde{v}\left(\frac{\partial\widetilde{v}}{\partial x} - \frac{\partial\widetilde{u}}{\partial y}\right)\ \mathrm{d}\Omega = \frac{1}{2}\int\limits_{\Omega}\frac{\partial\left(\widetilde{v}^2\right)}{\partial x}\ \mathrm{d}\Omega + \int\limits_{\Omega}\frac{\partial\widetilde{v}}{\partial y}\widetilde{u}\ \mathrm{d}\Omega \\ &= \frac{1}{2}\int\limits_{\Omega}\frac{\partial\left(\widetilde{v}^2\right)}{\partial x}\ \mathrm{d}\Omega - \int\limits_{\Omega}\frac{\partial\widetilde{u}}{\partial x}\widetilde{u}\ \mathrm{d}\Omega \\ &= \frac{1}{2}\int\limits_{\Omega}\frac{\partial\left(\widetilde{v}^2\right)}{\partial x}\ \mathrm{d}\Omega - \frac{1}{2}\int\limits_{\Omega}\frac{\partial\left(\widetilde{u}^2\right)}{\partial x}\ \mathrm{d}\Omega \\ &= 0,\end{aligned} \tag{3.38}$$

in which we had applied integration by parts to the second line that relies on either

$\widetilde{u} = 0$ or $\widetilde{v} = 0$ at the walls. The third line of (3.38) is due to the continuity equation, and the streamwise periodicity is applied to the fourth line for deducing the cancellation.

Moreover, the right-hand side of (3.37) reads

$$\frac{1}{R}\int\limits_{\Omega}\frac{\widetilde{\omega}}{\omega_l'}\nabla^2\widetilde{\omega}\,\mathrm{d}\Omega = \frac{1}{R}\int\limits_{-L}^{L}\left[\frac{\widetilde{\omega}}{\omega_l'}\frac{\partial\widetilde{\omega}}{\partial y}\right]_{y=-1}^{y=1}\mathrm{d}x - \frac{1}{R}\int\limits_{\Omega}\frac{|\nabla\widetilde{\omega}|^2}{\omega_l'}\,\mathrm{d}\Omega + \frac{1}{R}\int\limits_{\Omega}\frac{\omega_l''}{\omega_l'^2}\widetilde{\omega}\frac{\partial\widetilde{\omega}}{\partial y}\,\mathrm{d}\Omega. \tag{3.39}$$

Identity (3.37), thereby, reduces to the following

$$\begin{aligned}\frac{1}{2}\frac{\mathrm{d}}{\mathrm{d}t}\int\limits_{\Omega}\frac{\widetilde{\omega}^2}{\omega_l'}\,\mathrm{d}\Omega = \frac{1}{R}\int\limits_{-L}^{L}\left[\frac{\widetilde{\omega}}{\omega_l'}\frac{\partial\widetilde{\omega}}{\partial y}\right]_{y=-1}^{y=1}\mathrm{d}x - \frac{1}{R}\int\limits_{\Omega}\frac{|\nabla\widetilde{\omega}|^2}{\omega_l'}\,\mathrm{d}\Omega \\ + \frac{1}{R}\int\limits_{\Omega}\frac{\omega_l''}{\omega_l'^2}\widetilde{\omega}\frac{\partial\widetilde{\omega}}{\partial y}\,\mathrm{d}\Omega + V\int\limits_{\Omega}\frac{\widetilde{\omega}}{\omega_l'}\frac{\partial\widetilde{\omega}}{\partial y}\,\mathrm{d}\Omega,\end{aligned} \tag{3.40}$$

and the second line of (3.40) reads

$$\frac{1}{R}\int\limits_{\Omega}\frac{\omega_l''}{\omega_l'^2}\widetilde{\omega}\frac{\partial\widetilde{\omega}}{\partial y}\,\mathrm{d}\Omega + V\int\limits_{\Omega}\frac{\widetilde{\omega}}{\omega_l'}\frac{\partial\widetilde{\omega}}{\partial y}\,\mathrm{d}\Omega = \int\limits_{\Omega}\frac{1}{\omega_l'^2}\left(\frac{1}{R}\nabla^2\omega_l + V\omega_l'\right)\widetilde{\omega}\frac{\partial\widetilde{\omega}}{\partial y}\,\mathrm{d}\Omega = 0 \tag{3.41}$$

due to (3.11) expressed with respect to the base steady state $U_l(y)\mathbf{i} - V\mathbf{j}$.

Identity (3.35) follows from (3.40) and (3.41).

□

Theorem III.2 provides us with a novel weighted identity for streamwise translation-invariant shear flows. We present the following flow example taken from [12] for illustrating an application of Theorem III.2. We will elaborate this result further in Chapter 4, in which we will introduce a nonlinear enstrophy identity for flows with suction.

Example III.3. The viscous planar Couette flow with injection and suction

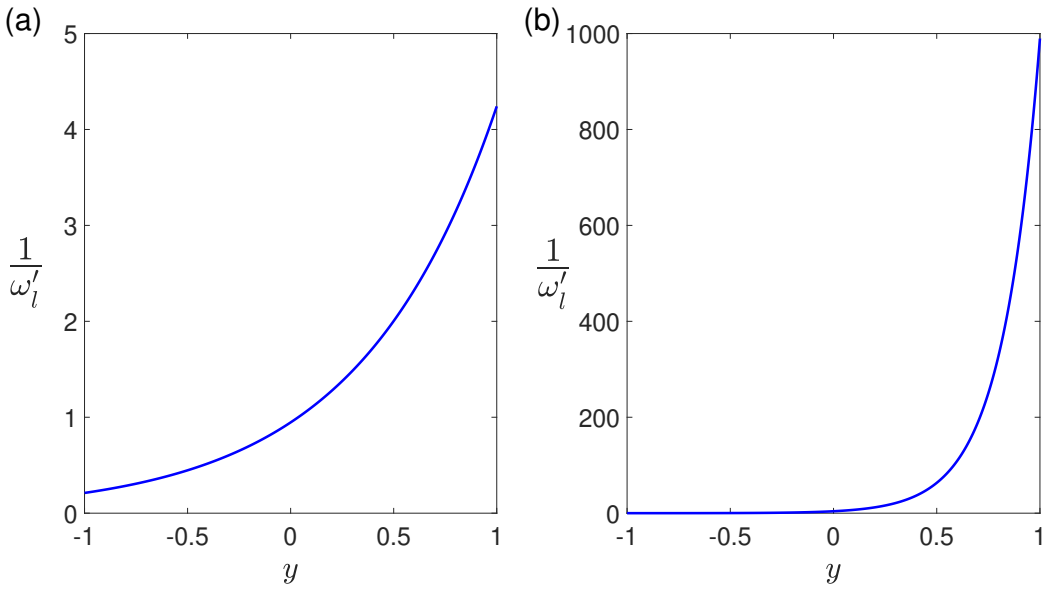

Figure 3.3: Plots of the weight function $\frac{1}{\omega_l'}$ for the viscous planar Couette flow with wall boundary injection and suction at $R = 10^6$ and (a): $V = 1.5 \times 10^{-6}$, (b): $V = 5.5 \times 10^{-6}$.

Consider the planar Couette flow with $U_0(y) = y$. Once after it is imposed with constant injection and suction rates $-V$ through the walls, its original linear streamwise velocity profile would then be disturbed, and a base steady state to the new flow system is of the form $U_l(y)\mathbf{i} - V\mathbf{j}$, with

$$U_l(y) := \frac{2 - 2\exp\left[-RV\left(y+1\right)\right]}{1 - \exp\left(-2RV\right)} - 1, \tag{3.42}$$

note that $U_l(y) \to U_0(y) = y$ when $V \to 0$. The corresponding weight function is

$$\frac{1}{\omega_l'(y)} = -\frac{1}{U_l''(y)} = \frac{1 - \exp\left(-2RV\right)}{2R^2V^2} \exp\left[RV\left(y+1\right)\right]. \tag{3.43}$$

Plots of the weight function at $R = 10^6$ with $V = 1.5 \times 10^{-6}$ and $V = 5.5 \times 10^{-6}$ are shown in Figure 3.3(a) and Figure 3.3(b), respectively. The weights in both cases exhibit relatively large magnitudes at a vicinity of the upper wall, whereas their values at the lower wall are relatively negligible. The presence of the weight function

reviews a significant fact, that the upper wall plays a much more dominant role than the lower in terms of their influence on stability of the flow. This is especially clear in the case $V = 5.5 \times 10^{-6}$, in which the magnitude of the weight function reaches to an exceedingly high magnitude of nearly $O(10^3)$ at the upper wall, whereas it remains to be of order $O(1)$ at the lower wall.

3.5 Imposing wall boundary conditions to (3.34) under global nonlinear dynamics

Let us take a step back to our study on strictly parallel non-inflectional shear flows. With the observation that ω_0' is a non-zero constant, applying the aforementioned procedure in §3.2 used to derive (3.34) under linear dynamics to the fully nonlinear viscous Arnold's identity (3.30) brings one to exactly the same identity as (3.34). Therefore, (3.34) also holds under global nonlinear dynamics for the no-slip wall condition. This is a direct consequence of the global nonlinear nature of our viscous Arnold's identity.

In fact, as noted in the work by Fraternale *et al* [17] [see also Appendix C of 46], the temporal rate of change of perturbation's enstrophy quantified by (3.34) is independent of the disturbance's amplitude. Thus, the perturbation's dynamics is governed by linear mechanisms only. Physically, this fact is related to the lack of vortex stretching in two dimensions. Fraternale *et al* [17] adopted this fact to justify the usage of linearized equation (3.34) for seeking improved bounds (in terms of the Reynolds number) on global nonlinear stability of viscous plane Couette flow and viscous plane Poiseuille flow.

With regards above evidence as inspiration, we rigorously examined the validity of (3.34) for strictly parallel shear flows under global nonlinear dynamics imposed with two categories of wall boundary conditions, and we obtained the following result. We

would like to point out, that Fraternale *et al* [17] did not prove the following result, we are the first in literature to prove it.

Theorem III.4. *Let $\widetilde{\omega}$ be the perturbation's vorticity of a strictly parallel viscous planar shear flow $U_0(y)\boldsymbol{i}$ ($\omega_0'(y)$ is a constant). Suppose that at each wall, either of the following two categories of boundary conditions are imposed*

1. *$\widetilde{v} = 0$ and another arbitrarily prescribed condition on a perturbation field.*

2. *$\widetilde{u} = 0$ and $\widetilde{\omega} = 0$.*

The temporal evolution of the perturbation's enstrophy is then still governed by (3.34) *under global nonlinear dynamics.*

Proof. Substituting $\psi = \psi_0(y) + \widetilde{\psi},\ \omega = \omega_0(y) + \widetilde{\omega}$ into (3.11), then integrating which over Ω to obtain the following

$$\begin{aligned}\frac{1}{2}\frac{\mathrm{d}}{\mathrm{d}t}\int\limits_{\Omega}\widetilde{\omega}^2\ \mathrm{d}\Omega = \int\limits_{\Omega}\widetilde{\omega}\frac{\partial\widetilde{\omega}}{\partial t}\ \mathrm{d}\Omega &= -\int\limits_{\Omega}\widetilde{\omega}\{\psi,\omega\}\ \mathrm{d}\Omega + \frac{1}{R}\int\limits_{\Omega}\widetilde{\omega}\nabla^2\omega\ \mathrm{d}\Omega \\ &= -\int\limits_{\Omega}\widetilde{\omega}\left[\{\psi_0,\widetilde{\omega}\} + \{\widetilde{\psi},\omega_0\} + \{\widetilde{\psi},\widetilde{\omega}\}\right]\ \mathrm{d}\Omega + \frac{1}{R}\int\limits_{\Omega}\widetilde{\omega}\nabla^2\widetilde{\omega}\ \mathrm{d}\Omega. \qquad (3.44)\end{aligned}$$

The first integral on the right-hand side of (3.44) is non-viscous, and it is equal to zero as demonstrated termwise below

$$\int\limits_{\Omega}\widetilde{\omega}\ \{\psi_0,\widetilde{\omega}\}\ \mathrm{d}\Omega = \int\limits_{\Omega}\widetilde{\omega}\ U_0(y)\frac{\partial\widetilde{\omega}}{\partial x}\ \mathrm{d}\Omega = \frac{1}{2}\int\limits_{\Omega}U_0(y)\frac{\partial(\widetilde{\omega}^2)}{\partial x}\ \mathrm{d}\Omega = 0, \qquad (3.45)$$

in which we have applied integration by parts and the streamwise periodicity;

$$\int\limits_{\Omega}\widetilde{\omega}\ \{\widetilde{\psi},\omega_0\}\ \mathrm{d}\Omega = \omega_0'\int\limits_{\Omega}\widetilde{\omega}\widetilde{v}\ \mathrm{d}\Omega = 0, \qquad (3.46)$$

in which we have used the fact that ω_0' is a constant number, and we have applied

(3.38) under either $\widetilde{u}=0$ or $\widetilde{v}=0$ at the walls;

$$\begin{aligned}\int_{\Omega}\widetilde{\omega}\{\widetilde{\psi},\widetilde{\omega}\}\mathrm{d}\Omega &= \int_{\Omega}\widetilde{\omega}\left(\widetilde{v}\frac{\partial\widetilde{\omega}}{\partial y}+\widetilde{u}\frac{\partial\widetilde{\omega}}{\partial x}\right)\mathrm{d}\Omega \\ &= -\frac{1}{2}\int_{\Omega}\left(\frac{\partial\widetilde{v}}{\partial y}+\frac{\partial\widetilde{u}}{\partial x}\right)\omega^2\mathrm{d}\Omega+\frac{1}{2}\int_{-L}^{L}\left[\widetilde{v}\widetilde{\omega}^2\right]_{y=-1}^{y=1}\mathrm{d}x+\frac{1}{2}\int_{-1}^{1}\left[\widetilde{u}\widetilde{\omega}^2\right]_{x=-L}^{x=L}\mathrm{d}y \\ &= 0, \end{aligned} \tag{3.47}$$

in which we have applied the continuity equation, the streamwise periodicity, and either $\widetilde{v}=0$ or $\widetilde{\omega}=0$ at the walls. (3.47) reveals a hidden relationship between $\widetilde{\omega}$ and $\widetilde{\psi}$, namely that $\widetilde{\omega}$ is always orthogonal to $\{\widetilde{\psi},\widetilde{\omega}\}$ with respect to the integral over Ω.

Moreover, applying integration by parts to the viscous term on right-hand side of (3.44) deduces the following, note that its right-hand side is of the same form as (3.34)

$$\frac{1}{R}\int_{\Omega}\widetilde{\omega}\nabla^2\widetilde{\omega}\ \mathrm{d}\Omega=\frac{1}{R}\int_{-L}^{L}\left[\widetilde{\omega}\frac{\partial\widetilde{\omega}}{\partial y}\right]_{y=-1}^{y=1}\mathrm{d}x-\frac{1}{R}\int_{\Omega}|\nabla\widetilde{\omega}|^2\ \mathrm{d}\Omega. \tag{3.48}$$

Above calculations are valid for any profile $U_0(y)$ with $\omega_0=-U_0'$ being a constant function, which includes the planar Couette flow (its $U_0(y)=y$) as a degenerate case. □

Theorem III.4 is novel, it extends the validity of (3.34) to be under global nonlinear dynamics, and it is valid for two sets of wall boundary conditions that include but not limited to the no-slip wall boundary condition (3.10). According to above theorem, the only production mechanism of perturbation's enstrophy is due to the enforced no-slip condition at the rigid walls, and the internal flow only contributes to the loss in perturbation's enstrophy. Moreover, it also shows that the inviscid mechanism has no quantitative contribution to the production and loss of perturbation's enstrophy

in viscous shear flows, the same holds true in Arnold's theory on inviscid shear flows [2]. However, as inferred by our mathematical derivations for the viscous extension of Arnold's inviscid theory, that the inviscid mechanism still serves an important role of transporting the perturbation's vorticity in a viscous flow.

We take the viscous planar Poiseuille flow with $U_0(y) = 1 - y^2$ as an example to substantiate the physical meaning of Theorem III.4. It is a well-known fact, that under the no-slip wall boundary condition $\widetilde{u} = \widetilde{v} = 0$, the critical Reynolds number corresponding to the onset of linear instability of the flow is $R_l = 5772$ associated with wave number $\alpha_l = 1.02$ [see 32, 36]. It has also been shown that a subcritical bifurcation would trigger in this flow at the Reynolds number R_l. Beyond the subcritical bifurcation, it has been validated that some initial conditions on the flow would lead to finite-amplitude two-dimensional equilibrated wave states, those were steady in a constantly moving frame of reference with respect to the base steady state.

These results are summarized in a review article by Bayly, Orszag and Herbert [6] [see also 20, 43] in form of a (E, α, R) plot, here E is the ratio between the kinetic energy of the wave disturbance and that of the base steady state, and it is directly proportional to the squared amplitude of the wave disturbance, α and R are the wave number and the Reynolds number, respectively. We display this plot as Figure 3.4 for convenience of the reader. The Reynolds number for the 'nose' of the nonlinear neutral surface is $R_{cr} = 2935$ with the corresponding wave number to be $\alpha_{cr} = 1.32$. The intersection of the neutral surface with the zero-energy plane coincides with the linear neutral stability curve of the viscous planar Poiseuille flow subject to infinitesimal wave disturbances, as shown by the red curve. The projection of the neutral surface onto the zero-energy plane is shown by the blue curve, which encloses the region of the (α, R)-plane associated with unstable two-dimensional wave disturbances of arbitrary amplitudes.

As an application of Theorem III.4 to the viscous planar Poiseuille flow, we first

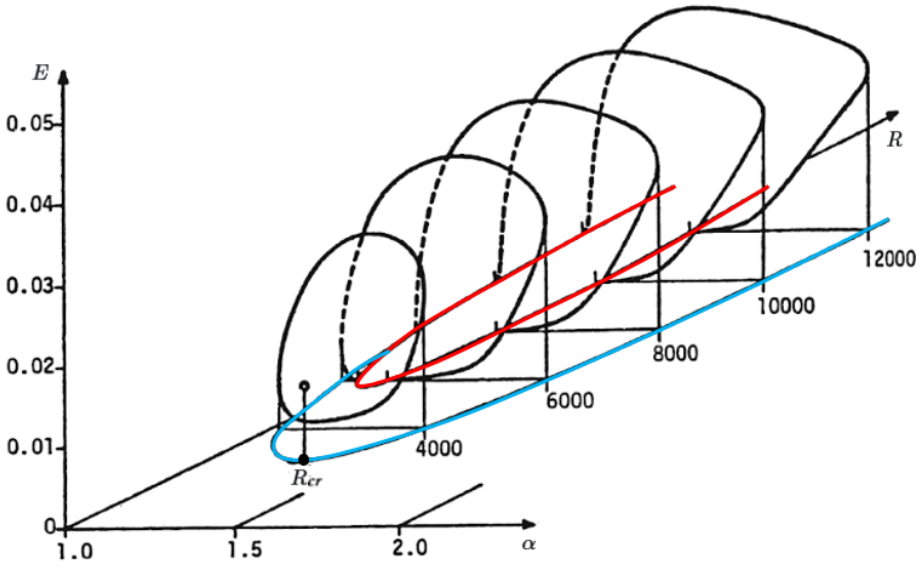

Figure 3.4: Nonlinear neutral surface for finite-amplitude two-dimensional wave disturbances in the viscous planar Poiseuille flow. The 'tip' of the neutral surface is located at $R_{cr} = 2935$ with $\alpha_{cr} = 1.32$.

consider the no-slip wall boundary condition $\widetilde{u} = \widetilde{v} = 0$. For an aforementioned two-dimensional equilibrated travelling wave disturbance $\widetilde{\omega}_T$, there holds $\frac{\mathrm{d}}{\mathrm{d}t}\int_\Omega \widetilde{\omega}_T^2 \,\mathrm{d}\Omega = 0$ for all time t, and thus

$$\frac{1}{R}\left(\int_{-L}^{L}\left[\widetilde{\omega}_T\frac{\partial\widetilde{\omega}_T}{\partial y}\right]_{y=-1}^{y=1}\mathrm{d}x - \int_\Omega |\nabla\widetilde{\omega}_T|^2 \,\mathrm{d}\Omega\right) = 0. \tag{3.49}$$

(3.49) clearly reveals a physical mechanism, that a wave disturbance is able to remain self-sustainable only if the internal damping in perturbation's vorticity was perfectly overcome by the production of perturbation's vorticity at the walls. Therefore, (3.49) stands as a crucial prerequisite for the existence of a nonlinear equilibrated wave disturbance.

The second category of wall conditions are compatible with the vorticity flow equations (3.11). Note that since $\widetilde{u}$ is prescribed at the walls, the other wall condition on $\widetilde{\omega}$ may be matched through controls on $\widetilde{v}$ at the walls. Note also that the

application of (3.34) into this case implies immediately global nonlinear stability for the base flow, and it leads to an upper bound for the decay rate of the disturbance's enstrophy. We elaborate this through the following Example.

Example III.5. Consider the viscous planar Poiseuille flow $(1-y^2)\mathbf{i}$ with its no-slip wall boundary condition

$$\begin{pmatrix} u \\ v \end{pmatrix}\Big|_{y=\pm 1} = \begin{pmatrix} 0 \\ 0 \end{pmatrix} \tag{3.50}$$

replaced by

$$\begin{pmatrix} u \\ \omega \end{pmatrix}\Big|_{y=\pm 1} = \begin{pmatrix} 0 \\ \pm 2 \end{pmatrix} \ \textit{or} \ \begin{pmatrix} v \\ \omega \end{pmatrix}\Big|_{y=\pm 1} = \begin{pmatrix} 0 \\ \pm 2 \end{pmatrix}. \tag{3.51}$$

Note that $U_0(y)\mathbf{i}$ remains to be the base steady state under the new wall boundary conditions (3.51), because of $\omega_0(y) = -U_0'(y)$.

Since the values of ω are prescribed to be those of ω_0 at $y = \pm 1$, it implies that $\widetilde{\omega} = 0$ at the walls. Application of Theorem III.4 into this case deduces that

$$\frac{1}{2}\frac{\mathrm{d}}{\mathrm{d}t}\int_\Omega \widetilde{\omega}^2 \,\mathrm{d}\Omega = -\frac{1}{R}\int_\Omega |\nabla\widetilde{\omega}|^2 \,\mathrm{d}\Omega < 0, \text{ for } \widetilde{\omega} \neq 0. \tag{3.52}$$

(3.52) implies that under wall condition (3.51), any given initial finite-amplitude perturbation of the viscous planar Poiseuille flow must decay with respect to time. For an estimation on the decay rate, we introduce the following Poincaré inequality that is compatible with the streamwise periodic condition on $\widetilde{\omega}$ and $\widetilde{\omega} = 0$ at the walls [1]

$$\int_\Omega \widetilde{\omega}^2 \,\mathrm{d}\Omega \leq M \int_\Omega |\nabla\widetilde{\omega}|^2 \,\mathrm{d}\Omega, \tag{3.53}$$

where M is a positive constant depending upon the domain Ω. To be precise, the constant M is determined by the Rayleigh quotient

$$M := \left[\min_{\widetilde{\omega}} \frac{\int_\Omega |\nabla \widetilde{\omega}|^2 \, \mathrm{d}\Omega}{\int_\Omega \widetilde{\omega}^2 \, \mathrm{d}\Omega} \right]^{-1}, \tag{3.54}$$

in which the minimization process is taken over all perturbation fields $\widetilde{\omega}$ that are admissible with the boundary conditions. By using (3.53), we find an upper bound for the right-hand side of (3.52) to be

$$\frac{\mathrm{d}\widetilde{\mathscr{W}}}{\mathrm{d}t} \leq -\frac{2}{MR}\widetilde{\mathscr{W}}, \tag{3.55}$$

where $\widetilde{\mathscr{W}}(t) := \frac{1}{2}\int_\Omega [\widetilde{\omega}(x,y,t)]^2 \, \mathrm{d}\Omega$. It yields the following analytical estimation on the upper bound for the decay of the perturbation's enstrophy $\widetilde{\mathscr{W}}$

$$\widetilde{\mathscr{W}}(t) \leq \widetilde{\mathscr{W}}(0) e^{-2t/(MR)}, \text{ for all times } t \geq 0. \tag{3.56}$$

We have therefore established global nonlinear stability for the flow.

The wall condition $\left(\widetilde{v}, \frac{\partial \widetilde{u}}{\partial y}\right) = (0,0)$ (*i.e.* $\widetilde{\omega} = 0$) is commonly referred to as the free-slip condition. [47] reviewed and studied the role of wall boundary conditions on stability of strictly parallel shear flows, and found that flows are linearly stable under the free-slip condition.

We would like to remark that the disturbance's vorticity $\widetilde{\omega}$ at the walls are generally unknown for other wall boundary conditions, in particular, for the no-slip wall condition. Thus, additional constraints on the disturbance fields are in general necessary to enable an estimate of the boundary term in (3.34). Fraternale *el al* [17] conducted a study on viscous planar Poiseuille flow and viscous planar Couette flow with the no-slip wall condition imposed for both flows, through the incorporation of a variational constraint, improved linear stability bounds were deduced for both flows.

An implementation of the proposed boundary conditions in Theorem III.4 may lead to effective flow control methodologies, we shall present a control scheme in §3.6.2 that transitions the wall settings from the no-slip condition to the free-slip condition.

3.6 Preliminary interpretation of linear instability/stability and wall boundary vorticity control for viscous plane Poiseuille flow

In the next two subsections, we investigate distributions of perturbation's enstrophy at/in-between the walls within the classical normal modal framework. The investigation includes a variety of flow parameters and wall conditions, aimed to acquire more quantitative understanding about the production/dissipation mechanisms of the perturbation's enstrophy. The viscous planar Poiseuille flow is selected to be the base state for our investigation. The no-slip wall condition is imposed throughout §3.6.1, followed by a flow control scheme that transitions the no-slip condition to the free-slip condition in §3.6.2.

The modal analysis presented in this section is new, they give rise to the first set of enstrophy-based perspectives on stability and instability for plane parallel shear flows. The modal analysis is based on the perturbation's enstrophy identity (3.34) under various boundary conditions allowed by Theorem III.4.

The framework established in this section will be applied to investigate the instability mechanism of the Couette flow subject to asymptotic suction rates in the next Chapter.

3.6.1 Interpretation of linear instability/stability under the no-slip wall condition

For classical normal-mode analysis, we propose perturbations to be of the following form

$$\begin{pmatrix} \widetilde{\psi} \\ \widetilde{u} \\ \widetilde{v} \\ \widetilde{\omega} \end{pmatrix} = \begin{pmatrix} \phi(y) \\ \widehat{u}(y) \\ \widehat{v}(y) \\ \widehat{\omega}(y) \end{pmatrix} \exp[i\alpha(x-ct)], \text{ with } \begin{pmatrix} \widehat{u} \\ \widehat{v} \\ \widehat{\omega} \end{pmatrix} = \begin{pmatrix} \phi' \\ -i\alpha\phi \\ \alpha^2\phi - \phi'' \end{pmatrix}, \tag{3.57}$$

in which α denotes a (positive) spatial wave number of perturbations and c denotes the complex phase velocity ($c := c_r + ic_i,\ i^2 = -1$), respectively.

Substituting (3.57) into the linearized equation (3.36) with $V \to 0$ and U_l replaced by U_0 to obtain the standard Orr-Sommerfeld stability equation

$$(i\alpha R)^{-1}(\mathscr{D}^2 - \alpha^2)^2\phi = (U_0 - c)(\mathscr{D}^2 - \alpha^2)\phi - U_0''\phi, \tag{3.58}$$

in which $\mathscr{D} := \frac{\mathrm{d}}{\mathrm{d}y}$, and with the no-slip wall condition

$$\widehat{u}(\pm 1) = 0 = \widehat{v}(\pm 1). \tag{3.59}$$

The growth rate of perturbations is hence computed from (3.34) to be

$$c_i = \frac{1}{\alpha R}\left(\int_{-L}^{L}\left[\mathrm{Real}(\widetilde{\omega})\frac{\partial \mathrm{Real}(\widetilde{\omega})}{\partial y}\right]_{y=-1}^{y=1}\mathrm{d}x - \int_{\Omega}|\nabla \mathrm{Real}(\widetilde{\omega})|^2\,\mathrm{d}\Omega\right) \Big/ \int_{\Omega}\mathrm{Real}(\widetilde{\omega})^2\,\mathrm{d}\Omega, \tag{3.60}$$

where $\mathrm{Real}(\widetilde{\omega})$ stands for the real-valued part of $\widetilde{\omega}$.

By setting $L = \pi/\alpha$ and substituting the normal-mode decomposition (3.57) into

(3.60), we obtain the following expression for the growth rate

$$c_i = \frac{1}{2\alpha R}\frac{\left[\frac{\mathrm{d}}{\mathrm{d}y}|\widehat{\omega}|^2\right]_{y=-1}^{y=1}}{\int_{-1}^{1}|\widehat{\omega}|^2\ \mathrm{d}y} - \frac{1}{\alpha R}\frac{\int_{-1}^{1}|\widehat{\omega}'|^2+\alpha^2|\widehat{\omega}|^2\ \mathrm{d}y}{\int_{-1}^{1}|\widehat{\omega}|^2\ \mathrm{d}y} \tag{3.61}$$

$$=: [B_\omega(y)]_{y=-1}^{y=1} - \int_{-1}^{1} I_\omega(y)\ \mathrm{d}y \tag{3.61-1}$$

$$=: p_B - p_I. \tag{3.61-2}$$

Besides, the Reynolds-Orr kinetic energy equation [see (1.11) on p. 9 of 41] imposed under (3.59) gives rise to the following

$$c_i = -\frac{1}{\alpha}\frac{\int_\Omega 2y\mathrm{Real}(\widetilde{u})\mathrm{Real}(\widetilde{v})\ \mathrm{d}\Omega}{\int_\Omega \mathrm{Real}(\widetilde{u})^2+\mathrm{Real}(\widetilde{v})^2\ \mathrm{d}\Omega} - \frac{1}{\alpha R}\frac{\int_\Omega |\nabla\mathrm{Real}(\widetilde{u})|^2+|\nabla\mathrm{Real}(\widetilde{v})|^2\ \mathrm{d}\Omega}{\int_\Omega \mathrm{Real}(\widetilde{u})^2+\mathrm{Real}(\widetilde{v})^2\ \mathrm{d}\Omega} \tag{3.62}$$

$$= -\frac{1}{\alpha}\frac{\int_{-1}^{1} y\left(\widehat{u}\overline{\widehat{v}}+\overline{\widehat{u}}\widehat{v}\right)\ \mathrm{d}y}{\int_{-1}^{1}|\widehat{u}|^2+|\widehat{v}|^2\ \mathrm{d}y} - \frac{1}{\alpha R}\frac{\int_{-1}^{1}|\widehat{u}'|^2+|\widehat{v}'|^2+\alpha^2\left(|\widehat{u}|^2+|\widehat{v}|^2\right)\ \mathrm{d}y}{\int_{-1}^{1}|\widehat{u}|^2+|\widehat{v}|^2\ \mathrm{d}y} \tag{3.62-1}$$

$$=: \int_{-1}^{1} S_{RO}(y)\ \mathrm{d}y - \int_{-1}^{1} D_{RO}(y)\ \mathrm{d}y \tag{3.62-2}$$

$$=: S - D. \tag{3.62-3}$$

Observe that $p_I > 0$ and $D > 0$ in all circumstances. Thus, p_B and S are the only constituents of c_i that may contribute to instability. Noticing that B_ω is an odd function over $y \in [-1, 1]$, while functions I_ω, S_{RO}, and D_{RO} are all even. It is thus sufficient to restrict our attention to be over $y \in [0, 1]$ when we display these functions. However, we refer actual physical quantities to the ones with respect to $y \in [-1, 1]$.

We set $U_0(y) = 1 - y^2$ in (3.58) which is solved numerically by using the standard Chebyshev collocation technique [7] in the spanwise direction under the no-slip wall boundary condition (3.59). We started with input parameters $\alpha = 1$ and $R = 10\ 000$, and the first 50 largest growth rates are reconfirmed by corresponding results com-

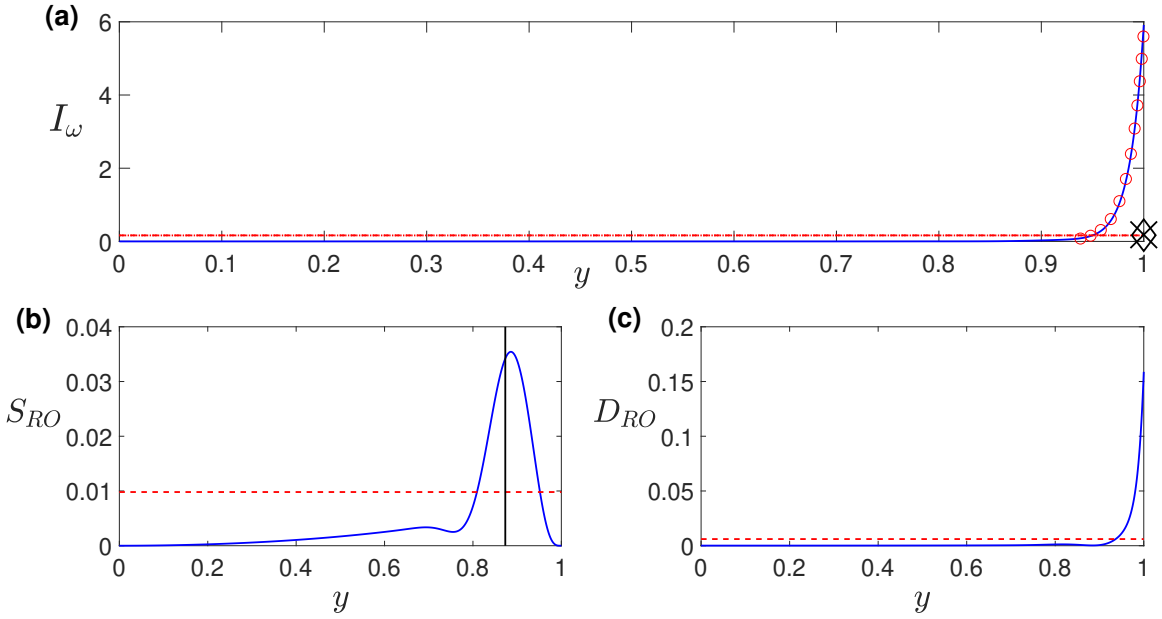

Figure 3.5: Production and damping of perturbation's enstrophy and kinetic energy for the unstable mode of the viscous planar Poiseuille flow under $\alpha = 1, R = 10\ 000$ with $c = 0.2375 + 0.0037i$: (a) The solid curve represents the vorticity damping function I_ω over $0 \le y \le 1$, the dashed horizontal line represents the integral of I_ω over $-1 \le y \le 1$, which is equal to $p_I = 0.1657$, and the diamond at $y = 1$ stands for the vorticity production quantity $p_B = 0.1694$. In addition, the circles represent $I_{\omega_{bl}}$ due to the boundary layer solution (3.64) at a vicinity of $y = 1$, the dotted horizontal line represents the vorticity damping resultant near $y = \pm 1$, namely $p_I^* = 0.1640$, and the cross label at $y = 1$ stands for the vorticity production quantity due to wall boundary layers near $y = \pm 1$, namely $p_{B_{bl}} = 0.1820$; (b) The solid curve represents the Reynolds stress function $S_{RO}(y)$ over $0 \le y \le 1$, the dashed horizontal line represents the integral of S_{RO} over $-1 \le y \le 1$, which is equal to $S = 0.0098$, and the solid vertical line stands for the critical point $y_c = \sqrt{1 - c_r} = 0.8732$; (c) The solid curve represents the kinetic energy damping function $D_{RO}(y)$ over $0 \le y \le 1$, the dashed horizontal line represents the integral of D_{RO} over $-1 \le y \le 1$, which is equal to $D = 0.0061$.

puted by Orszag [36]. Following discussions are based on two pre-selected modes, with the first being unstable and the second being stable, related plots are presented in Figure 3.5 and Figure 3.7, respectively.

The unique unstable mode has its associated $c = 0.2375 + 0.0037i$. As shown in Figure 3.5(a), that the vorticity production term B_ω at the walls gives rise to $p_B = 0.1694$ (the diamond label). Besides, the damping of perturbation's vorticity is primarily sustained within a neighbourhood of $y = \pm 1$, with an accumulated value $p_I = 0.1657$ (the dashed line). The overall contribution of the perturbation's vorticity is measured by $c_i = p_B - p_I = 0.0037$, which is only a small portion of p_B. Specifically, we find that $c_i/p_B \approx 2.18\%$.

Identity (3.61) and Figure 3.5(a) suggest an interconnection between values of p_B and p_I for this unstable mode. That is, p_B is strongly related to the gradient of perturbation's vorticity across the walls, which in turn quantifies the steepness of the vorticity damping function I_ω (the solid curve) at a vicinity of $y = \pm 1$, and hence it affects the area under the I_ω curve near the walls, namely the value of p_I. Such interconnection between p_B and p_I near the wall boundaries explains the small difference in their magnitudes. Moreover, it infers that the wall boundary layer effect had played a predominant role for sustaining the growth of the mode.

To validate our hypothesis regarding the wall boundary layer effect, we define

$$p_I^* := \int\limits_{\pm[0.9,1]} I_\omega(y)\ \mathrm{d}y. \tag{3.63}$$

Besides, we adopt the following wall boundary layer solution that holds for a vicinity of $y = \pm 1$ [see (27.5) on p. 167 of 13]

$$\phi_{bl}(y) \sim \exp\left[(\pm y - 1)\sqrt{\alpha Rc}\ e^{-\frac{\pi i}{4}}\right],\ y \sim \pm 1 \tag{3.64}$$

and denote its associated quantities by the aforementioned symbols with a subscript

bl.

The $I_{\omega_{bl}}$ function is shown in Figure 3.5(a) as circles over $y \in [0.9, 1]$, from which we observe an evident agreement between I_ω and $I_{\omega_{bl}}$. Moreover, the value $p_I^* = 0.1640$ (the dotted line) is close to the value $p_I = 0.1657$ (the dashed line), and the value $p_{B_{bl}} = 0.1820$ (the cross label) is close to the value $p_B = 0.1694$ (the diamond label). The growth of the mode is thus predominantly sustained by the wall boundary layer.

Figure 3.5(b) represents the contribution to the growth rate due to the Reynolds stress function S_{RO} that appears in (3.62-2). It exhibits two contrasting features in comparison to the vorticity based quantity B_ω. First, the shape of the S_{RO} function indicates that the production of the perturbation's kinetic energy is spread out over the entire range of the fluid domain, with its peak value reached slightly to the right of the critical layer $y_c = \sqrt{1 - c_r} = 0.8732$ (the solid vertical line). This observation was also made by Drazin [see 13, p. 223]. Secondly, there is zero energy production at the wall boundary. The overall energy production is quantified by the area under the S_{RO} curve, which is $S = 0.0098$ (the dashed line). On the other hand, as shown by Figure 3.5(c), that the energy damping function D_{RO} demonstrates a similar trend to that of the vorticity damping function I_ω, with an integrated value $D = 0.0061$ (the dashed line).

As a validation of the observations made above for an unstable mode, we selected ten further unstable modes with R ranges from 5772 (the critical Reynolds number corresponding to the onset of linear instability) to 10 000. These modes are located halfway through the stability boundaries in the (α, R) plane, as shown by the dots in Figure 3.6. The stability parameters associated with these modes are presented in Table 1.

To demonstrate the stability mechanism for this flow, we consider another symmetric (even) mode under the same set of parameters but $c = 0.5129 - 0.2866i$. The corresponding plots are shown in Figure 3.7, with the critical point $y_c = 0.6979$ shown

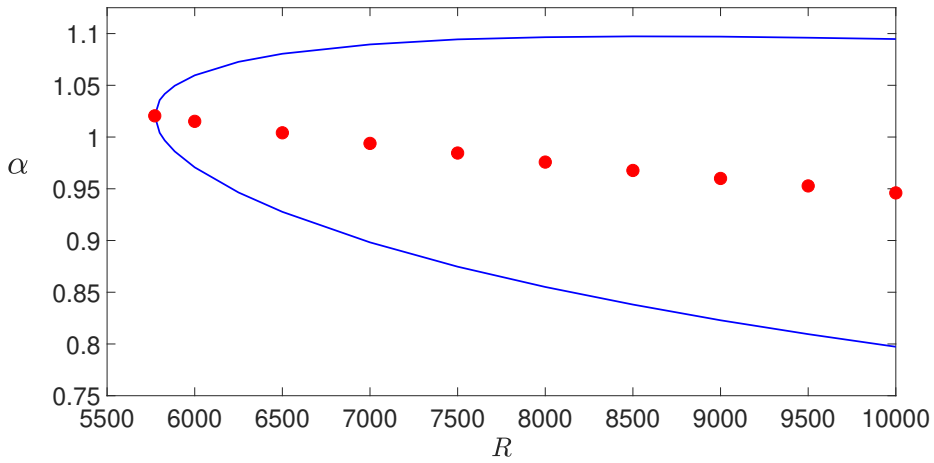

Figure 3.6: Marginal linear stability boundary (the solid curve) of the planar Poiseuille flow. The region enclosed by the stability boundary consists of unstable modes.

as a solid vertical line in each plot. It is evident that the Reynolds stress S_{RO} and the energy damping function D_{RO} are both almost symmetrically distributed around the critical point, so is the vorticity damping function I_ω. The corresponding integrated quantities are $p_I = 0.2866, S = -0.0289$, and $D = 0.2578$, respectively (dashed lines).

The vorticity production quantities of this mode are $p_B = -1.014 \times 10^{-7}$ (the diamond label) and $p_{B_{bl}} = -1.109 \times 10^{-7}$ (the cross label), which are both negligible, it hence exhibits little vorticity production at the walls. Besides, the vorticity damping function I_ω is accumulated over the subinterval $[0.48, 0.9]$, outside which the value of I_ω is relatively negligible, this indicates that there is also little damping of the perturbation's vorticity at a vicinity of $y = \pm 1$. These phenomena are consistent with the aforementioned interconnection between p_B and the portion of p_I near the walls.

Similar observations were made through carefully examining other stable symmetric modes under the same set of prescribed parameters, see a summary of these modes in form of Figure 3.8. Specifically, we observe in those stable modes that the damping of vorticity are all accumulated at a neighbourhood of their corresponding critical points away from the boundary layers, and there is considerably less vortic-

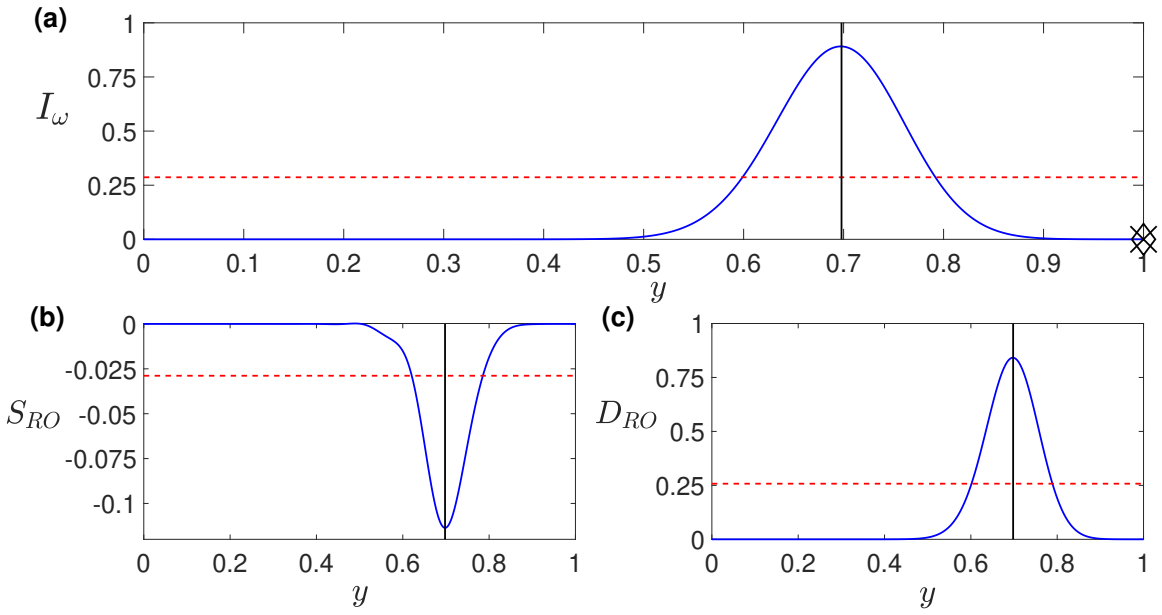

Figure 3.7: Production and damping of perturbation's enstrophy and kinetic energy for the stable symmetric mode of the viscous planar Poiseuille flow under $\alpha = 1, R = 10\ 000$ with $c = 0.5129 - 0.2866i$. In all plots, the solid vertical line stands for the critical point $y_c = 0.6979$: (a) The solid curve represents the vorticity damping function I_ω over $0 \leq y \leq 1$, the dashed horizontal line represents the integral of I_ω over $-1 \leq y \leq 1$, which is equal to $p_I = 0.2866$, the diamond at $y = 1$ stands for the vorticity production quantity $p_B = -1.014 \times 10^{-7}$, and the cross label at $y = 1$ stands for the vorticity production quantity due to wall boundary layers, namely $p_{B_{bl}} = -1.109 \times 10^{-7}$; (b) The solid curve represents the Reynolds stress function S_{RO} over $0 \leq y \leq 1$, the dashed horizontal line represents the integral of S_{RO} over $-1 \leq y \leq 1$, namely $S = -0.0289$; (c) The solid curve represents the kinetic energy damping function $D_{RO}(y)$ over $0 \leq y \leq 1$, the dashed horizontal line represents the integral of D_{RO} over $-1 \leq y \leq 1$, namely $D = 0.2578$.

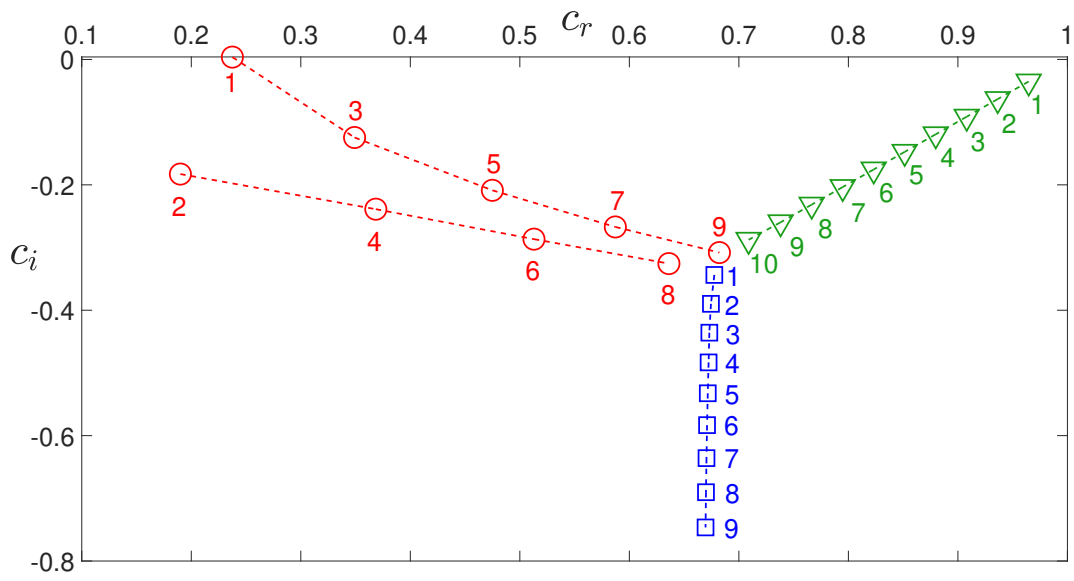

Figure 3.8: Distribution of eigenvalues of symmetric modes for viscous planar Poiseuille flow at $\alpha = 1$ and $R = 10\,000$. The circles, wedges and squares stand for modes of the A family, P family and S family, respectively (notations adopted by Mack [33]).

ity production at the walls. These are different from the observations made for the boundary layer dominant case, where production and damping of vorticity both sustain with similar magnitudes within the boundary layer. In other words, from the perspective of vorticity, a sufficiently strong wall boundary layer effect is necessary for the onset of instability.

Remark: Above study on shear flow stability was based on (3.34) establised under the no-slip wall boundary condition. This preliminary study provides a different view from the one based on the classical Reynolds-Orr kinetic energy equation. In particular, the current approach has its root in the vorticity motion of the flow. As it was remarked by Küchemann [29], that vortices are 'the sinews and muscles of fluid motion'. Indeed, by pursuing the 'sinews', one would be able to ascribe precisely the unique production source of perturbation's enstrophy to the walls, over which the flow is rubbed due to the enforced no-slip wall boundary condition.

It is evident that the internal flow always makes a direct contribution to the perturbation's enstrophy only as a damping constituent, which was quantified by the

term $-p_I$ in (3.61-2). Specifically, the critical layer is a primary source of damping in perturbation's enstrophy at high Reynolds numbers. The relatively large magnitude of the damping source at high Reynolds numbers is a consequence of the singularity that forms at the critical layer in the inviscid limit of the flow.

In summary, the current study shows a natural interconnection between viscous and inviscid flow stability mechanisms for non-inflectional shear flows. The viscous and inviscid stability mechanisms are hence two sides of the same coin. Besides, formulations based on enstrophy and kinetic energy tell different faces of the same physical reality, they enrich and complement each other.

3.6.2 A control scheme on wall boundary's vorticity for viscous plane Poiseuille flow

Recall from Example III.5 that the wall condition $(\widetilde{u}, \widetilde{\omega}) = (0, 0)$ would imply global nonlinear stability for the base planar Poiseuille flow. It is also clear that the same is true under the free-slip wall condition, namely $(\widetilde{v}, \widetilde{\omega}) = (0, 0)$.

We propose the following wall boundary control scheme, in which $l_s \in [0, 1]$ is the control parameter

$$\begin{cases} \widehat{v}(\pm 1) = 0, \\ (1 - l_s)\widehat{u}(\pm 1) \mp l_s \widehat{\omega}(\pm 1) = 0. \end{cases} \tag{3.65}$$

This control scheme can be regarded as an extension (or a relaxation) of the free-slip wall condition $(\widetilde{v}, \widetilde{\omega}) = (0, 0)$ that corresponds to the special case when $l_s = 1$. On the other hand, the case with $l_s = 0$ corresponds to the uncontrolled unstable base flow under the no-slip wall condition. The control scheme is aimed to seek an intermediate value of the control parameter for which the base Poiseuille flow under wall conditions (3.65) becomes stable. Note that for each l_s, the vorticity wall condition in (3.65) can be realized by matching the velocity $\widetilde{u}(x, \pm 1, t)$ (e.g. through an actuator in

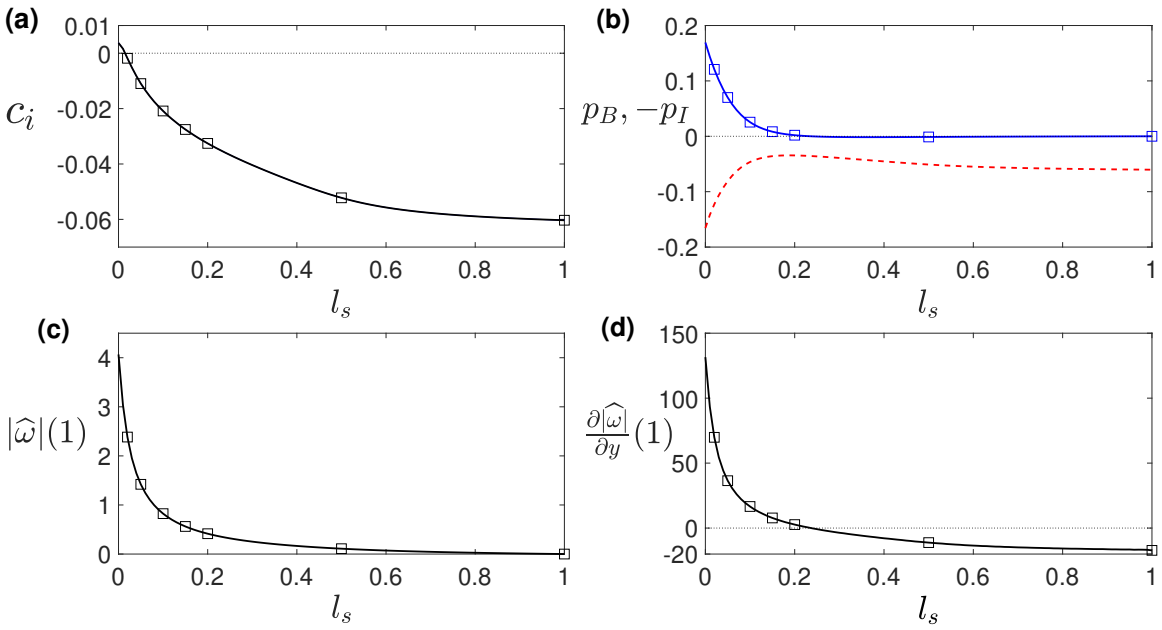

Figure 3.9: The largest growth rate c_i and its constituents as functions of the control parameter l_s for the viscous planar Poiseuille flow at $\alpha = 1, R = 10\ 000$. Pre-selected points for further display are marked by squares, and the horizontal dotted lines are the zero reference lines: (a) Growth rate c_i as a function of l_s; (b) The two constituents p_B (solid curve) and $-p_I$ (dashed curve) as functions of l_s based on (3.61); (c) The modulus of $\widehat{\omega}$ at $y = 1$ as a function of l_s; (d) The normal derivative of $|\widehat{\omega}|$ at $y = 1$ as a function of l_s.

engineering practice) according to the instantly measured $\frac{\partial \widetilde{u}}{\partial y}$ $(= -\widetilde{\omega})$.

To further understand the qualitative behavior of the control scheme, we conduct a linear stability analysis of the base Poiseuille flow under wall conditions (3.65).

Noticing that in accordance with Theorem III.2 (in the limit as $V \to 0$) or Theorem III.4, the vorticity based identity (3.61) is still valid under proposed wall boundary conditions due to $\widetilde{v} = 0$ at the walls, but the Reynolds-Orr kinetic energy equation (3.62) is no longer valid for $l_s \neq 0$.

As a test for above wall vorticity control scheme, we consider the viscous planar Poiseuille flow studied in §3.6.1 with $\alpha = 1, R = 10\ 000$. Equation (3.58) imposed under (3.65) is numerically solved for $0 \leq l_s \leq 1$ by using the standard Chebyshev collocation method [7]. Note that we are looking for the mode corresponding to

the largest growth rate for each l_s. Results are summarized in Figure 3.9. Figure 3.9(a) shows that the growth rate c_i (the solid curve) monotonically decreases as l_s increases, and the flow is stabilized at $l_s = 1.481\%$. Such rapid decreasing trend of c_i with respect to l_s indicates that stability of the flow is sensitive to the proposed control scheme. Besides, the successively added vorticity component in (3.65), namely $\mp l_s \widehat{\omega}''(\pm 1)$, would always shift the flow into a more stable state.

To further illustrate the change in flow stability with respect to the control parameter, we present in Figure 3.9(b) the constituents p_B and p_I of the growth rate as a function of l_s. Clearly, that the constituent p_B (the solid curve) strictly decreases over $0 \leq l_s \leq 20\%$, with zero reached at about $l_s = 20\%$, thereafter it remains to be approximately a constant that is slightly below zero until l_s reaches 100%. Moreover, Figure 3.9(c) and 3.9(d) indicate that a decrease in the wall boundary's vorticity would also lead to a decrease in its normal derivative across the walls. However, it is evident that the magnitude of $\widehat{\omega}(1)$ is always much less than that of $\frac{\partial \widehat{\omega}}{\partial y}(1)$ at each given l_s. Thus, the test suggests that instability of the flow is primarily restrained by the amount of perturbation's vorticity at the walls, namely $\widehat{\omega}(\pm 1)$ itself, but not its normal derivative across the walls.

3.7 Discussion

A viscous extension of Arnold's theory on planar non-inflectional shear flows was developed. The extension in form of the viscous Arnold's identity (Theorem III.1) complements Arnold's stability theory on inviscid shear flows subject to arbitrary two-dimensional perturbations. The viscous Arnold's identity contains viscous terms only, it led to a number of perturbation's enstrophy identities that are valid for a variety of flow motions under various wall boundary conditions.

As a first application of our viscous Arnold's identity, we found an alternative derivation of the classical perturbation's enstrophy identity under linear dynamics

that was established earlier by Synge [44] and Fraternale *el* [17]. The enstrophy identity consists of a boundary component at the walls and a damping component in the fluid bulk, with the presence of viscosity in both components being a feature that is consistent with our viscous Arnold's identity.

We had established a new weighted perturbation's enstrophy identity in form of Theorem III.2 based on the viscous Arnold's identity, which is valid for non-inflectional streamwise translation-invariant base laminar states under linear dynamics. The weighted identity holds under two classes of relaxed wall boundary conditions.

We showed that the perturbation's enstrophy identity for strictly parallel base states is preserved under global nonlinear dynamics, this is a direct consequence of the fully nonlinear viscous Arnold's identity. Furthermore, we examined the validity of the perturbation's enstrophy identity under more general wall boundary conditions than the no-slip condition. The results are summarized as Theorem III.4.

As a case study, the enstrophy identity under global nonlinear dynamics imposed with the free-slip (zero disturbance's vorticity) wall condition was applied to viscous plane Poiseuille flow, thereby it rigorously deduced unconditional global stability for the flow. The corresponding decay rate of a vorticity disturbance was estimated through Example III.5. The case study illustrates a novel stabilization mechanism that inhibits the growth of any two-dimensional disturbance, implementation of the mechanism may lead to effective flow control methodologies.

To explore physical mechanisms of linear instability/stability from the perspective of enstrophy, we carried out a preliminary study in §4 for the viscous planar Poiseuille flow. Distributions of disturbance's enstrophy at/in-between the walls were investigated within the classical normal modal framework. We found that the critical layer is always a direct source of damping in disturbance's enstrophy for all cases computed.

We observed a subtle interaction between a critical layer and its adjacent boundary

layer, which determines the stability nature of a shear flow. We would like to remark that the underlying inviscid mechanism also plays a role in the interaction between the two layers, although it is not explicitly included the viscous enstrophy identity.

As an implementation of those relaxed wall conditions imposed for the enstrophy identity, we proposed a control scheme on wall boundary's vorticity disturbance. The control scheme transitions wall settings from the no-slip condition to the free-slip condition. The linearly unstable viscous planar Poiseuille flow originally imposed under the no-slip wall condition becomes stabilized after addition of about 2% of the free-slip wall effect.

It should be remarked that the current study is limited to two-dimensional disturbances. On the other hand, it is well known, that flow three-dimensionality can develop in two-dimensional boundary layers relatively fast [see 26]. Thus, a three-dimensional disturbance may cause a linearly stable (against two-dimensional disturbances) laminar boundary layer to undergo an intricate transition into a turbulent state. The effectiveness of the control method proposed in the current study, therefore, must be re-assessed in future studies for cases where three-dimensional disturbances arise.

CHAPTER IV

Viscous extension of Arnold's non-viscous stability theory for shear flows with suction

In this section and the next, we consider a layer of two-dimensional incompressible (unit density) Newtonian fluid with kinematic viscosity ν confined between parallel rigid plates separated by distance h. The velocity vector field is $\mathbf{u}^* = u^*\mathbf{i} + v^*\mathbf{j}$ where **i, j** are the unit vectors in the x^* and y^* directions, respectively. We confine the fluid domain to be over the streamwise periodic cell $(x^*, y^*) \in [-L_x, L_x] \times \left[-\frac{h}{2}, \frac{h}{2}\right]$ with half-period L_x.

We impose an arbitrary translation-invariant base laminar state in the form $U_l^*(y^*)\mathbf{i} - V^*\mathbf{j}$, for which fluid is uniformly injected into the layer with speed V^* at the top plate and uniformly removed at the bottom plate. Assume that U_l^* is a smooth profile with $U_l^{*''}(y^*) \neq 0$ for $y^* \in \left(-\frac{h}{2}, \frac{h}{2}\right)$, denote

$$U^* := \max_{y_1^*, y_2^* \in \left[-\frac{h}{2}, \frac{h}{2}\right]} |U_l^*(y_1^*) - U_l^*(y_2^*)|. \tag{4.1}$$

Unless otherwise stated, we enforce the no-slip condition to $\mathbf{u}^*$ with respect to the base laminar solution at each wall, as illustrated in Figure 4.1.

Introducing following dimensionless quantities, in which t^*, p^*, Re, θ are the dimensional time, dimensional pressure normalized by the constant density of the fluid,

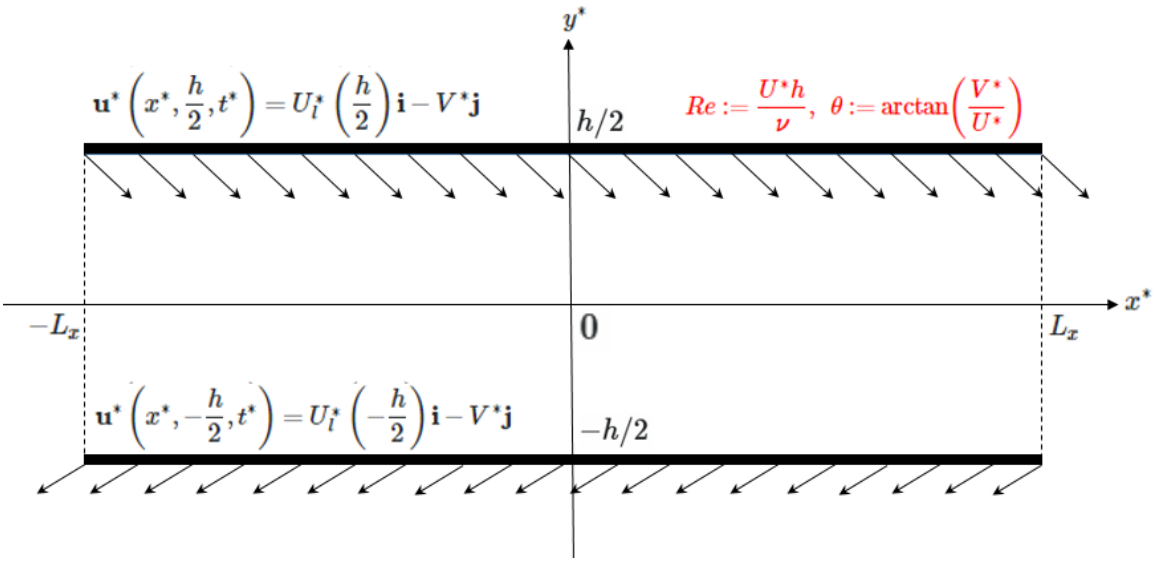

Figure 4.1: Sketch of boundaries and boundary conditions for flows under consideration.

Reynolds number and angle of injection, respectively.

$$\mathbf{u} := \frac{1}{U^*}\mathbf{u}^*,\ (x, y, L) := \frac{1}{h}(x^*, y^*, L_x),\ t := \frac{U^*}{h}t^*,\ p := \frac{p^*}{U^{*2}},\ Re := \frac{U^* h}{\nu},\ \tan\theta := \frac{V^*}{U^*}. \tag{4.2}$$

The fluid motion over $(x, y) \in \Omega := [-L, L] \times \left[-\frac{1}{2}, \frac{1}{2}\right]$ is governed by Navier-Stokes equations

$$\begin{cases} \frac{\partial \mathbf{u}}{\partial t} + \mathbf{u} \cdot \nabla \mathbf{u} + \nabla p = \frac{1}{Re}\nabla^2 \mathbf{u}, \\ \nabla \cdot \mathbf{u} = 0, \end{cases} \tag{4.3}$$

under wall boundary conditions

$$\mathbf{u} = U_l\left(\pm\frac{1}{2}\right)\mathbf{i} - \tan\theta\mathbf{j} \text{ at } y = \pm\frac{1}{2}. \tag{4.4}$$

Let p_l denote the pressure field associated with the base laminar state $U_l(y)\mathbf{i} - \tan\theta\mathbf{j}$, equations (4.3) imply that $\frac{\partial p_l}{\partial y} = 0$. A solution $\mathbf{u}$ of (4.3) can be expressed as

$$\mathbf{u} = [U_l(y) + \widetilde{u}(x, y, t)]\,\mathbf{i} + [-\tan\theta + \widetilde{v}(x, y, t)]\,\mathbf{j},\ p = p_l(x) + \widetilde{p}(x, y, t), \tag{4.5}$$

in which $(\widetilde{u}, \widetilde{v}, \widetilde{p})$ are the perturbation fields. (4.4) and (4.5) imply

$$(\widetilde{u}, \widetilde{v}) = (0, 0) \text{ at } y = \pm\frac{1}{2}. \tag{4.6}$$

For a vorticity form of (4.3), we introduce a stream function $\psi(x, y)$ such that $u = \frac{\partial \psi}{\partial y}$ and $v = -\frac{\partial \psi}{\partial x}$, the corresponding vorticity is $\omega := \frac{\partial v}{\partial x} - \frac{\partial u}{\partial y} = -\nabla^2 \psi$. The vorticity formulation of (4.3) is hence

$$\frac{\partial \omega}{\partial t} + \{\psi, \omega\} = \frac{1}{Re}\nabla^2 \omega, \tag{4.7}$$

in which $\{\psi, \omega\} := \frac{\partial \psi}{\partial y}\frac{\partial \omega}{\partial x} - \frac{\partial \psi}{\partial x}\frac{\partial \omega}{\partial y}$.

Let $\psi_l(x, y)$ be the stream function associated with the base laminar state $U_l(y)\mathbf{i} - V\mathbf{j}$ and let $\omega_l(y) := -U_l'(y)$, it follows from (4.7) that

$$\tan\theta \omega_l' + \frac{1}{Re}\omega_l'' = 0, \tag{4.8}$$

which further implies

$$\omega_l' \omega_l''' = \omega_l''^2. \tag{4.9}$$

A solution (ψ, ω) of (4.7) can be expressed as

$$\psi = \psi_l(x, y) + \widetilde{\psi}(x, y, t),\ \omega = \omega_l(y) + \widetilde{\omega}(x, y, t). \tag{4.10}$$

Following wall boundary conditions on $\widetilde{\psi}$ are consistent with (4.6)

$$\left(\widetilde{\psi}, \frac{\partial \widetilde{\psi}}{\partial y}\right) = (0, 0) \text{ at } y = \pm\frac{1}{2}. \tag{4.11}$$

The streamwise periodic condition applies to $\widetilde{u}, \widetilde{v}$ and $\widetilde{\psi}$ throughout this study.

4.1 Viscous extension of Arnold's inviscid theory

We now extend the nonlinear stability criterion of [2] on inviscid planar shear flows to a viscous base laminar flow of the form $U_l(y)\mathbf{i} - \tan\theta\mathbf{j}$. We assume without loss of generality that $\omega_l' = -U_l'' > 0$ throughout this study, note that this restricts U_l to be non-inflectional. The extension closely follows the procedure established by [30] for viscous strictly parallel shear flows, with additional aspects highlighted in present study due to the suction component.

Denoting the total kinetic energy of a flow field $\mathbf{u}$ as $\mathcal{E} := \frac{1}{2}\int_\Omega \mathbf{u}\cdot\mathbf{u}\ \mathrm{d}\Omega$, the kinetic energy of the laminar state $U_l(y)\mathbf{i} - \tan\theta\mathbf{j}$ is thus $\mathcal{E}_l := \frac{1}{2}\int_\Omega U_l^2 + \tan^2\theta\ \mathrm{d}\Omega$. Let $\widetilde{\mathcal{E}} := \mathcal{E} - \mathcal{E}_l$. We define an associated Casimir function to be $\mathcal{C}_s := \int_\Omega F(\omega)\ \mathrm{d}\Omega$, where F is an arbitrary real-valued smooth function. In particular, let $\mathcal{C}_{sl} := \int_\Omega F(\omega_l)\ \mathrm{d}\Omega$ and $\widetilde{\mathcal{C}}_s := \mathcal{C}_s - \mathcal{C}_{sl}$.

The first step of the extension procedure is to select an F function that makes $\widetilde{\mathcal{E}} + \widetilde{\mathcal{C}}_s$ a positive-definite quadratic form for which to be used as a norm in stability analysis. In accordance with (4.5) and (4.6) to obtain

$$\widetilde{\mathcal{E}} = \int_\Omega \frac{\widetilde{u}^2 + \widetilde{v}^2}{2} + U_l\widetilde{u} - \tan\theta\widetilde{v}\ \mathrm{d}\Omega. \tag{4.12}$$

On the other hand, the Taylor expansion of F about ω_l with a second-order remainder reads

$$F(\omega) = F(\omega_l + \widetilde{\omega}) = F(\omega_l) + F'(\omega_l)\widetilde{\omega} + F''(\omega_l + \eta\widetilde{\omega})\frac{\widetilde{\omega}^2}{2} \text{ for some } \eta \in (0,1), \tag{4.13}$$

this implies that

$$\widetilde{\mathcal{C}}_s = \int_\Omega F'(\omega_l)\widetilde{\omega} + F''(\omega_l + \eta\widetilde{\omega})\frac{\widetilde{\omega}^2}{2}\ \mathrm{d}\Omega. \tag{4.14}$$

We need to select an F with $F'' > 0$, under which first-order perturbation terms

in $\widetilde{\mathcal{E}} + \widetilde{\mathcal{C}_s}$ cancel each other out. The sum of first-order terms in $\widetilde{\mathcal{E}} + \widetilde{\mathcal{C}_s}$ reads

$$\begin{aligned}\int_\Omega F'(\omega_l)\widetilde{\omega} + U_l\widetilde{u} - \tan\theta\widetilde{v}\ \mathrm{d}\Omega &= \int_\Omega F'(\omega_l)\left(\frac{\partial\widetilde{v}}{\partial x} - \frac{\partial\widetilde{u}}{\partial y}\right) + U_l\widetilde{u} + \tan\theta\frac{\partial\widetilde{\psi}}{\partial x}\ \mathrm{d}\Omega \\ &= \int_\Omega -F'(\omega_l)\frac{\partial\widetilde{u}}{\partial y} + U_l\widetilde{u}\ \mathrm{d}\Omega \\ &= \int_\Omega \left[F''(\omega_l)\omega_l' + U_l\right]\widetilde{u}\ \mathrm{d}\Omega. \end{aligned} \tag{4.15}$$

Based on (4.15), F needs to be defined according to $F''(\omega_l)\omega_l' + U_l = 0$. We introduce an arbitrary constant velocity shift $\overline{U}$ that is to be added into the base laminar state's streamwise velocity profile U_l, with the observation that ω_l as well as all perturbation fields are preserved under such a shift. Therefrom, the function F depends on $\overline{U}$ and it fulfills

$$F''(\omega_l)\omega_l'(y) + U_l(y) + \overline{U} = 0. \tag{4.16}$$

The positivity of F'' can hence be ensured by a sufficiently negative $\overline{U}$.

The next step of the extension procedure is to verify the cancellation of first-order perturbation terms in the temporal derivative of $\widetilde{\mathcal{E}} + \widetilde{\mathcal{C}_s}$, which needs to hold for the same F defined by (4.16). We assume without loss of generality that $\overline{U} = 0$ throughout following derivations.

Using (4.3), (4.6), and following the derivation for (A2) in [30] to obtain the following, which has two first-order terms on its right-hand side.

$$\frac{\mathrm{d}\widetilde{\mathcal{E}}}{\mathrm{d}t} = -\frac{1}{Re}\int_\Omega |\nabla\widetilde{u}|^2 + |\nabla\widetilde{v}|^2\ \mathrm{d}\Omega + \int_\Omega U_l\frac{\partial\widetilde{p}}{\partial x}\ \mathrm{d}\Omega + \frac{1}{Re}\int_\Omega U_l\frac{\partial^2\widetilde{u}}{\partial y^2}\ \mathrm{d}\Omega + \tan\theta\int_\Omega U_l\frac{\partial\widetilde{u}}{\partial y}\ \mathrm{d}\Omega. \tag{4.17}$$

Using (4.7) and following the derivation for (A3) in [30] to obtain

$$\frac{\mathrm{d}\mathcal{C}_s}{\mathrm{d}t} = \frac{1}{Re}\int_{-L}^{L}\left[F'(\omega)\frac{\partial\omega}{\partial y}\right]_{y=-\frac{1}{2}}^{y=\frac{1}{2}}\mathrm{d}x - \frac{1}{Re}\int_{\Omega}F''(\omega)|\nabla\omega|^2\ \mathrm{d}\Omega + \tan\theta\int_{-L}^{L}\left[F(\omega)\right]_{y=-\frac{1}{2}}^{y=\frac{1}{2}}\mathrm{d}x. \tag{4.18}$$

Through replacing the argument ω on right-hand side of (4.18) by $\omega_l + \lambda\widetilde{\omega}$, it defines a function in argument λ with ω_0 and $\widetilde{\omega}$ regarded as constant terms herein, we denote this function by $g_\theta(\lambda)$.

The Taylor expansion of $g_\theta(\lambda)$ centered at $\lambda = 0$ with increment 1 up to the second-order reads

$$g_\theta(1) = g_\theta(0) + g'_\theta(0) + \frac{1}{2}g''_\theta(\xi) \text{ for some } \xi \in (0,1), \tag{4.19}$$

Recall from (4.10) that $\omega = \omega_l + \widetilde{\omega}$, the definition of $g_\theta(\lambda)$ implies that $\frac{\mathrm{d}\widetilde{\mathcal{C}_s}}{\mathrm{d}t} = g_\theta(1) - g_\theta(0)$. Following the derivation for (A8) in [30] and applying (4.8) to obtain

$$\begin{aligned}
\frac{\mathrm{d}\widetilde{\mathcal{C}_s}}{\mathrm{d}t} \quad &= g_\theta(1) - g_\theta(0) = g'_\theta(0) + \frac{1}{2}g''_\theta(\xi) \\
&= -\frac{1}{Re}\int_{-L}^{L}\left[F'(\omega_l)\frac{\partial^2\widetilde{u}}{\partial y^2}\right]_{y=-\frac{1}{2}}^{y=\frac{1}{2}}\mathrm{d}x + \frac{1}{Re}\int_{\Omega}F''(\omega_l)\omega'_l\frac{\partial^2\widetilde{u}}{\partial y^2}\ \mathrm{d}\Omega \\
&\quad - \tan\theta\int_{-L}^{L}\left[F'(\omega_l)\frac{\partial\widetilde{u}}{\partial y}\right]_{y=-\frac{1}{2}}^{y=\frac{1}{2}}\mathrm{d}x + \tan\theta\int_{\Omega}F''(\omega_l)\omega'_l\frac{\partial\widetilde{u}}{\partial y}\ \mathrm{d}\Omega + \frac{1}{2}g''_\theta(\xi) \\
&= -\int_{\Omega}U_l\frac{\partial\widetilde{p}}{\partial x}\ \mathrm{d}\Omega - \frac{1}{Re}\int_{\Omega}U_l\frac{\partial^2\widetilde{u}}{\partial y^2}\ \mathrm{d}\Omega - \tan\theta\int_{\Omega}U_l\frac{\partial\widetilde{u}}{\partial y}\ \mathrm{d}\Omega + \frac{1}{2}g''_\theta(\xi).
\end{aligned} \tag{4.20}$$

Note that the last line of (4.20) is based upon (4.16) and the following relation

$$\left(-\tan\theta\frac{\partial\widetilde{u}}{\partial y} + \frac{\partial\widetilde{p}}{\partial x} - \frac{1}{Re}\frac{\partial^2\widetilde{u}}{\partial y^2}\right)\Bigg|_{y=\pm\frac{1}{2}} = 0. \tag{4.21}$$

It is clear that the first-order terms on right-hand side of of (4.20) are exactly the

opposite of those in (4.17). Therefore, first-order terms in the temporal derivative of $\widetilde{\mathcal{E}} + \widetilde{\mathcal{C}}_s$ indeed cancel each other out. Note that the sum of (4.17) and (4.20) is equal to the sum of the temporal derivatives of (4.12) and (4.14) under the F chosen according to (4.16). This establishes our first main result below.

Theorem IV.1. *(The viscous Arnold's identity with suction) The following identity is valid for a laminar non-inflectional shear flow $U_l(y)\boldsymbol{i} - \tan\theta\boldsymbol{j}$ under global nonlinear dynamics enforced by the no-slip wall condition (4.6)*

$$\frac{1}{2}\frac{\mathrm{d}}{\mathrm{d}t}\int\limits_{\Omega}\left[\widetilde{u}^2+\widetilde{v}^2+F''(\omega_l+\eta\widetilde{\omega})\widetilde{\omega}^2\right]\mathrm{d}\Omega = -\frac{1}{Re}\int\limits_{\Omega}|\nabla\widetilde{u}|^2+|\nabla\widetilde{v}|^2\ \mathrm{d}\Omega+\frac{1}{2}g''_\theta(\xi), \quad (4.22)$$

where F is a function that obeys (4.16) for a sufficiently negative constant $\overline{U}$ such that $F'' > 0$, and $\frac{1}{2}g''_\theta(\xi)$ is evaluated explicitly to be

$$\begin{aligned}\frac{1}{2}g''_\theta(\xi) = {}& \frac{1}{2Re}\int\limits_{-L}^{L}\left[F'''\left(\omega_l+\xi\widetilde{\omega}\right)\widetilde{\omega}^2\left(\omega_l'+\xi\frac{\partial\widetilde{\omega}}{\partial y}\right)+2F''\left(\omega_l+\xi\widetilde{\omega}\right)\widetilde{\omega}\frac{\partial\widetilde{\omega}}{\partial y}\right]_{y=-\frac{1}{2}}^{y=\frac{1}{2}}\mathrm{d}x\\ &-\frac{1}{2Re}\int\limits_{\Omega}\left\{F''''\left(\omega_l+\xi\widetilde{\omega}\right)\widetilde{\omega}^2\left|\nabla\left(\omega_l+\xi\widetilde{\omega}\right)\right|^2+4F'''\left(\omega_l+\xi\widetilde{\omega}\right)\widetilde{\omega}\left[\nabla\left(\omega_l+\xi\widetilde{\omega}\right)\cdot\nabla\widetilde{\omega}\right]\right.\\ &\left.+2F''\left(\omega_l+\xi\widetilde{\omega}\right)|\nabla\widetilde{\omega}|^2\right\}\mathrm{d}\Omega+\frac{\tan\theta}{2}\int\limits_{-L}^{L}\left[F''\left(\omega_l+\xi\widetilde{\omega}\right)\widetilde{\omega}^2\right]_{y=-\frac{1}{2}}^{y=\frac{1}{2}}\mathrm{d}x, \end{aligned} \quad (4.23)$$

in which $\eta(x,y,t), \xi(x,y,t)$ are two functions with range $(0,1)$ that depend upon $\widetilde{\omega}(x,y,t)$.

Taking the limit $\theta \to 0$ in (4.22) and (4.23) recover the viscous Arnold's identity for a strictly parallel base shear flow [see (3.6) and (3.7) of 30]. In contrasting to a strictly parallel base flow, the quantity ω_l' is no longer a constant for cases with $\theta \neq 0$. Above result serves as a ground for derivation of further viscous identities. We present a viscous identity in the coming section that quantifies perturbation's enstrophy.

4.2 Quantification of weighted perturbation's enstrophy under global nonlinear dynamics

We observed through (4.16) that $F''(\omega_0)$ has a freedom due to an arbitrary constant shift $\overline{U}$. We exploit such freedom in this section to derive an identity that quantifies perturbation's enstrophy under global nonlinear dynamics. The function $\omega_l \mapsto F(\omega_l)$ defined by (4.16) acted upon an argument $\bullet$ reads

$$F''(\bullet) = -\frac{U_l(Y(\bullet)) + \overline{U}}{\omega_l'(Y(\bullet))}, \tag{4.24}$$

in which $\bullet \mapsto Y(\bullet)$ is the inverse function of $y \mapsto \omega_l(y)$. From (4.24) we obtain

$$F'''(\bullet) = \frac{\omega_l(Y(\bullet))\omega_l'(Y(\bullet)) + \left[U_l(Y(\bullet)) + \overline{U}\right]\omega_l''(Y(\bullet))}{\omega_l'(Y(\bullet))^3} \tag{4.25}$$

and

$$\begin{aligned} F''''(\bullet) = \frac{1}{\omega_l'(Y(\bullet))^2} \quad & + \frac{\left[U_l(Y(\bullet)) + \overline{U}\right]\omega_l'''(Y(\bullet)) - 3\omega_l(Y(\bullet))\omega_l''(Y(\bullet))}{\omega_l'(Y(\bullet))^4} \\ & - \frac{3\left[U_l(Y(\bullet)) + \overline{U}\right]\omega_l''(Y(\bullet))^2}{\omega_l'(Y(\bullet))^5}. \end{aligned} \tag{4.26}$$

Let $-\mathbb{N}$ denote the set of non-positive integers. For each $\overline{U} \in -\mathbb{N}$, there exists an F function that fulfills (4.16) and a corresponding $\xi_{\overline{U}} \in (0,1)$ that fufills (4.19). Since the sequence $(\xi_{\overline{U}})_{\overline{U}=0}^{-\infty}$ is bounded within $[0,1]$, there exists a subsequence $(n_k)_{k=1}^{\infty} \subset -\mathbb{N}$ and a number $\xi_\infty \in [0,1]$ such that $\xi_{n_k} \to \xi_\infty$ as $k \to \infty$. Moreover, there exists a subsequence $(n_{k_s})_{s=1}^{\infty} \subset (n_k)_{k=1}^{\infty}$ and a number $\eta_\infty \in [0,1]$ such that $\eta_{n_{k_s}} \to \eta_\infty$ as $s \to \infty$.

Denote $\odot := \omega_l + \eta_\infty\widetilde{\omega}$ and $\bullet := \omega_l + \xi_\infty\widetilde{\omega}$. Substituting (4.24), (4.25), and (4.26) into (4.22) and (4.23), dividing both sides of (4.22) by $\overline{U}$, then taking the limit as

$\overline{U} = n_{k_s} \to -\infty$ whilst $s \to \infty$ on both sides of the resulting equality to obtain

$$
\begin{aligned}
-\frac{1}{2}\frac{\mathrm{d}}{\mathrm{d}t}\int\limits_{\Omega}\frac{\widetilde{\omega}^2}{\omega_l'(Y(\odot))}\,\mathrm{d}\Omega &= \frac{1}{2Re}\int\limits_{-L}^{L}\left[\frac{\omega_l''(Y(\bullet))}{\omega_l'(Y(\bullet))^3}\widetilde{\omega}^2\frac{\partial \bullet}{\partial y} - \frac{2}{\omega_l'(Y(\bullet))}\widetilde{\omega}\frac{\partial\widetilde{\omega}}{\partial y}\right]_{y=-\frac{1}{2}}^{y=\frac{1}{2}}\mathrm{d}x \\
&+\frac{1}{Re}\int\limits_{\Omega}\frac{\omega_l'''(Y(\bullet))}{\omega_l'(Y(\bullet))^4}\widetilde{\omega}^2|\nabla \bullet|^2\,\mathrm{d}\Omega - \frac{2}{Re}\int\limits_{\Omega}\frac{\omega_l''(Y(\bullet))}{\omega_l'(Y(\bullet))^3}\widetilde{\omega}\left[\nabla\widetilde{\omega}\cdot\nabla\bullet\right]\,\mathrm{d}\Omega \\
&+\frac{1}{Re}\int\limits_{\Omega}\frac{1}{\omega_l'(Y(\bullet))}|\nabla\widetilde{\omega}|^2\,\mathrm{d}\Omega - \frac{\tan\theta}{2}\int\limits_{-L}^{L}\left[\frac{1}{\omega_l'(Y(\bullet))}\widetilde{\omega}^2\right]_{y=-\frac{1}{2}}^{y=\frac{1}{2}}\mathrm{d}x, \qquad (4.27)
\end{aligned}
$$

in which we had applied (4.9). The second integral on the second line of (4.27) is further evaluated through using integration by parts to be

$$
\begin{aligned}
&\int\limits_{\Omega}\frac{\omega_l''(Y(\bullet))}{\omega_l'(Y(\bullet))^3}\widetilde{\omega}\left[\nabla\widetilde{\omega}\cdot\nabla\bullet\right]\,\mathrm{d}\Omega \\
&= \frac{1}{2}\int\limits_{\Omega}\frac{\omega_l''(Y(\bullet))}{\omega_l'(Y(\bullet))^3}\left[\nabla(\widetilde{\omega}^2)\cdot\nabla\bullet\right]\,\mathrm{d}\Omega \\
&= \frac{1}{2}\int\limits_{-L}^{L}\left[\frac{\omega_l''(Y(\bullet))}{\omega_l'(Y(\bullet))^3}\widetilde{\omega}^2\frac{\partial\bullet}{\partial y}\right]_{y=-\frac{1}{2}}^{y=\frac{1}{2}}\mathrm{d}x + \frac{1}{2}\int\limits_{-\frac{1}{2}}^{\frac{1}{2}}\left[\frac{\omega_l''(Y(\bullet))}{\omega_l'(Y(\bullet))^3}\frac{\partial\bullet}{\partial x}\right]_{x=-L}^{x=L} \\
&\quad -\frac{1}{2}\int\limits_{\Omega}\left(\frac{\mathrm{d}}{\mathrm{d}\bullet}\left[\frac{\omega_l''(Y(\bullet))}{\omega_l'(Y(\bullet))^3}\right]\right)\widetilde{\omega}^2|\nabla\bullet|^2\,\mathrm{d}\Omega - \frac{1}{2}\int\limits_{\Omega}\frac{\omega_l''(Y(\bullet))}{\omega_l'(Y(\bullet))^3}\widetilde{\omega}^2\nabla^2\bullet\,\mathrm{d}\Omega \\
&= \frac{1}{2}\int\limits_{-L}^{L}\left[\frac{\omega_l''(Y(\bullet))}{\omega_l'(Y(\bullet))^3}\widetilde{\omega}^2\frac{\partial\bullet}{\partial y}\right]_{y=-\frac{1}{2}}^{y=\frac{1}{2}}\mathrm{d}x \\
&\quad +\int\limits_{\Omega}\frac{\omega_l'''(Y(\bullet))}{\omega_l'(Y(\bullet))^4}\widetilde{\omega}^2|\nabla\bullet|^2\,\mathrm{d}\Omega - \frac{1}{2}\int\limits_{\Omega}\frac{\omega_l''(Y(\bullet))}{\omega_l'(Y(\bullet))^3}\widetilde{\omega}^2\nabla^2\bullet\,\mathrm{d}\Omega, \qquad (4.28)
\end{aligned}
$$

in which we had applied (4.9) and the streamwise periodicity.

Substituting (4.28) into (4.27) and using (4.8) to obtain the following result.

Theorem IV.2. *The following identity holds for $\widetilde{\omega}$ determined by the global nonlinear*

dynamics under the no-slip wall condition (4.6)

$$\frac{1}{2}\frac{\mathrm{d}}{\mathrm{d}t}\int\limits_{\Omega}\frac{\widetilde{\omega}^2}{\omega_l'(Y(\odot))}\,\mathrm{d}\Omega=\frac{1}{Re}\int\limits_{-L}^{L}\left[\frac{1}{\omega_l'(Y(\bullet))}\widetilde{\omega}\frac{\partial\widetilde{\omega}}{\partial y}\right]_{y=-\frac{1}{2}}^{y=\frac{1}{2}}\mathrm{d}x-\frac{1}{Re}\int\limits_{\Omega}\frac{|\nabla\widetilde{\omega}|^2}{\omega_l'(Y(\bullet))}\,\mathrm{d}\Omega$$
$$+\frac{1}{2Re}\int\limits_{-L}^{L}\left[\frac{\omega_l''(Y(\bullet))}{\omega_l'(Y(\bullet))^3}\left(\omega_l'(y)-\omega_l'(Y(\bullet))+\xi_\infty\frac{\partial\widetilde{\omega}}{\partial y}\right)\widetilde{\omega}^2\right]_{y=-\frac{1}{2}}^{y=\frac{1}{2}}\mathrm{d}x$$
$$-\frac{1}{Re}\int\limits_{\Omega}\frac{\omega_l''(Y(\bullet))}{\omega_l'(Y(\bullet))^3}\left(\omega_l''(y)-\omega_l''(Y(\bullet))+\xi_\infty\nabla^2\widetilde{\omega}\right)\widetilde{\omega}^2\,\mathrm{d}\Omega$$
$$+\frac{1}{Re}\int\limits_{\Omega}\frac{\omega_l'''(Y(\bullet))}{\omega_l'(Y(\bullet))^4}\left(\omega_l'(y)^2-\omega_l'(Y(\bullet))^2+2\omega_l'(y)\xi_\infty\frac{\partial\widetilde{\omega}}{\partial y}+\xi_\infty^2|\nabla\widetilde{\omega}|^2\right)\widetilde{\omega}^2\mathrm{d}\Omega \quad (4.29)$$

where $\odot:=\omega_l+\eta_\infty\widetilde{\omega}$ *and* $\bullet:=\omega_l+\xi_\infty\widetilde{\omega}$ *for some* $\eta_\infty,\xi_\infty\in[0,1]$.

We would like to remark that (4.29) contains terms of order greater than 2 for cases with $\eta_\infty\neq 0$ or/and $\xi_\infty\neq 0$, this applies to the general situation under global nonlinear dynamics. On the other hand, by letting $\eta_\infty\to 0$ and $\xi_\infty\to 0$ in (4.29) would reduce which to the weighted enstrophy identity (3.35) that holds under linear dynamics, with only the two quadratic terms of (4.29) present therein.

Theorem IV.2 stands as an example that illustrates the distinction in forms of disturbance's enstrophy identity under linear versus nonlinear dynamics. However, as noted by Fraternale *et al* [17], the distinction is not observed for a strictly parallel base flow due to the fact that $\omega_l''\to 0$ as $\theta\to 0$. For such a special case, Fraternale *et al* [17] applied the enstophy identity under linear dynamics to study nonlinear transient growth of perturbations in viscous Couette and Poiseuille flows.

4.3 Enstrophy-based views on instability at asymptotic suction rates

The viscous planar Couette flow becomes linearly unstable subject to asymptotic wall suction under sufficiently large Re [34, 12]. The physical mechanism underneath

the onset of instability remains unclear in literature [27, 31]. With the aid of the weighted enstrophy identity and numerical computation, we provide a preliminary investigation through this section on the vorticity-based instability mechanism for the flow.

We impose U_l to be of the following form throughout this section [12]

$$U_l(y) := \frac{1-\exp\left[-\frac{1}{2}Re\tan\theta\,(2y+1)\right]}{1-\exp\left(-Re\tan\theta\right)}-\frac{1}{2}, \tag{4.30}$$

note that $U_l(y)\to y$ as $\theta\to 0$.

Linearizing (4.7) about the base laminar state $U_l(y)\mathbf{i}-\tan\theta\mathbf{j}$ to obtain

$$\frac{\partial\widetilde{\omega}}{\partial t}+U_l(y)\frac{\partial\widetilde{\omega}}{\partial x}-\tan\theta\frac{\partial\widetilde{\omega}}{\partial y}+\omega_l'(y)\widetilde{v}=\frac{1}{Re}\nabla^2\widetilde{\omega}. \tag{4.31}$$

For a classical normal-mode analysis, we propose perturbations to be of the following form [30]

$$\begin{pmatrix}\widetilde{\psi}\\ \widetilde{u}\\ \widetilde{v}\\ \widetilde{\omega}\end{pmatrix}=\begin{pmatrix}\phi(y)\\ \widehat{u}(y)\\ \widehat{v}(y)\\ \widehat{\omega}(y)\end{pmatrix}\exp\left[i\alpha\left(x-ct\right)\right],\ \text{with}\begin{pmatrix}\widehat{u}(y)\\ \widehat{v}(y)\\ \widehat{\omega}(y)\end{pmatrix}=\begin{pmatrix}\phi'(y)\\ -i\alpha\phi(y)\\ \alpha^2\phi(y)-\phi''(y)\end{pmatrix} \tag{4.32}$$

in which α denotes a (positive) spatial wave number of perturbations and c denotes the complex phase velocity ($c:=c_r+ic_i,\ i^2=-1$), respectively.

Substituting (4.32) into (4.31) to obtain the following stability equation

$$\begin{cases}(i\alpha Re)^{-1}(\mathcal{D}^2-\alpha^2)^2\phi+\frac{\tan\theta}{i\alpha}\mathcal{D}(\mathcal{D}^2-\alpha^2)\phi=(U_l-c)(\mathcal{D}^2-\alpha^2)\phi-U_l''\phi,\\ \phi\left(\pm\frac{1}{2}\right)=0=\phi'\left(\pm\frac{1}{2}\right).\end{cases} \tag{4.33}$$

in which $\mathcal{D}:=\frac{\mathrm{d}}{\mathrm{d}y}$.

The growth rate of perturbations is expressed according to the linearized form of (4.29), by letting $\eta_\infty \to 0$ and $\xi_\infty \to 0$ therein to obtain

$$c_i = \frac{1}{\alpha Re} \frac{\int_{-L}^{L} \left[\frac{1}{\omega_l'} \mathrm{Real}(\widetilde{\omega}) \frac{\partial \mathrm{Real}(\widetilde{\omega})}{\partial y} \right]_{y=-\frac{1}{2}}^{y=\frac{1}{2}} \mathrm{d}x - \int_\Omega \frac{1}{\omega_l'} |\nabla \mathrm{Real}(\widetilde{\omega})|^2 \, \mathrm{d}\Omega}{\int_\Omega \frac{1}{\omega_l'} \mathrm{Real}(\widetilde{\omega})^2 \, \mathrm{d}\Omega}, \tag{4.34}$$

where $\mathrm{Real}(\widetilde{\omega})$ stands for the real-valued part of $\widetilde{\omega}$.

By setting $L = \frac{\pi}{\alpha}$ in (4.34) and substituting (4.32) into which to obtain

$$\begin{aligned} c_i \quad &= \frac{1}{2\alpha Re} \frac{\left[\frac{1}{\omega_l'} \frac{\mathrm{d}}{\mathrm{d}y} |\widehat{\omega}|^2 \right]_{y=-\frac{1}{2}}^{y=\frac{1}{2}}}{\int_{-\frac{1}{2}}^{\frac{1}{2}} \frac{1}{\omega_l'} |\widehat{\omega}|^2 \, \mathrm{d}y} - \frac{1}{\alpha Re} \frac{\int_{-\frac{1}{2}}^{\frac{1}{2}} \frac{1}{\omega_l'} \left(|\widehat{\omega}'|^2 + \alpha^2 |\widehat{\omega}|^2 \right) \, \mathrm{d}y}{\int_{-\frac{1}{2}}^{\frac{1}{2}} \frac{1}{\omega_l'} |\widehat{\omega}|^2 \, \mathrm{d}y} \\ &=: \left[B_\omega(y) \right]_{y=-\frac{1}{2}}^{y=\frac{1}{2}} - \int_{-\frac{1}{2}}^{\frac{1}{2}} I_\omega(y) \, \mathrm{d}y \\ &=: p_B - p_I. \end{aligned} \tag{4.35}$$

It is manifest that $p_I > 0$ in all circumstances. Thus, p_B is the only constituent of c_i that may contribute to instability.

We fix $\alpha = 1$ without loss of generality, equation (4.33) is solved numerically for a range of (Re, θ) parameters by using the standard Chebyshev collocation technique [7]. The stability boundary is presented in Figure 4.2(a) by the solid curve, below which the base flow is linearly stable. For the fixed $Re = 4.5 \times 10^6$, we computed the growth rate c_i versus $\tan\theta$ starting from $\tan\theta = 10^{-8}$, and we found that the maximum growth is reached at $\tan\theta = 3 \times 10^{-6}$ with a magnitude of $c_i = 0.0047$.

The plot of c_i and its constituents p_B, p_I versus $\tan\theta$ that ranges from 10^{-8} to 3×10^{-6} is presented in Figure 4.2(b), from which we observe the closeness in magnitudes of p_B and p_I that well corresponds to small growth rates observed over the designated range of $\tan\theta$. Moreover, $B_\omega\left(\pm\frac{1}{2}\right)$ (the constituents of p_B) versus $\tan\theta$ is presented in Figure 4.2(c). It is evident that the contribution to p_B from the upper wall, namely

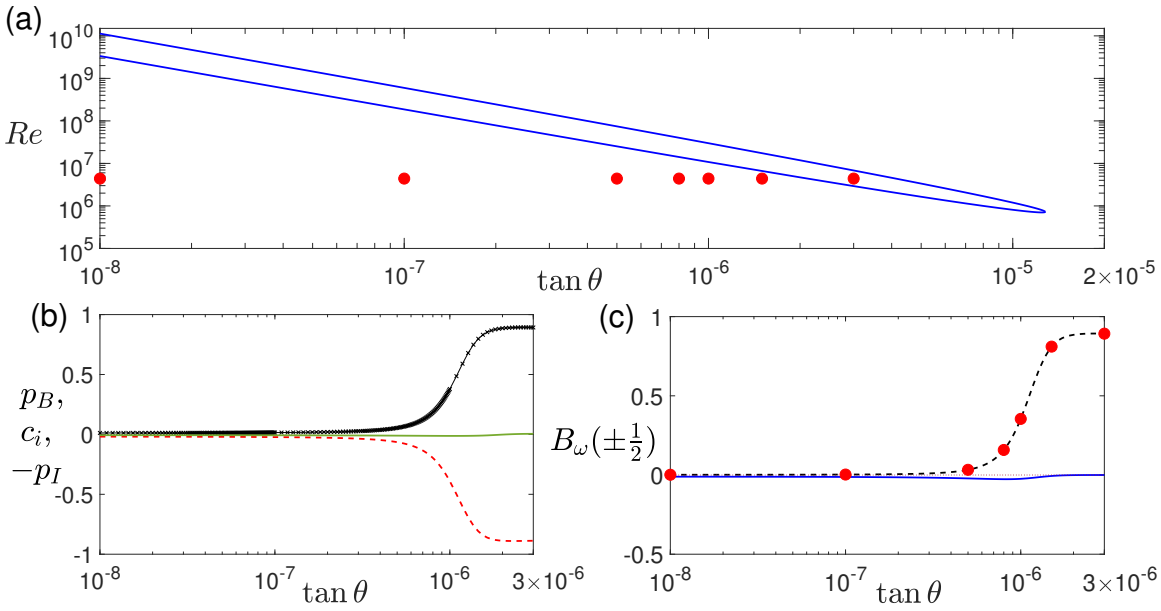

Figure 4.2: Stability boundary and enstrophy parameters for fixed $\alpha = 1$.

$B_\omega\left(\frac{1}{2}\right)$ (the dashed curve) becomes significantly larger than that due to the lower wall (solid curve) as $\tan\theta$ approaches the stability boundary. This suggests that the upper wall had played a predominant role in the onset of instability.

4.4 Discussion

The viscous extension of Arnold's identity for the suction problem closely follows the procedure established in the previous Chapter. However, there was a 'risk' at the first step of the extension procedure which was not observed for the case of strictly parallel flows, namely the presence of $\tan\theta \int_\Omega \widetilde{v}\ \mathrm{d}\Omega$ in (4.15). Though this term vanishes due to streamwise periodicity of the perturbation's stream function $\widetilde{\psi}$, it rang the alarm for us to think about whether the viscous extension of Arnold's non-viscous theory might be carried out for a universal shear flow. Nevertheless, one thing we know for sure is that the extension would work only if there was a (unique) F function that cancels first-order terms in $\widetilde{\mathcal{E}} + \widetilde{\mathcal{C}}_s$.

Note that (4.29) in Theorem IV.2 is the nonlinear version of (3.35) in Theorem

III.2. The drastic difference in forms of the two enstrophy identities were not seen in the case for strictly parallel flows (recall Theorem III.4). This reveals a fact that the identities which govern the perturbation's enstrophy are of different forms under linear versus nonlinear dynamics. In fact, the perturbation's enstrophy identity possesses the same form under both linear and nonlinear dynamics only for strictly parallel plane shear flows.

One other fact about our enstrophy identities (3.34), (3.35) and (4.29) is related to the challenging task of using these to carry out a rigorous Sobolev-type estimation on the marginal stability boundary. The reason is due to the presence of boundary terms in these identities. Specifically, one has to know apriori the range of $\frac{\partial\widetilde{\omega}}{\partial y}$ based on information of admissible $\widetilde{\psi}$ up to the second-order derivative, but the Sobolev embedding theorem does not serve for that purpose! The physical reasoning for such difficulty arises from the Arnold's procedure, namely the non-viscous portion of the flow dynamics had been completely 'wiped off' from the Arnold's function $\widetilde{\mathcal{E}}+\widetilde{\mathcal{C}}_s$ by the unique choice of F, and hence the inviscid information is no longer recorded in our enstrophy identities. Therefore, to enable an analytical estimation based on our enstrophy identity, one needs to couple our enstrophy identity with the original set of equations of motion in order to determine higher-order information on $\widetilde{\omega}$. Of course, as far as physical interpretations are concerned, numerical solutions are adequate.

CHAPTER V

Future works

Viscous extension of Arnold's theory to plane shear flows had been established in the last two chapters. Our viscous theory needs to be continually developed for more sophisticated flows. Meanwhile, the novel theory up-to-date is readily applicable to a variety of problems in fluid dynamics, such as the two outlined below.

5.1 Rigiorous proof of global nonlinear stability for viscous plane-parallel Couette flow

The plane-parallel Couette flow is one of the most fundamental plane wall-driven flows. Despite its formal simplicity and the general belief that the flow is stable against arbitrary 2D perturbations, there is no rigorous proof of global nonlinear stability for the flow in literature. On the other hand, there are numerical computations which strive to push forward the best up-to-date stability bounds [14]. A rigorous proof of *linear* stability for the plane-parallel Couette flow is due to V. A. Romanov which dates back to 1973 [40]. Mathematicians since after have attempted to prove nonlinear stability for the flow, but the traditional energy approach limited the arguments to hold only under small Reynolds numbers [14].

Not withstanding the limitation of those traditional energy-type estimations, I plan to re-visit the problem from the perspective of enstrophy (vorticity). The starting

point is Theorem III.4 in Chapter 3, which enables one to use the enstrophy quantity in global nonlinear stability analysis. In contrasting to an energy-type approach, the enstrophy approach needs to be closely tied to flow equations in order to obtain faithful estimations on the vorticity perturbation at the wall boundary. I foresee the potential of such new approach in reviving interest of study on classical viscous flows.

5.2 The exact cause of instability in viscous pipe Hagen-Poiseuille flow

The onset of turbulence in fluid flows has stood as a major challenge in physics since the early past century. Shortly after the essential discovery by scientific giants Lord Kevin and Lord Rayleigh [38], a classical methodology based on linearized Navier-Stokes equations had then been developed, and it is commonly referred to as the 'normal-mode analysis'. Despite its enormous success in recognizing early stages of transition into turbulence for a great majority of fluid flows [13], there remain a few flows of crucial importance that behave differently from the prediction made according to the normal-mode analysis.

The Pipe Poiseuille Flow is one such flow that has perplexed fluid dynamists for over a century. A first experiment on this flow was conducted by Osborne Reynolds in 1883, in which turbulence was observed at a moderately high flow speed. Thereafter, a vast amount of research in literature strives to explore the cause of instability (onset of turbulence) for the flow. The actual cause, however, remains to be a mystery at the present. It is worth mentioning that the flow was predicted to be linearly stable under arbitrary flow speeds, since the long-established normal-mode analysis fails to predict any instability for the flow! It prompts us to make the conjecture that the instability in the pipe Poiseuille flow is very likely due to nonlinear effects, for which our novel nonlinear enstrophy identity shall be useful for re-visiting the problem.

BIBLIOGRAPHY

BIBLIOGRAPHY

[1] R. A. Adams and J. J. F. Fournier. *Sobolev Spaces*. 2nd Ed. Academic Press, 2003.

[2] V. I. Arnold. Conditions for the nonlinear stability of the stationary plane curvilinear flows of an ideal fluid. *Doklady Akademii Nauk*, 162:975–978, 1965.

[3] V. I. Arnold. On a priori estimate in the theory of hydrodynamic stability. *American Mathematical Society Translations*, 19:267–269, 1969.

[4] V. I. Arnold and B. A. Khesin. *Topological Methods in Hydrodynamics*. volume 125 of *Applied Mathematical Sciences*. Springer, 1998.

[5] G. K. Batchelor. *An introduction to Fluid Dynamics*. Cambridge University Press, 1967.

[6] B. J. Bayly, S. A. Orszag, and T. Herbert. Instability Mechanisms in Shear-Flow Transition. *Annual Review of Fluid Mechanics*, 20:359–391, 1988.

[7] J. P. Boyd. *Chebyshev and Fourier Spectral Methods*. 2nd Ed. Dover, New York, 2000.

[8] F. H. Busse. Bounds for turbulent shear flow. *J. Fluid Mech*, 41:219, 1970.

[9] P. Constantin and C. R. Doering. Variational bounds on energy dissipation in incompressible flows: II. channel flow. *Physical Review E*, 51:3192, 1995.

[10] C. R. Doering and P. Constantin. Energy dissipation in a shear driven turbulence. *Physical Review Letters*, 69:1648, 1992.

[11] C. R. Doering and P. Constantin. Variational bounds on energy dissipation in incompressible flows: Shear flow. *Physical Review E*, 49:4087, 1994.

[12] C. R. Doering, E. A. Spiegel, and R. A. Worthing. Energy dissipation in a shear layer with suction. *Physics of Fluids*, 12:1955–1968, 2000.

[13] P. G. Drazin and W. H. Reid. *Hydrodynamic Stability*. Cambridge University Press, 2nd edition, 2004.

[14] P. Falsaperla, A. Giacobbe, and G. Mulone. Nonlinear stability results for plane couette and poiseuille flows. *Physcal Review E*, 100:013113, 2019.

[15] R. Fjørtoft. Application of integral theorems in deriving criteria of stability for laminar flows and for the baroclinic circular vortex. *Geofysiske publikasjoner*, 17(6):1–52, 1950.

[16] J. Frank, A. King, and D. Raine. *Accretion Power in Astrophysics, Cambridge Astrophysics Series, Vol. 21.* Cambridge University Press, 1992.

[17] F. Fraternale, L. Domenicale, G. Staffilani, and D. Tordella. Internal waves in sheared flows: Lower bound of the vorticity growth and propagation discontinuities in the parameter space. *Physical Review E*, 97:063102, 2018.

[18] B. Gallet, C. R. Doering, and E. A. Spiegel. Destabilizing taylor-couette flow with suction. *Phys. Fluids*, 22:034105, 2010.

[19] S. Grossmann, D. Lohse, and C. Sun. High-Reynolds Number Taylor-Couette Turbulence. *Annual Review of Fluid Mechanics*, 48:53–80, 2016.

[20] T. Herbert. Periodic secondary motions in a plane channel. In A. I. van de Vooren and P. J. Zandbergen, editors, *Proceedings of the Fifth International Conference on Numerical Methods in Fluid Dynamics*, volume 59 of *Lecture Notes in Physics*, pages 235–240. Springer-Verlag, Berlin, 1976.

[21] E. Hopf. Ein allgemeiner endlichkeitssatz der hydrodynamik. *Mathematische Annalen*, 117:764, 1941.

[22] K. Ilin and M. Andrey. Instability of a two-dimensional viscous flow in an annulus with permeable walls to two-dimensional perturbations. *Phys. Fluids*, 27:044107, 2015.

[23] A. Ishak, R. Nazar, and I. Pop. Uniform suction/blowing effect on flow and heat transfer due to a stretching cylinder. *Applied Mathematical Modelling*, 32:2059, 2008.

[24] D. D. Joseph. Nonlinear stability of the Boussinesq equations by the method of energy. *Arch. Rational Mech. Anal.*, 22:163, 1966.

[25] D. D. Joseph. *Stability of Fluid Motions.* Springer-Verlag, Berlin, 1976.

[26] Y. S. Kachanov. Physical mechanisms of laminar-boundary-layer transition. *Annual Review of Fluid Mechanics*, 26:411–482, 1994.

[27] R. R. Kerswell. Instability driven by boundary inflow across shear: a way to circumvent Rayleigh's stability criterion in accretion disks? *J. Fluid Mech*, 784:619, 2015.

[28] H. Kozono and T. Yanagisawa. Leray's problem on the stationary Navier-Stokes equations with inhomogeneous boundary data. *Mathematische Zeitschrift*, 262:27, 2009.

[29] D. Küchemann. Report on the I.U.T.A.M. symposium on concentrated vortex motions in fluids. *Journal of Fluid Mechanics*, 21:1–20, 1965.

[30] H. Lee and S. Wang. Extension of classical stability theory to viscous planar wall-bounded shear flows. *Journal of Fluid Mechanics*, 877:1134–1162, 2019.

[31] H. Lee, B. Wen, and C. R. Doering. Improved upper bounds on the energy dissipation rate for shear flow with injection and suction. *Physics of Fluids*, 31:085102, 2019.

[32] C. C. Lin. *The Theory of Hydrodynamic Stability*. Cambridge University Press, 1955.

[33] L. M. Mack. A numerical study of the temporal eigenvalue spectrum of the Blasius boundary layer. *Journal of Fluid Mechanics*, 73:497–520, 1976.

[34] F. Nicoud and J. R. Angilella. Effects of uniform injection at the wall on the stability of Couette-like flows. *Phys. Rev. E*, 56:3000, 1997.

[35] W. McF. Orr. The Stability or Instability of the Steady Motions of a Perfect Liquid and of a Viscous Liquid; Part II. A Viscous Liquid. In *Proceedings of the Royal Irish Academy, Sec. A*, volume 27, pages 69–204. 1907.

[36] S. A. Orszag. Accurate solution of the Orr-Sommerfeld stability equation. *Journal of Fluid Mechanics*, 50:689–703, 1971.

[37] S. C. Plasting and R. R. Kerswell. Improved upper bound on the energy dissipation rate in plane Couette flow: the full solution to Busse's problem and the Constantin-Doering-Hopf problem with one-dimensional background field. *Journal of Fluid Mechanics*, 477:363–379, 2003.

[38] L. Rayleigh. On the stability, or instability, of certain fluid motions. *Proceedings of the London Mathematical Society*, 11:57–70, 1880.

[39] O. Reynolds. An experimental investigation of the circumstances which determine whether the motion of water shall be direct or sinuous, and of the law of resistance in parallel channels. *Philosophical Transactions of the Royal Society A*, 174:935–982, 1883.

[40] V. A. Romanov. Stability of plane-parallel couette flow. *Functional Analysis and Its Applications*, 7(2):137–146, 1973.

[41] P. J. Schmid and D. S. Henningson. *Stability and Transition in Shear Flows*. volume 142 of *Applied Mathematical Sciences*. Springer, 2001.

[42] J. Serrin. On the stability of viscous fluid motions. *Archive for Rational Mechanics and Analysis*, 3:1–13, 1959.

[43] J. T. Stuart. On the non-linear mechanics of wave disturbances in stable and unstable parallel flows. Part 1: The basic behaviour in plane Poiseuille flow. *Journal of Fluid Mechanics*, 9:353–370, 1960.

[44] J. L. Synge. The stability of plane Poiseuille motion. In *Proceedings of the Fifth International Congress for Applied Mechanics*, pages 326–332. John Wiley & Sons, Inc., 1938.

[45] I. Tobasco, D. Goluskin, and C. R. Doering. Optimal bounds and extremal trajectories for time averages in nonlinear dynamical systems. *Phys. Lett. A*, 382:382, 2018.

[46] A. Tsinober. *An Informal Introduction to Turbulence*. volume 63 of *Fluid Mechanics and Its Applications*. Kluwer, Dordrecht, 2001.

[47] F. Waleffe and K. Kerswell. *Shear Turbulence: Onset and Structure (lecture notes)*. pages 79–91. Woods Hole Oceanographic Institution, 2011.

[48] B. Wen, G. P. Chini, N. Dianati, and C. R. Doering. Computational approaches to aspect-ratio-dependent upper bounds and heat flux in porous medium convection. *Physics Letters A*, 377:2931, 2013.

[49] B. Wen, G. P. Chini, R. R. Kerswell, and C. R. Doering. Time-stepping approach for solving upper-bound problems: Application to two-dimensional Rayleigh-Bénard convection. *Physical Review E*, 92:043012, 2015.

[50] B. Wen and Gregory P. Chini. Inclined porous medium convection at large Rayleigh number. *Journal of Fluid Mechanics*, 837:670–702, 2018.

[51] P. W. Yau, S. Wang, and Z. Rusak. Extension to nonlinear stability theory of the circular Couette flow. *Journal of Fluid Mechanics*, 795:455–493, 2016.